MODELING AND SIMULATION OF THE INYAN KARA FORMATION TO ESTIMATE SALTWATER DISPOSAL POTENTIAL: FINAL REPORT

Final Report

Prepared by:

Jun Ge
Nicholas W. Bosshart
Lawrence J. Pekot
Bethany A. Kurz
Charles D. Gorecki
Jun He
Benjamin S. Oster

Energy & Environmental Research Center
University of North Dakota
15 North 23rd Street, Stop 9018
Grand Forks, ND 58202-9018

TABLE OF CONTENTS

LIST OF FIGURES

LIST OF TABLES

MODELING AND SIMULATIONS OF THE INYAN KARA FORMATION TO ESTIMATE SALTWATER DISPOSAL POTENTIAL: FINAL REPORT

EXECUTIVE SUMMARY

The rapid increase in oil and gas production within the Bakken petroleum system has resulted in a substantial increase in the volume of produced brine requiring disposal in western North Dakota. As of 2016, approximately 94% of produced brines (by volume) was disposed of via deep well injection into the sandstone units of the Inyan Kara Formation, raising questions about the long-term viability of the Inyan Kara as a disposal target. Through the Bakken Production Optimization Program, the Energy & Environmental Research Center developed a reservoir simulation model of a portion of the Inyan Kara Formation to evaluate the effects of current and possible future saltwater disposal (SWD) operations on reservoir pressure and long-term disposal potential.

The reservoir simulation model developed for this effort encompassed most of McKenzie County and a portion of northwestern Dunn County. The geologic model was built using Schlumberger's Petrel software (Schlumberger, 2016), and a numerical simulation model was developed using Computer Modelling Group's (CMG's) GEM software. The data inputs for the geologic model included well logs, formation tops, and core sample descriptions and analyses, as well as injected volumes and pressure measurements at individual SWD wells. Injection rate, volume, and pressure data was compiled for the 103 SWD wells in the modeled area and used to history-match the numerical simulation model. Adjustments were made in the model to better account for local permeability and porosity and to account for skin factor and periodic well operations such as acid treatment.

The simulation model was used to estimate the current distribution of reservoir pressure and injected salinity plumes as a result of SWD beginning in 1961. Several potential future scenarios were also simulated to evaluate the distribution of pressure and salinity within the Inyan Kara Formation and to evaluate long-term disposal potential out to the year 2050. Three simulation scenarios were evaluated: one that assumed that each of the 103 SWD wells in the area (both those that are currently operational and those that have ceased injection) continued injecting until 2050 at their last reported rate, one scenario that assumed that only the operational SWD wells in the area (93 total) continued injecting at their last reported rate, and one scenario that assumed that the 93 active SWD wells operated at their maximum allowable rate (based on wellhead injection pressure) until 2050. Each of the three primary scenarios had two cases. One case assumed that all boundaries surrounding the model were open, meaning no impediments to fluid flow along the model boundaries. The second case in each scenario assumed closed boundaries (no fluid flow allowed) on all but the eastern edge, which was considered open because it is adjacent to an area with a low occurrence of SWD wells.

In addition to the results generated by the simulation model, a simplistic equation was used to calculate the volumetric storage potential of the Inyan Kara within the modeled area under closed boundary conditions. This calculation assumed that all of the available pore space would be accessible via injection wells and that the formation fluid pressure would be at the maximum allowable without exceeding the permitted injection pressure. This simple estimate of maximum

storage potential under closed boundary conditions was calculated for comparison to the disposal potential estimated by the reservoir simulation model.

The cumulative water injection into the Inyan Kara at the beginning of 2017 was approximately 644 million barrels (bbl). Results of the numerical simulation suggest the cumulative brine injection at the end of 2050 will range from 3.86 to 5.27 billion bbl based on the different scenarios evaluated. This represents an increase of 500% to 670% over the 2017 cumulative injection volume for all of the simulation cases. Comparison of the results from the numerical simulation to the estimated storage potential using the volumetric approach also indicates that there would be pore space available for storage at the end of 2050. The closed system volumetric estimate was 7.19 billon bbl, compared to the highest predicted cumulative injection volume of 5.27 billion bbl. Although the closed system estimate is highly conservative (and likely low) because it assumes no flow from the model boundaries or resulting pressure dissipation, a comparison of the estimate storage potential suggests that as much as 73% of the storage potential (of a closed system) could be utilized by 2050. A comparison of the simulated injection rates over time indicates that, in each case, rates of injection will have to decline to avoid exceeding the injection pressure limitations.

Despite the large predicted storage potential of the Inyan Kara, maps of the predicted reservoir pressure indicate that localized areas of pressurization have already occurred, and predictive model simulations suggest that the areas of elevated pressure could expand in size and magnitude with continued long-term injection, especially in the northern portion of McKenzie County. These areas exhibit behavior of a system with semiclosed boundary conditions, and continued injection could result in operators curtailing injection rates and/or injected volumes to avoid exceeding the injection pressure limitations established by the North Dakota Department of Mineral Resources (DMR). The model predictions also suggest that there is a large portion (e.g., southern half) of the simulated area that could support an additional pressure increase even after more than 30 years of injection.

Maps depicting the brine plume extents surrounding individual SWD wells illustrate the influence of geology of the brine migration pathways. Many of the brine plumes appear to follow preferential flow pathways that result from variability in the extent and thickness of the sandstone layers within the Inyan Kara. The model results reinforce the importance of understanding the local geology prior to siting a SWD well.

The goal of this modeling effort was not to conduct a comprehensive analysis of multiple potential injection scenarios, but rather to provide some general insight into the overall disposal potential of the Inyan Kara. An additional goal was to identify areas within the Inyan Kara reservoir that may already exhibit pressurization effects as a result of SWD, to evaluate the effects of possible future injection scenarios on reservoir fluid pressure and, ultimately, to aid in identification of areas that may be conducive or problematic for siting of new SWD wells. This model was meant to provide insight over a broad region of SWD in the Bakken region. Additional work could be performed to expand the model extent, to increase the spatial resolution of the model, and/or to improve the resolution of the publically available SWD well operational data with partner-supplied data.

MODELING AND SIMULATIONS OF THE INYAN KARA FORMATION TO ESTIMATE SALTWATER DISPOSAL POTENTIAL: FINAL REPORT

INTRODUCTION

The increase in oil and gas production in North Dakota because of Bakken petroleum system (Bakken) development has resulted in a threefold increase in produced water over the past decade (Kurz and others, 2016). In 2016, approximately 431 million bbl of water was injected into SWD wells located in North Dakota (Kurz, 2016), and this trend is expected to increase in the coming decades with the continued extraction of oil, gas, and associated water from the Bakken petroleum system. As of 2016, 94% of all SWD wells (on a volumetric basis) were developed in the Inyan Kara Formation (Inyan Kara) of the Dakota Group (Kurz and others, 2016), a sandstone formation of Early Cretaceous age (Figure 1).

Because of industry's current reliance on the Inyan Kara as a SWD target, an effort is under way through the Bakken Production Optimization Program (BPOP) to estimate local and regional pressure effects that have occurred as a result of historic SWD and to evaluate areas that may be suitable or problematic for disposal through reservoir simulation of hypothetical future injection scenarios. An additional goal was to evaluate the overall disposal potential of the Inyan Kara in the areas that are currently targeted for injection. In this effort, disposal potential (or storage potential) is defined as the total volume of saltwater that can be injected into the subsurface without exceeding the injection pressure limitations established by the Underground Injection Control (UIC) program at the North Dakota DMR.

BPOP is a consortium comprising the Energy & Environmental Research Center (EERC), the North Dakota Industrial Commission (NDIC), several of the largest oil producers in North Dakota, and representatives from the oil and gas service industry. The program was initially funded for 3 years to accomplish a wide range of projects focused on improving oil recovery from the Bakken petroleum system while simultaneously reducing the environmental footprint associated with oil and gas extraction. Program funding has since been expanded to include an additional 3 years, referred to as Phase 2 of the Bakken Production Optimization Program, to continue to address critical issues surrounding oil and gas extraction from the Bakken, such as water disposal.

To accomplish the goals of the Inyan Kara disposal potential assessment, a reservoir simulation model was developed to enable the assessment of current and potential future SWD scenarios in a portion of western North Dakota with a high concentration of SWD wells. The model's areal extent encompasses most of McKenzie County and a portion of northwestern Dunn County, as shown in Figure 2. This area was selected to coincide with an effort being conducted by the North Dakota DMR to map the total thickness of injectable (i.e., "clean") sand intervals within the Inyan Kara based on 1:100,000-scale (100K) quadrangle maps (Bader, 2015). The first unit mapped by the DMR was the Watford City quadrangle, and the information contained within that map was used to guide the development of the geologic model and the simulation discussed herein.

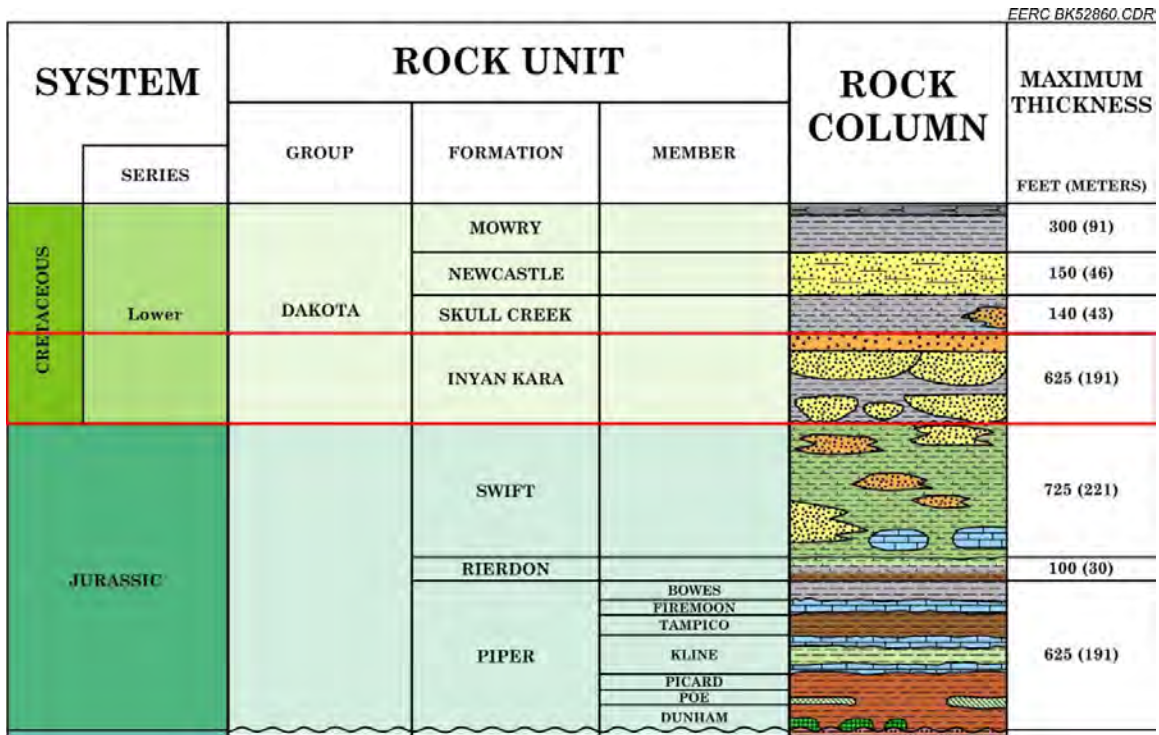| SYSTEM		ROCK UNIT			ROCK COLUMN	MAXIMUM THICKNESS
	SERIES	GROUP	FORMATION	MEMBER		FEET (METERS)
CRETACEOUS	Lower	DAKOTA	MOWRY			300 (91)
			NEWCASTLE			150 (46)
			SKULL CREEK			140 (43)
			INYAN KARA			625 (191)
JURASSIC			SWIFT			725 (221)
			RIERDON			100 (30)
		PIPER		BOWES		
				FIREMOON		
				TAMPICO		
			KLINE			625 (191)
				PICARD		
				POE		
				DUNHAM		

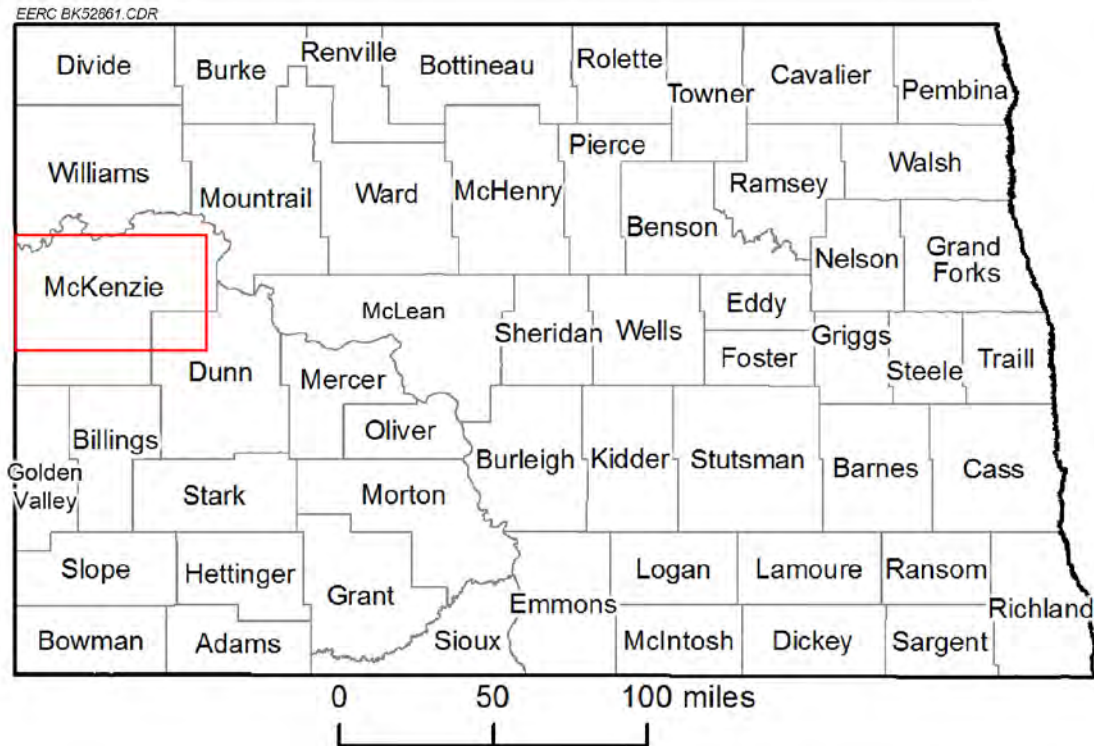Figure 1. Williston Basin stratigraphic column (adapted from Murphy and others, 2009).

Figure 2. Map view of the model area (red rectangle). The model area encompasses approximately 2100 mi^2.

This report summarizes model development, the assumptions used to develop the predictive simulation scenarios and the key findings and conclusions of the effort. Because this effort was intended as a first step to evaluate localized pressure effects resulting from SWD and to estimate the SWD potential of the Inyan Kara within the modeled area, a comprehensive assessment of multiple future injection scenarios was not conducted. The model was intended as a tool for use in evaluating potential future injection scenarios of interest that are defined by BPOP members.

GEOLOGIC MODEL DEVELOPMENT

For the purposes of this investigation, a simple deterministic model was developed for a portion of the Inyan Kara Formation. A probabilistic approach may be an appropriate next step to better capture the uncertainty with respect to property distributions and will affect the resulting distributions of brine and pressure within the modeled area. The Inyan Kara model was built using Schlumberger's Petrel software (Schlumberger, 2016), with model inputs compiled from publicly available data sets, most of which were available from NDIC. The input data sets include well logs, formation tops, and core sample descriptions and analyses as well as injected volumes and pressure measurements at individual SWD wells.

As shown in Figure 3, limited core data were available for the Inyan Kara. According to the available core analyses, the Inyan Kara comprises layers of sand, silty sand, and shale with limited lateral continuity between key lithotypes. The sandstone units of the Inyan Kara comprise quartz, with minor components such as feldspar, coal, and interspersed plant fragments, siderite nodules/concretions, iron staining, and calcitic cement. The average core porosity and average core permeability (geometric mean) for the Inyan Kara sandstone are 26% and 72 mD, respectively.

Structure

Formation top depths were picked based upon gamma ray (GR) well log characteristics, using logs from 585 wells, to develop the model's structural framework (Figure 4). Structural surfaces were created for the Mowry (K-M), Newcastle (K-N), Inyan Kara (K-IK), Swift (J-S), and Rierdon (J-R) Formations. An isopach map of the Inyan Kara (Figure 5) shows the Williston Basin depositional center lies in the west-central portion of the study area.

The Mowry Formation comprises the uppermost unit of the model, and the base of the model is defined by the Rierdon Formation top structure. A cell size of 1640 ft × 1640 ft was used for this study. Four zones were correlated across the area of review: the Mowry, Newcastle, Inyan Kara, and Swift intervals. There are a total of 983,268 cells within the entire model (Mowry top through Swift bottom) and 893,880 cells within the Inyan Kara portion of the model. For simulation purposes, the Inyan Kara cell sizes were split into 40 layers, with an average cell thickness of about 11 feet. This resolution was much finer than that of the surrounding formations.
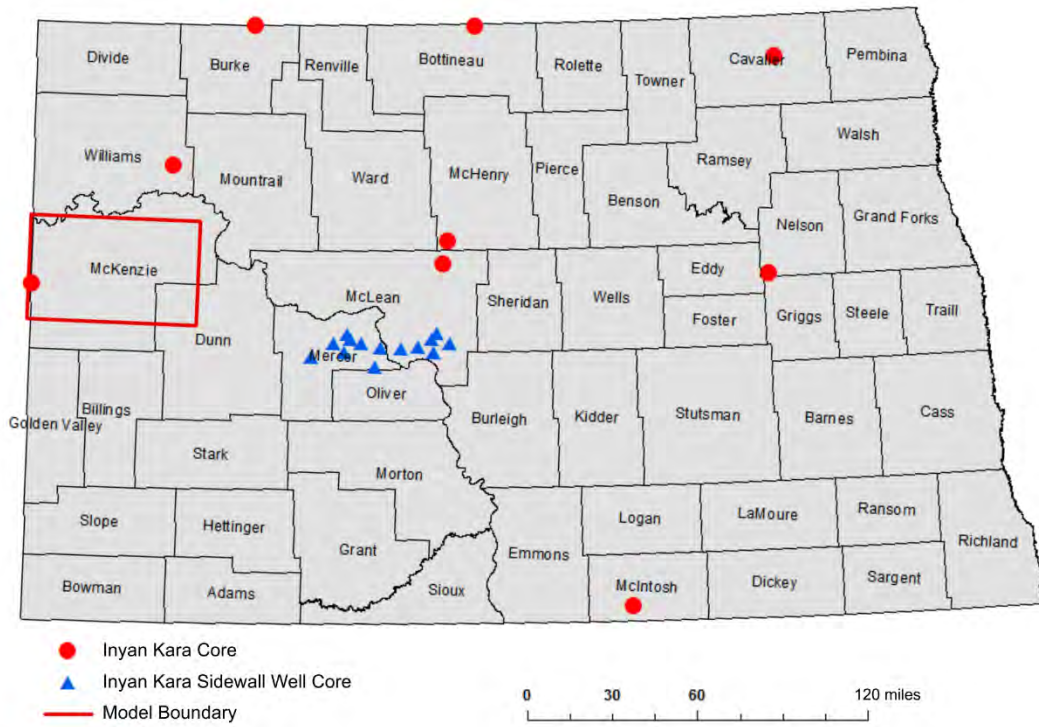
3

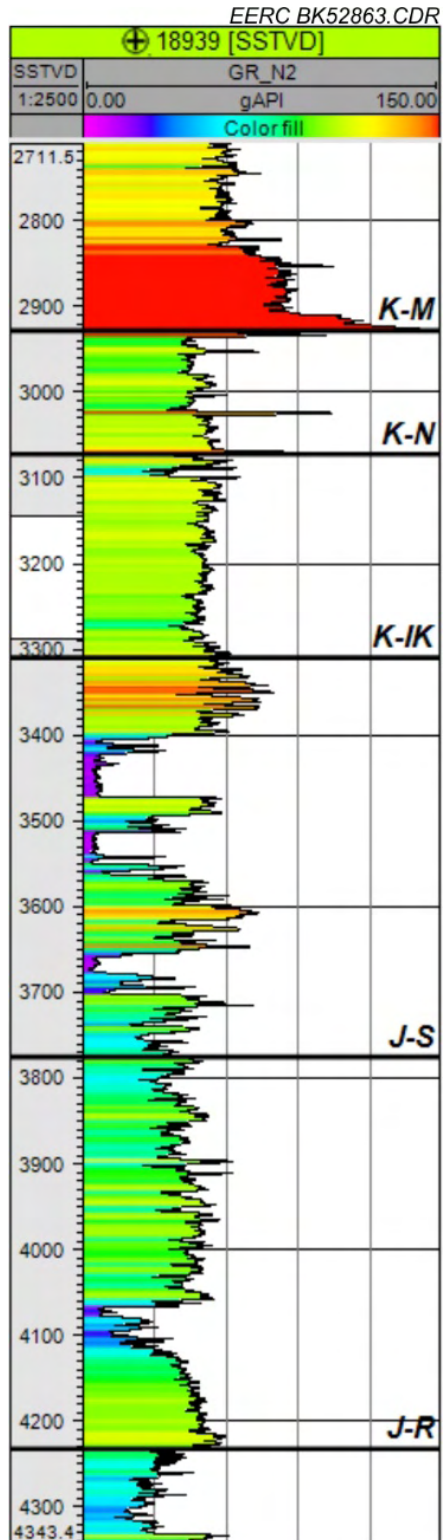Figure 3. Inyan Kara Formation cored well locations and model boundary.

Figure 4. An example of formation tops determined using a GR log (Mowry: K-M, Newcastle: K-N, Inyan Kara: K-IK, Swift: J-S, and Rierdon: J-R).
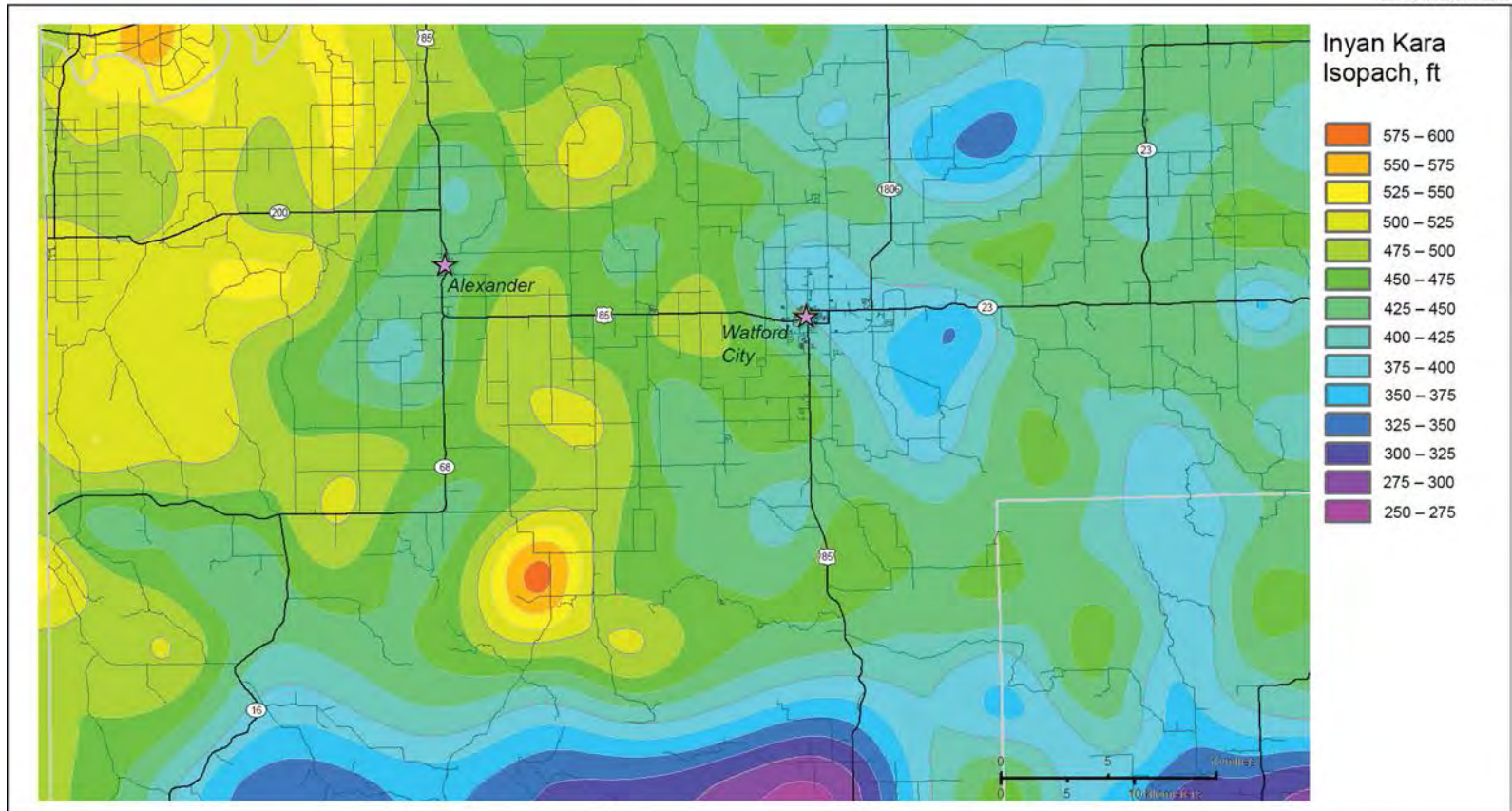
Figure 5. Isopach map of the Inyan Kara Formation.

Lithofacies

The Inyan Kara consists of heterogeneous clastic sequences deposited in several different environments (i.e., shallow marine, marginal marine, fluvial–deltaic, etc.). Examination of well logs and associated analyses of geologic core samples verified that normalized GR logs were able to provide reliable lithofacies interpretations. Normalized GR logs were used to separate the formation into three basic lithofacies: sand, silty sand, and shale. These lithofacies intervals were identified and upscaled into the grid to serve as control points for geostatistical distribution (Figures 6 and 7). Figure 6 is an excellent example of the lateral heterogeneity of sand (and other) units within the formation. The lithofacies percentages were 27.5%, 44.7%, and 27.8% for sand, silty sand, and shale, respectively (Figure 7). The distribution of Inyan Kara total sand thickness in the study area is shown by the isopach map in Figure 8, and a net/gross thickness map (Figure 9) shows the portion of the total formation thickness that comprises sand.

Petrophysical Properties

The petrophysical properties (porosity and permeability) were distributed in the geologic model with conditioning to the lithofacies model. A porosity–permeability crossplot was developed from the available geologic core sample measurements, as shown in Figure 10. Porosity and permeability measurements were examined with respect to each lithofacies (Figure 11) to guide geostatistical distribution throughout the model (Figures 12 and 13). Permeability distribution was subsequently modified during the history-matching process. Table 1 shows the volumetric characteristics for each lithofacies.
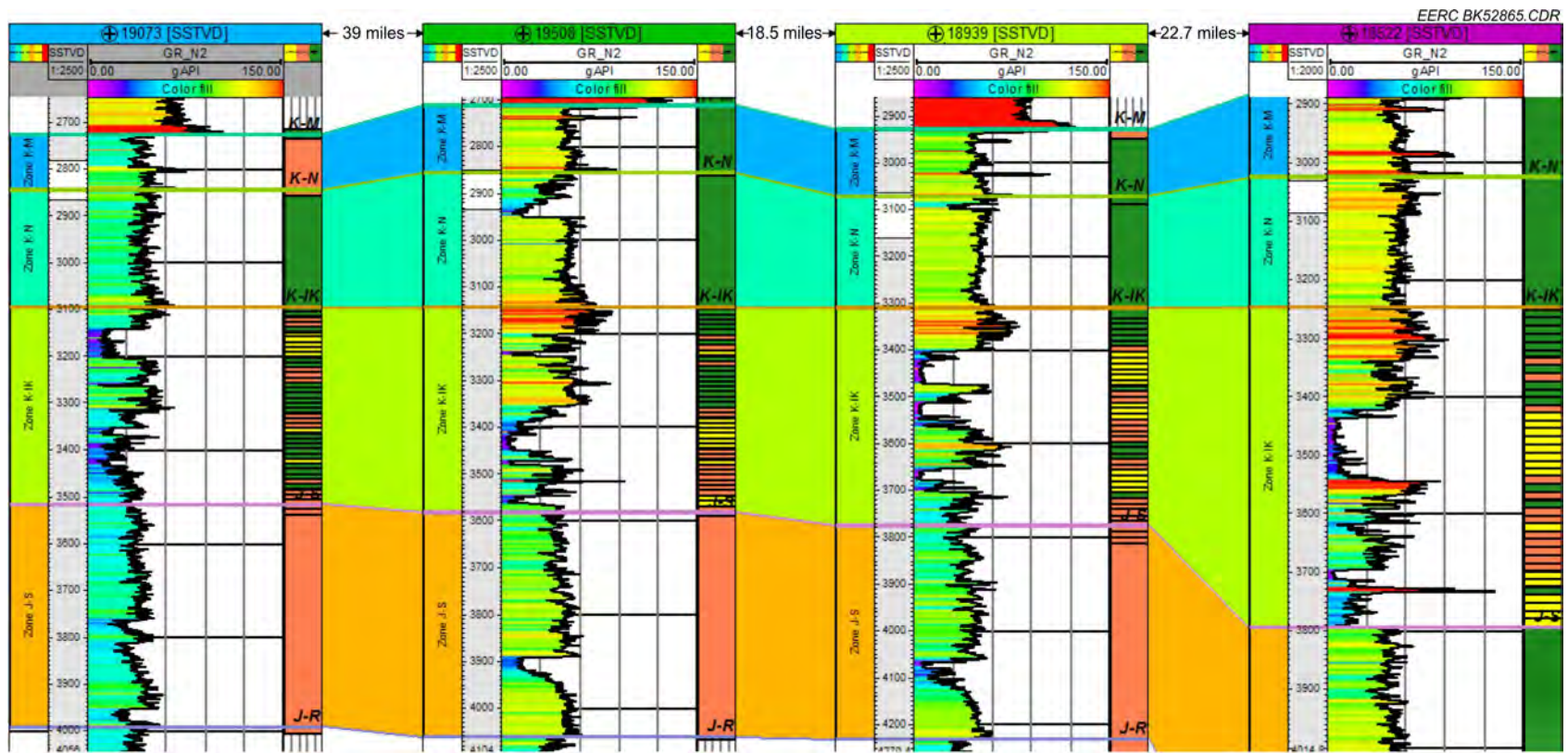
Figure 6. Well cross section showing the generalized lithofacies in the last track of each plot. Sand is shown in yellow, silty sand is shown in orange, and shale is shown in green. Depth is relative to mean sea level.

8
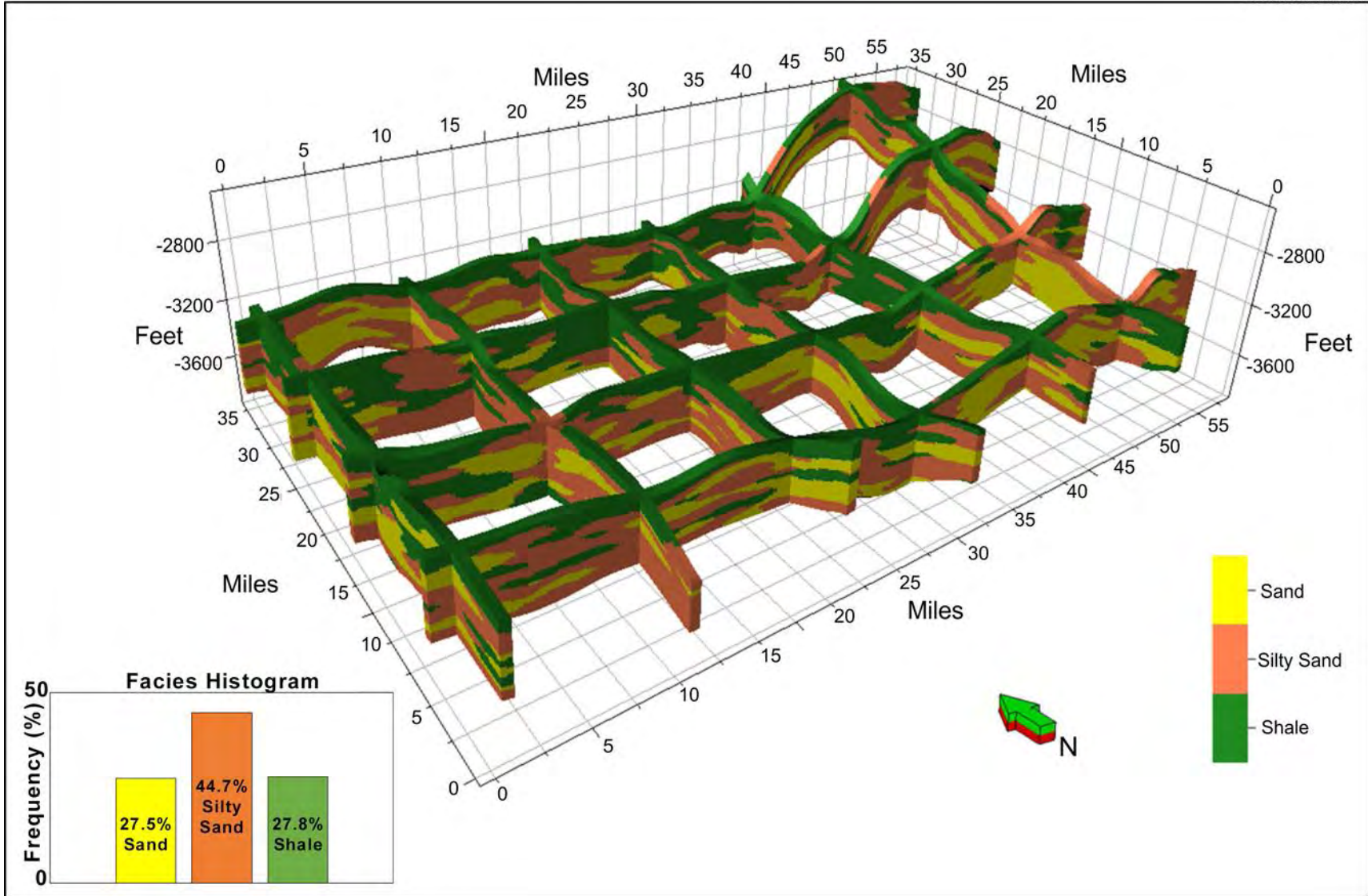
Figure 7. Fence diagram and histogram of the modeled facies distribution. Units are in miles along the X and Y axes and in feet (below mean sea level) along the Z axis.

Figure 8. Cumulative sand thickness within the Inyan Kara model.

Figure 9. Map showing the percentage of sandstone thickness in comparison to gross Inyan Kara thickness within the model.
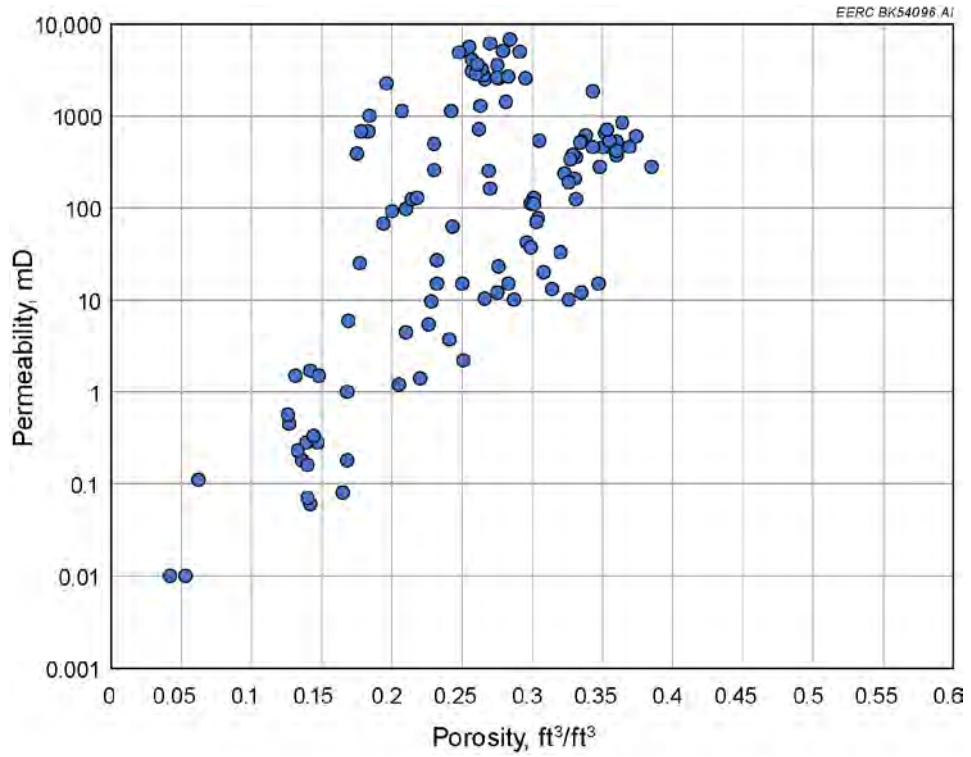
Figure 10. Crossplot of measured core sample porosity and permeability.
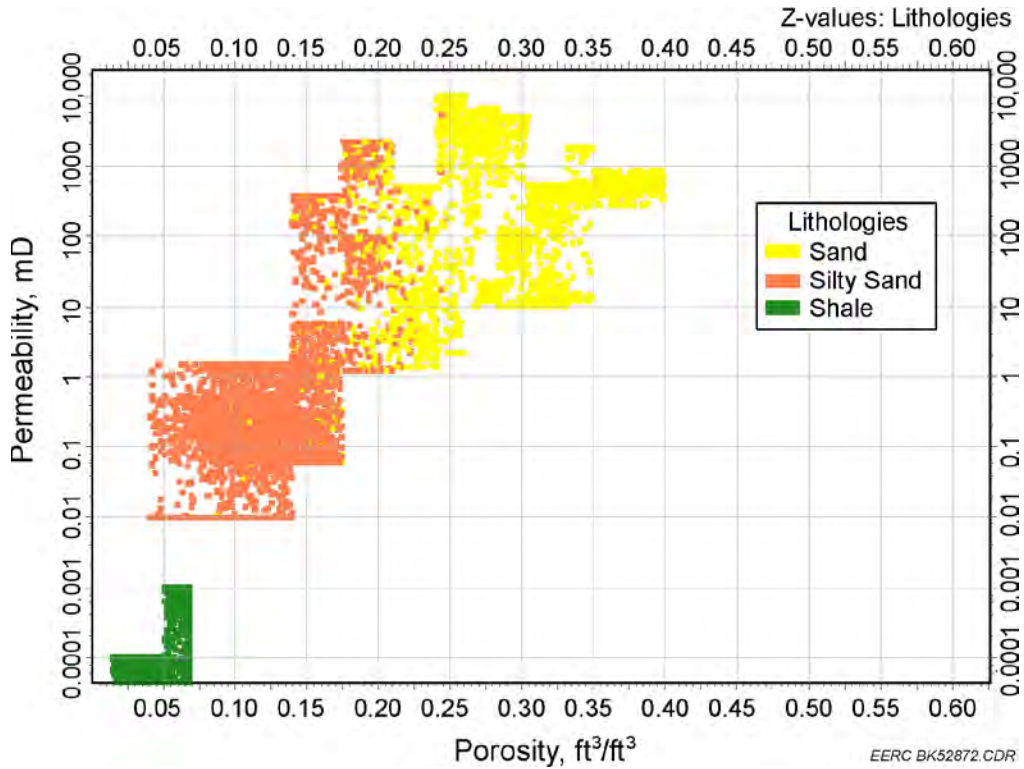
Figure 11. Crossplot of the distributed porosity and permeability values illustrating the trends for each facies.

12
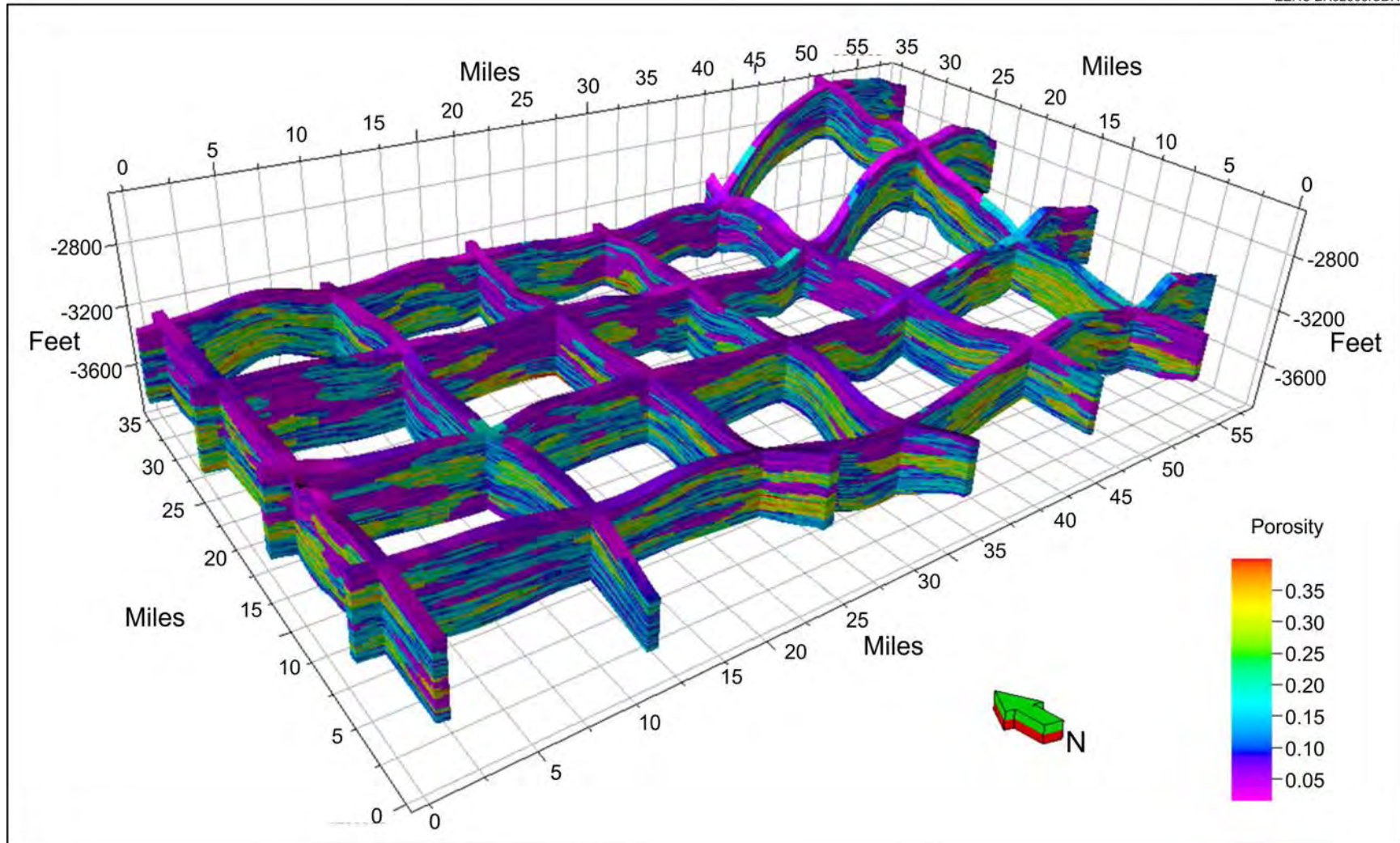
Figure 12. Fence diagram of the modeled porosity distribution. Units are in miles along the X and Y axes and in feet (below mean sea level) along the Z axis.
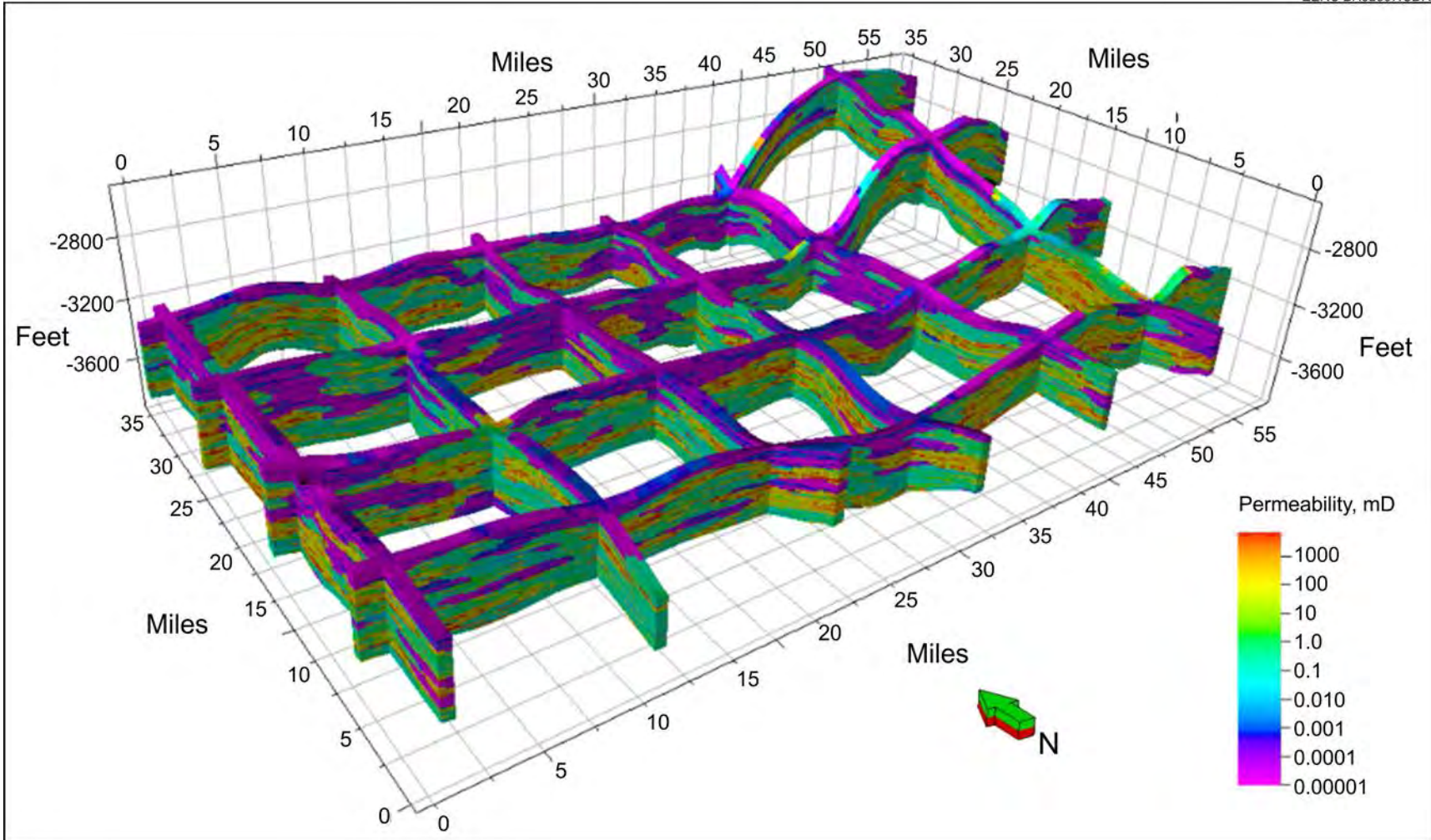
Figure 13. Fence diagram of the modeled permeability distribution (mD). Units are in miles along the X and Y axes and in feet (below mean sea level) along the Z axis. Vertical exaggeration = 5.

Table 1. Volumetric Characteristics for Each Lithofacies

Lithofacies	Bulk Volume, 10^6 ft^3	Pore Volume, 10^6 ft^3	Average Porosity, %
Sand	7,367,318	1,888,763	25.6
Silty Sand	12,125,981	1,621,396	13.4
Shale	7,567,889	413,363	5.5
Total	27,061,188	3,923,522	14.5

BOUNDARY CONDITIONS AND VOLUMETRIC DISPOSAL POTENTIAL

To better frame the storage potential within the modeled area of the Inyan Kara Formation, a simple equation can be used to define the maximum storage potential of the reservoir under closed boundary conditions and assuming that the fluid pressure in the reservoir is allowed to reach the 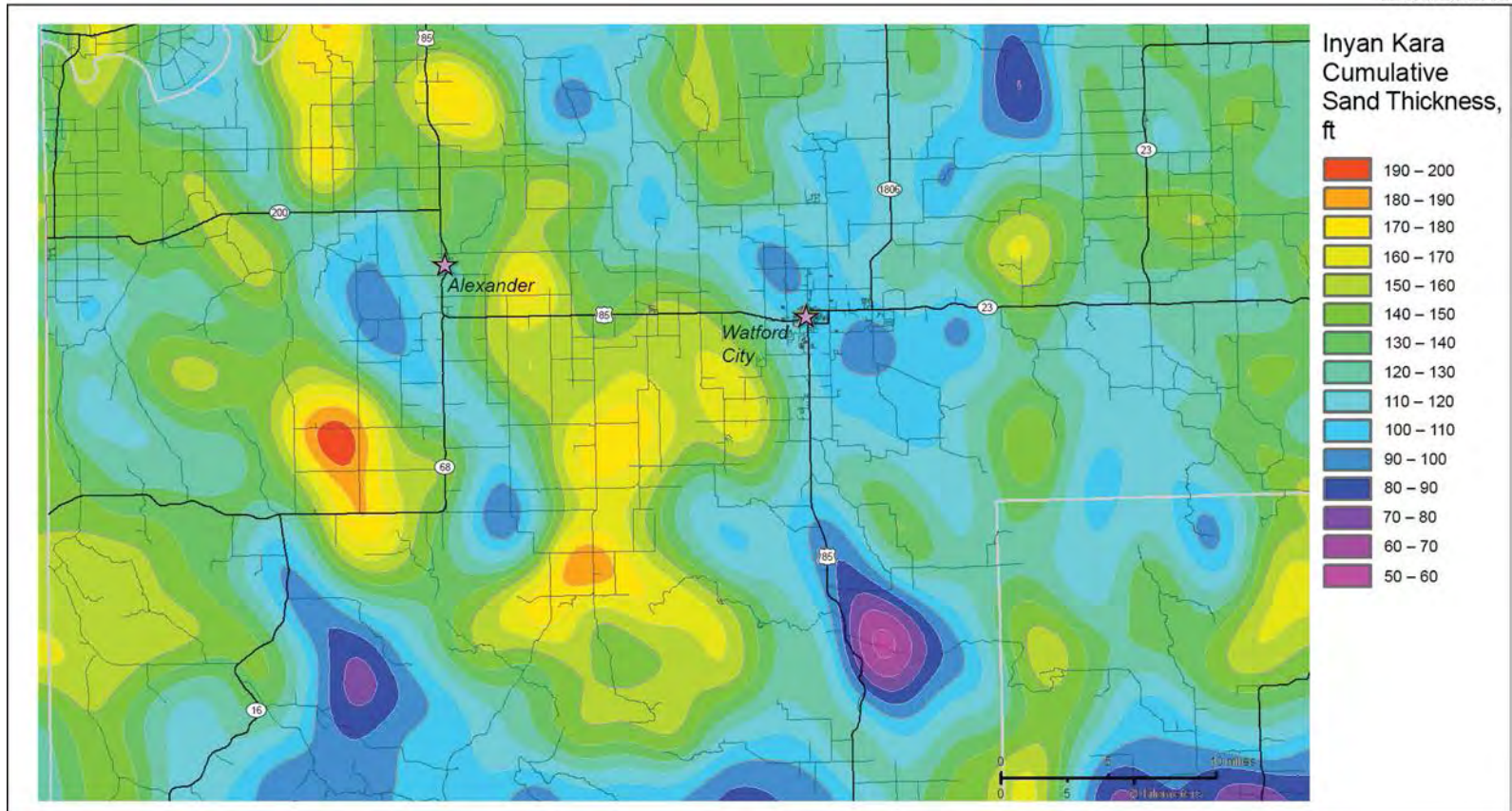maximum value without exceeding regulatory requirements. With the growing interest in storage of carbon dioxide (CO_2) in subsurface formations as a means to sequester carbon, the EERC and others have conducted several efforts to estimate the CO_2 storage resource potential of saline formations and to better understand the formation properties that affect storage (Zhou and others, 2008; Gorecki and others, 2009, 2014, and 2015; Craig and others, 2014). One of the key factors that impacts the CO_2 storage potential of a subsurface reservoir is the boundary conditions surrounding or within the injection target because they control brine movement and the rate of pressure increase or decrease within the formation. Disposal of brine within deep saline formations (DSFs) is controlled by the same boundary conditions that affect subsurface CO_2 storage; thus a discussion of the different types of boundary conditions are relevant to SWD in the Inyan Kara.

As described by Zhou and others (2008), the three primary types of boundary conditions include open, closed, and semiclosed. Laterally continuous saline formations that cover a large extent can be considered open or an "infinite acting" system because the native formation fluids can migrate laterally in response to gas or fluid injection. This allows for dissipation of the pressure caused by injection. However, if low permeability zones exist above, below, and/or laterally within the reservoir, the saline formation can be considered as a closed or semiclosed system. In these cases, gas or fluid injection may be limited by pressure increases that occur when the formation fluids become trapped by an impermeable boundary or the rate of formation fluid migration is restricted by areas of low permeability. If a storage reservoir is completely surrounded by impervious seal or areas of very low permeability zones, it is referred to as a closed system. If the sealing units or lateral barriers are not perfect seals and allow for some fluid migration and pressure dissipation (albeit at rate lower than the injection target), the storage reservoir is considered semiclosed. The pressure front generated by nearby SWD wells can also begin to affect reservoir pressure, and if enough SWD wells inject at a rate that does not allow for dissipation of the pressure front, an open system can begin to behave more like a semiclosed or even closed system.

Volumetric calculations to estimate storage potential rely on an accurate geologic description of the study area to determine the effective pore volume that can be filled with brine at the specified allowable pressure and reservoir temperature. Several methods have been previously developed to estimate the CO_2 storage potential of DSFs, including methods developed by the U.S. Department of Energy (DOE) (2007, 2008, 2010), the the IEA Greenhouse Gas R&D Programme (IEAGHG) (Gorecki and others, 2009), and Zhou and others (2008). The simplified

equation from Gorecki and others (2009) was used here to estimated storage potential in a closed system.

As pointed out by Gorecki and others (2009), saline formations targeted for storage are typically at 100% water saturation (this is also an important assumption in our dynamic simulation cases). With this assumption, the pore volume and the water volume are equal, as well as the pore pressure and the water pressure. Therefore, the total storage potential volume is:

$$\Delta V = \left(c_w + c_p\right) * V_{po} * \Delta P \qquad \text{[Eq. 1]}$$

Where ΔV is formation volume change, c_w is water compressibility, c_p is formation pore compressibility, V_{po} is the pore volume, and ΔP is the formation pressure change. This equation assumes that the pore volume is the effective pore volume. The pressure difference is the maximum average pressure that can be increased over the initial reservoir pressure.

The above equation was used to estimate the volumetric brine storage potential of the modeled portion of the Inyan Kara reservoir using parameters derived from the model. The total effective pore volume was calculated from the total reservoir volume and the average effective porosity, equating to a value of approximately 700 billion bbl. The formation rock compressibility was estimated at 4.9×10^{-6} 1/psi using Hall's correlation (1953) and the porosity parameters in the model. The default value for water compressibility from the CMG model was used, which was 3×10^{-6} 1/psi. The average maximum allowable wellhead pressure of the SWD wells in the model was used to roughly estimate the pressure capacity of the reservoir, which was approximately 1350 psi. The frictional loss in the well tubing was estimated as a few psi to 50 psi using the equations given by Bourgoyne and others (1986). In this estimation, at the maximum allowable wellhead pressure, the injection rate will be high, and the frictional loss was considered as a worst-case scenario condition at 50 psi. Therefore, a pressure difference of 1300 psi was used to calculate the volumetric brine storage potential if the modeled area was considered a closed system.

By applying the above parameters into Equation 1, the calculated volumetric saltwater storage potential for the modeled area of the Inyan Kara Formation is 7.19 billion bbl. This calculation was performed to estimate a maximum potential brine storage volume if all of the pore space in the model area was utilized. In reality, the amount of storage potential currently being accessed in the Inyan Kara is less than this total because there are many areas that contain no SWD wells and those areas may or may not be hydraulically connected to the current injection wells. This was a primary reason why the numerical simulation modeling was conducted so as to provide insight into areas that might be experiencing significant pressure increases as a result of ongoing SWD disposal or because of geologic constraints. The comparison between the volumetric storage potential and the numerical simulated disposal potentials will be discussed following the numerical simulation portion of the report. In addition, the differences between the predicted pressure distribution and brine plumes will be discussed in a later portion of this report.

NUMERICAL SIMULATION

To conduct dynamic simulations of the Inyan Kara's injection potential, the geologic model was exported from Petrel and imported into CMG's Builder to initialize the model for simulation. Figure 14 illustrates the grid layout of the model, including the three formations that overlie the Inyan Kara. Other properties representative of native reservoir conditions were specified, including pressure, water saturation, and global composition. The Inyan Kara was assumed to be fully saturated with a brine consisting of 10,000 ppm total dissolved solids (TDS). The injected water salinity was assumed to have an average value of 250,000 ppm TDS. General properties for the Inyan Kara portion of the simulation are summarized in Table 2. The average permeability and porosity values given in Table 2 are the numerical average values of all of the grid cells, which include all of the lithofacies of the Inyan Kara. The values of both permeability and porosity are, therefore, different than the average porosity and permeability values obtained from the limited set of core sample measurements. The water compressibility from the default value (3.0×10^{-6} 1/psi) in CMG was used in the model, and the rock compressibility was estimated by Hall's correlation between compressibility and porosity (1953) (4.9×10^{-6} 1/psi).

The simulation cases were run in CMG Gem and included both open and partially closed boundary conditions. The fully closed boundary condition case that was discussed in the previous section was not included as one of the dynamic simulation cases. In all cases, lateral water flux was allowed through the eastern boundary of the model, which is adjacent to the Fort Berthold Reservation and contains few SWD wells. The partially closed simulations assumed all other sides of the model (north, west, and south) were closed, simulating pressure interference from existing SWD wells beyond these boundaries (representing a conservative case). The open boundary cases were simulated with no restrictions to fluid movement (infinite-acting aquifer) on all sides of the model, representing an optimistic case with no pressure interference from disposal wells beyond the model boundaries. In all of the simulation cases, the formations underlying and overlying the Inyan Kara were considered as closed boundaries.

A total of 103 SWD wells were included in this model. Of that number, only 93 were operational at the time of this effort. Well perforations and well treatment activities, including acidizing or hydraulic fracturing, were included in the model to account for real-world operations at each SWD well. A wellbore model was used to calculate the pressure change in the direction of flow between the wellhead and the bottom-hole pressure of the well. The wellbore model estimated the change in pressure due to the hydrostatic head at the specific well depth, the frictional loss due to interaction between the injected brine and the walls of the tubing, and the kinetic energy gain resulting from fluid injection. Because this was a single-phase model (only water present in the formation), capillary pressure was neglected. Geochemical changes were not simulated because little supporting chemical reaction data were available. The well names were changed to short names in the model for the convenience of salinity data input, and the corresponding well number and names are listed in Appendix A.
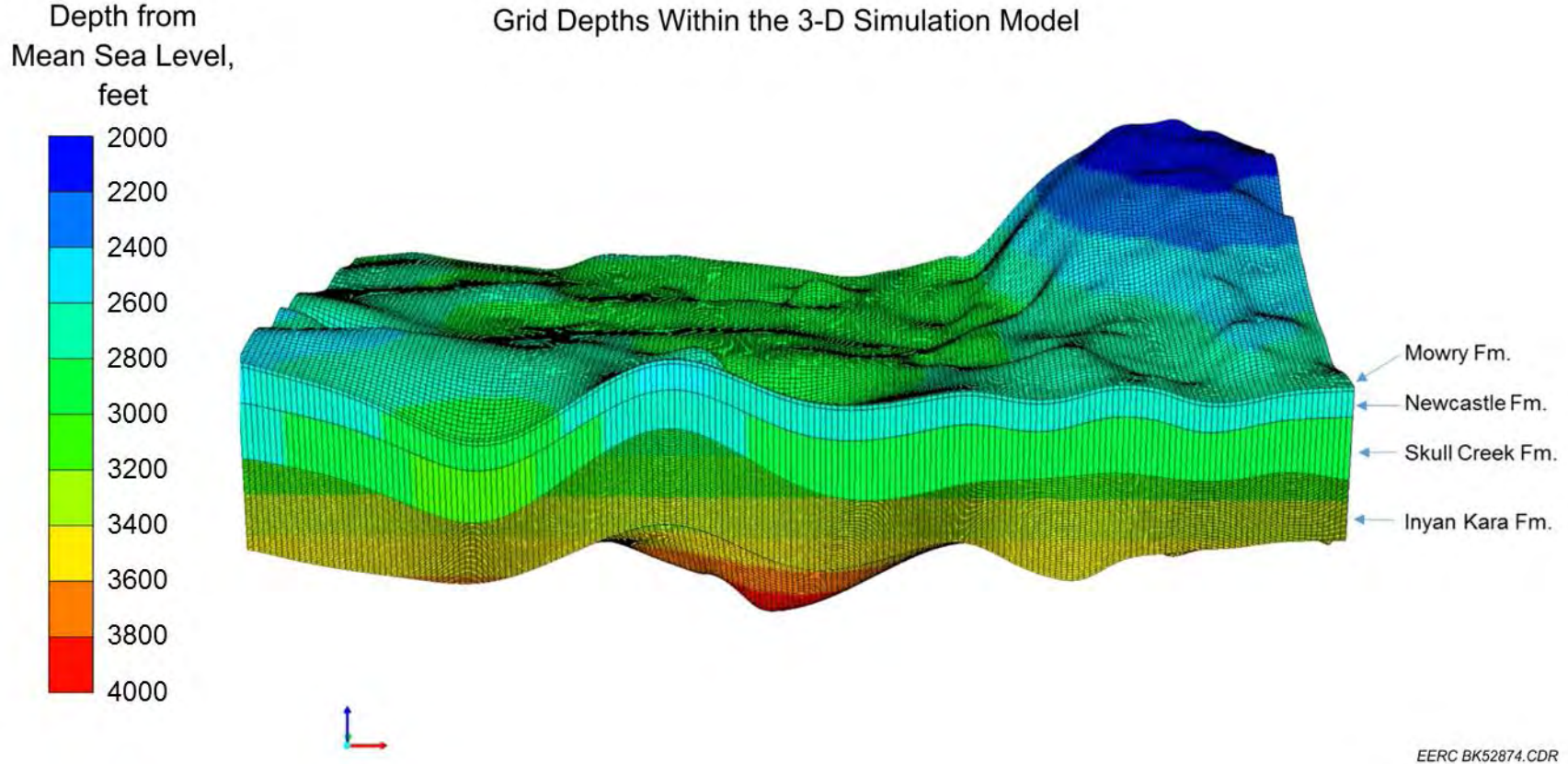
Figure 14. Subsea depth of the reservoir simulation model. The formations overlying the Inyan Kara were single layers, whereas the Inyan Kara was divided into 40 layers. Vertical exaggeration = 63×. With this vertical exaggeration, the Nesson Anticline is very apparent on the eastern side of the modeled area.

Table 2. General Properties for the Inyan Kara Portion of the Reservoir Model

Reservoir Property	Minimum	Maximum	Average
Permeability, mD	0.000001	10000	311
Porosity	0.015	0.34	0.15
Initial Pressure, psi	1938	2925	2454
Reservoir Salinity, ppm	–	–	10,000
Injected Water Salinity, ppm	–	–	250,000
Rock Compressibility, 1/psi (Hall, 1953)	–	–	4.9E-6
Formation Fluid Compressibility, 1/psi (CMG, 2014)	–	–	3.0E-6
Water Saturation	–	–	1
Temperature, °F	152	178	165
Grid Dimensions, miles	–	–	40×60
Grid Cell Dimensions, ft	–	–	1640×1640
Grid Cell Thickness, ft	6.4	15.6	11.3

After model initialization, simulation activities were conducted using CMG's GEM (Computer Modelling Group, 2014), a fully compositional reservoir simulation module. As summarized in Figure 15, before the simulation results were generated, several parameters were adjusted in the model to better match historical SWD well injection volume and pressure data. This step, referred to as history matching, is described in the following section.
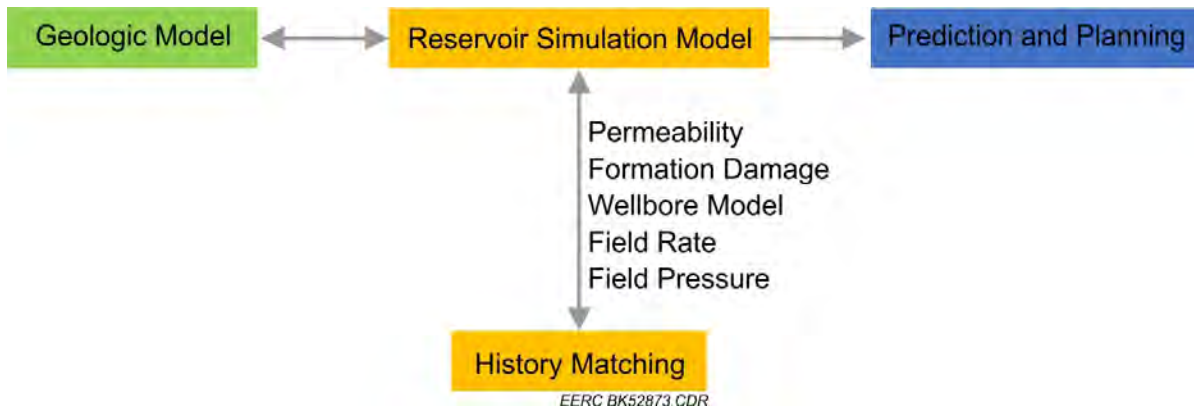

Figure 15. Workflow depicting the reservoir simulation, history-matching, and prediction process.

History Matching

Reservoir simulation began with history matching using operational data from the 103 SWD wells within the model area. This process involved matching the simulated pressure response,

water injection rates, and water injection volumes with the field-reported values, enabling more accurate predictions of future reservoir performance. This was achieved by adjusting and tuning specific model properties such as permeability, tubing roughness, and well skin factor. The history match included injection data beginning in 1961 through February 2017, which totaled 644 million bbl of cumulative injection in the simulated area.

Historical water injection (rates and volumes) and wellhead pressure data for the SWD wells located in the area of review were incorporated in history-matching the model. These field data, reported to NDIC on a monthly basis and spanning a time frame from as early as 1961 to present, were averaged for 6-month intervals to increase computational efficiency (shorter simulation run time). In general, the history match was most improved by adjustment to permeability (commonly 0.1 to 10 times), both throughout the simulated area and by more local adjustments for individual wells. Skin factor (–5 to 100) and tubing roughness coefficient (0.0004–0.002) were also adjusted during the life of individual wells as indicated by well records or otherwise as needed. Of the 103 wells, 62 wells were considered to have a good history match, 14 wells had a fair match quality, 21 wells were considered a poor match, and six wells could not be matched to the recorded field data, which were considered unreliable. The history-matching results for individual wells are listed in Table A-1 of Appendix A, with the current operator for each well.

An example of history matching of wellhead pressure for one of the SWD wells is shown in Figure 16. Additional history-matching curves for select wells are provided in Appendix A.
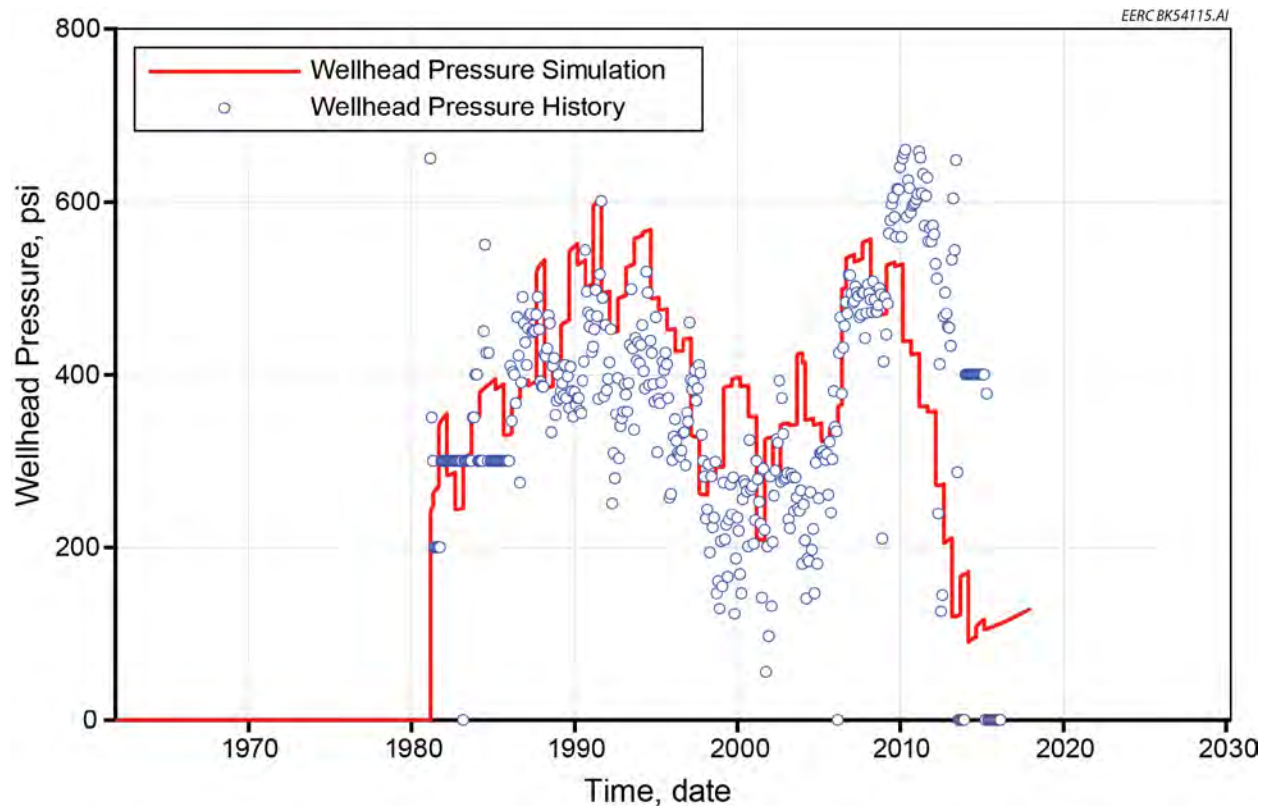

Figure 16. Example of a good-quality wellhead pressure history match for Well 5336.

Predictive Simulations

Six different cases were simulated using the reservoir model to evaluate the long-term injection potential of the Inyan Kara Formation within the study area. The scenarios that were evaluated were not meant to comprehensively define all of the possible SWD situations that might occur in the future. Instead, a select number of possible scenarios were evaluated to gain a sense of long-term injection potential of the Inyan Kara in the areas that currently contain SWD wells and at current injection rates and volumes. The time span for which the future scenarios were evaluated was also selected somewhat arbitrarily (out to 2050), with the thinking that it is impossible to predict the number of producing Bakken or Three Forks wells in the future or the potential SWD needs. The idea was also that additional scenarios can be simulated if desired by partners in the BPOP Program.

The assumptions used in each simulation case are shown in Table 3. Three cases (1_C, 2_C, and 3_C) assumed closed boundary conditions on all but the eastern edge of the model, which was considered an open boundary with unimpeded lateral flux. These scenarios are referred to as partially closed boundary scenarios. These scenarios were conducted because there are few permitted wells within the Fort Berthold Reservation that borders the eastern edge of the modeled area, and anecdotal evidence from industry partners (Personal communication, 2016–2017) suggests that the number of SWD wells on the reservation will remain low in the future

Table 3. Cumulative Water Injection for Each Predictive Simulation Case at Year 2050

Cases	Case Description	Cumulative Water Injection, billion bbl
1	All 103 SWD wells in model are operational from 2017 to 2050; open boundary conditions.	4.02
1_C	Same as above except closed boundaries to the north, west, and south.	3.89
2	The 93 SWD wells that are currently operational continue injection until 2050; open boundary conditions.	3.98
2_C	Same as above except closed boundaries to the north, west, and south.	3.86
3	The 93 operational wells continue injection until 2050 at the maximum rate without exceeding pressure constraints; open boundary conditions.	5.27
3_C	Same as above except closed boundaries to the north, west, and south.	4.97
Closed System Equation	$V_{inj} = (c_w + c_p) * A * H * \emptyset * \Delta P$	7.19

21

compared to surrounding areas. The three other cases (1, 2, and 3) assumed open boundary conditions by allowing lateral infinite-acting flux through all four sides. Cases 1_C and 1 assumed continued injection for all 103 SWD wells, some of which are no longer operational, using their final reported injection rates and starting from the end of the history match in 2017 to the year 2050. Cases 2_C and 2 simulated continued injection from the 93 SWD wells that are currently operational in the modeled area using the last reported injection rate. Cases 3_C and 3 assumed continued injection at the maximum allowable regulated constraints of injection rate and wellhead pressure for the 93 operating wells. These last two cases tested the theoretical maximum injection capability of the current system.

Results and Discussion

The cumulative water injection at the end of year 2050 (for a total of 33 years of injection) for each simulated case is listed in Table 3. The cumulative water injected at the beginning of the year 2017 was about 644 million bbl. The cumulative water injected at the year 2050 showed an increase of 500% to 670% for all of the simulation cases and an increase of ~ 1000% in comparison to the closed system equation method. The cumulative water injection at the end of the year 2050 from the open boundary cases was about 3%–6% greater than that estimated from the partially closed boundary cases, which indicates that the modeled boundary conditions have relatively small effect on the injection potential of the modeled area (few wells are in close proximity to the model boundaries). This would indicate that the boundary conditions of the system as a whole are behaving as open; however, there are localized areas experiencing pressure increases and behaving more like a semiclosed or closed system. This is likely due to the fact that the offset injectors are causing pressure feedback on each other such that most injection wells do not have an infinite pore volume for the pressure to dissipate.

Comparison of the results from the dynamic simulation to the estimated storage potential using the volumetric approach also indicates that there would be pore space available for storage at the end of 2050 (given the assumptions used in each simulation case). The closed system volumetric estimate was 7.19 billon bbl, compared to the highest cumulative injection volume (from Case 3) of 5.27 billion bbl. Although the closed system estimate is highly conservative (and likely low) because it assumes no flow from the model boundaries or resulting pressure dissipation, a comparison of the estimate storage potential suggests that as much as 73% of the storage potential (of a closed system) could be utilized by 2050. This assumes no increase in the number of SWD wells or volume of produced water requiring disposal in the next 33 years – a simplistic assumption considering that, on average, the volume of produced water generated by individual Bakken wells has increased every year, with wells completed in 2008 generating far less water than those completed in 2017 (Kurz and others, 2016; recent data analysis conducted at the EERC).

In addition, comparing the total estimated injection volume at end of 2050 to the maximum potential capacity based on a closed system volumetric approach can be misleading because, from a practical standpoint, SWD wells are typically located in areas with reasonable road access and where there is demand associated with oil and gas production. There are areas, such as in really rugged badlands-type terrain or in Theodore Roosevelt National Park, where SWD wells do not currently exist and are very unlikely to exist in the future. An advantage of the dynamic simulation is that the results indicate where pressure increases may start inhibiting injection volume and/or

rate across the modeled area; thus locations where there is a higher concentration of SWD wells can be evaluated for potential pressurization issues.

To illustrate the overall trends in cumulative injection and injection rate over time, the partially closed and closed cases for each of the scenarios are compared in Figures 17–19. In each of the cases, the injection rates declined through time because of pressure constraints. As injection volumes increased over time, the pressure also increased, resulting in a decrease in the rate of injection to avoid exceeding maximum pressure limits. These curves indicate that although there appears to be sufficient storage potential in the Inyan Kara under the various modeled conditions, the overall rate of injection will be forced to decrease over time to meet regulated pressure requirements. The curves also indicate that the injection rate decline is greatest in the cases with closed boundary conditions on the northern, western, and southern edges of the model. Overall, the results suggest that the system will begin behaving more like a semiclosed or closed system as injection continues into the future.

To better understand localized areas of pressure increase, pressure difference maps between the original pore pressure in 1961 and the year 2017 and from 2017 to 2050 were created for each simulation case. A key challenge with illustrating the pressure differences in the modeled area over time is deciding which of the 40 layers to use for illustrating pressure differences as they vary significantly from layer to layer. This variability is caused by geology, variations in which sandstone layers are targeted for injection, injection rate, cumulative volume of injection, etc. To
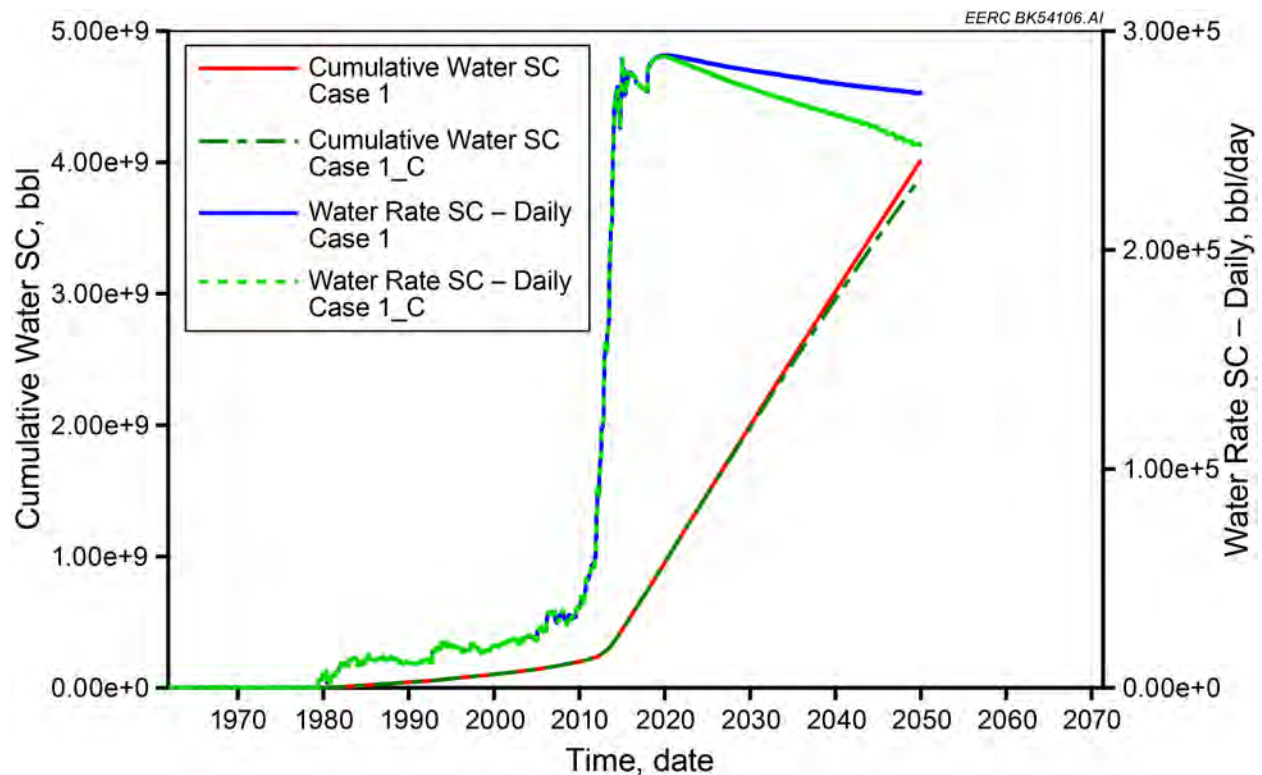

Figure 17. Comparison of predictive simulation Cases 1 and 1_C. Note that "SC" indicates standard conditions (e.g., 14.7 psi and 60°F).
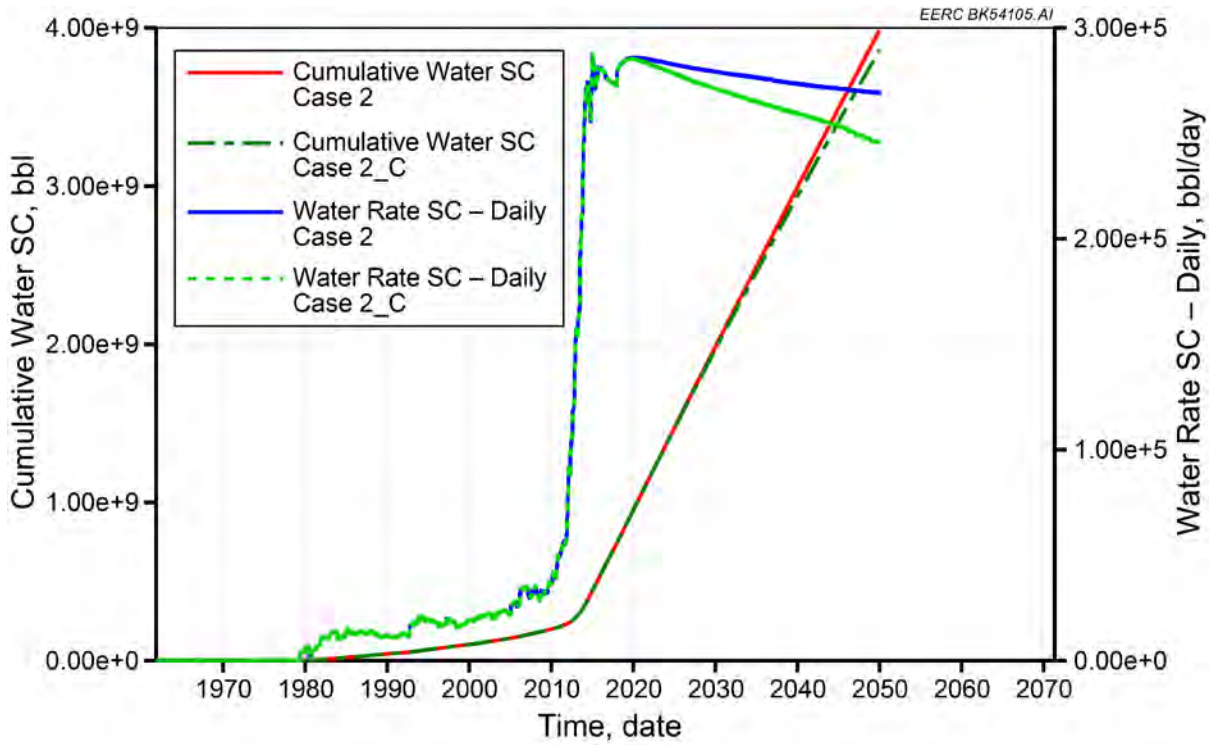
23

Figure 18. Comparison of predictive simulation Cases 2 and 2_C. Note that "SC" indicates standard conditions (e.g., 14.7 psi and 60°F).
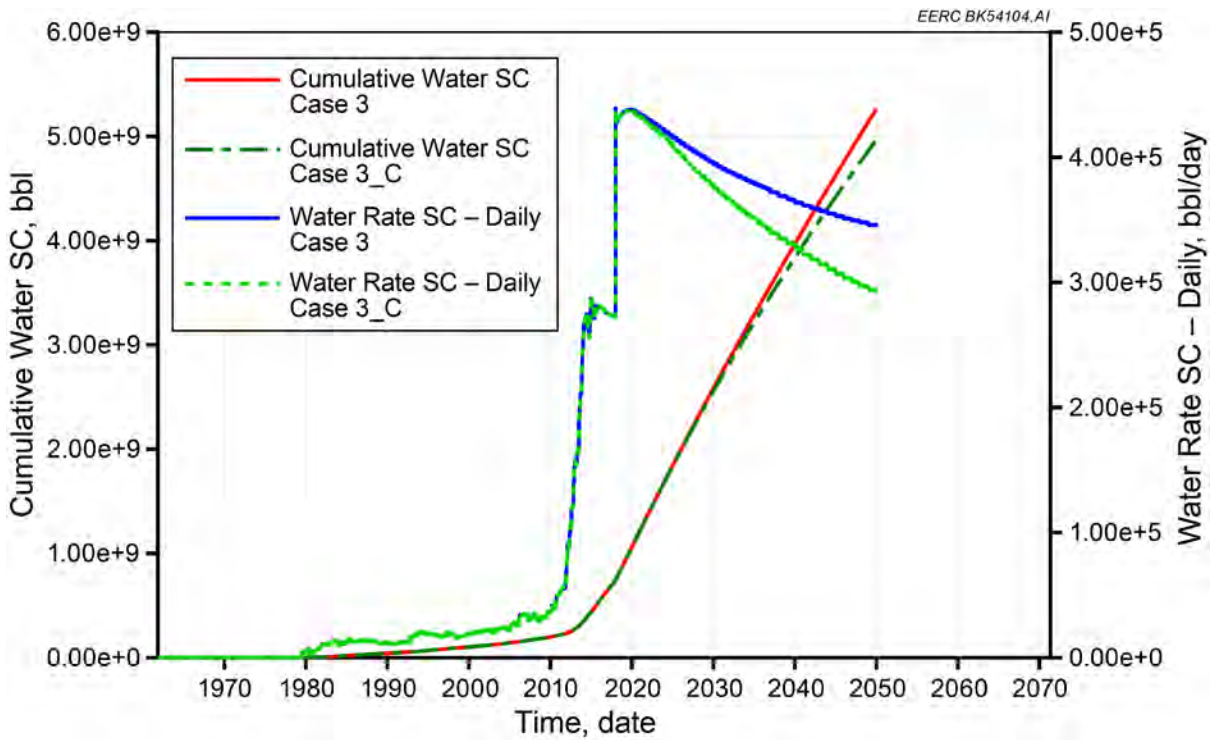

Figure 19. Comparison of predictive simulation Cases 3 and 3_C. Note that "SC" indicates standard conditions (e.g., 14.7 psi and 60°F).

24

illustrate the areas that might start to have pressurization issues, Figure 20 illustrates the maximum increase in pressure from 1961 to 2017 for any of the 40 reservoir layers in the corresponding grid cell. In this example, there were no differences between the simulation cases because this represents past, not forecasted, injection. The pressure difference is also shown in Figure 21 as a fence diagram and indicates large portions of the area of review (over half of the areal coverage of the model from visual inspection) likely experienced no significant pressure change over the time interval from 1961 to 2017. A few areas experienced pressure increases exceeding 300 psi, and only a few wellsite locations exhibited pressure increases nearing 500 psi. As would be expected, the pressure increase was highest in the immediate vicinity of the SWD wells. In addition, most areas in the model do not appear to experience pressure interferences between wells.

The hypothetical pressure differences from 2017 to the year 2050 for Cases 2_C and 3_C are shown in Figures 22–25, respectively. Similar to Figure 20, Figures 22 and 24 represent the maximum pressure increase exhibited within the 40 model layers for the corresponding grid cell. The partially closed cases were selected to estimate the pressure changes expected to occur with the currently operating SWD wells (93 wells). A comparison of the pressure distribution in Figures 22–25 indicates the case with the maximum allowable injection rate and/or pressure and the largest injection volume caused a much greater pressure increase across the area. As would be expected, both figures illustrate that the biggest pressure difference within the Inyan Kara occurs in the areas surrounding the existing injection wells, which have already experienced some pressure increase.

The areas near the northern edge of the simulation are estimated to have the greatest pressure increase by 2050. There are several reasons for this:

- Injection wells are more densely spaced.

- Cumulative injection is, in general, higher in northern wells which are closer to the core production area.

- In 2017, most of the northern boundary areas have not yet seen significant pressure increase, although significant injection and resulting pressure changes have occurred nearby. By 2050, these areas of pressure increase have spread farther north.

- The Inyan Kara in the northern area appears to have less continuity of high permeability sand. Areas with low permeability act as barriers or restrictions to flow in the region and contribute to local pressure buildup. These low permeability areas appear in Figures 22 to 25 as dark blue in color.
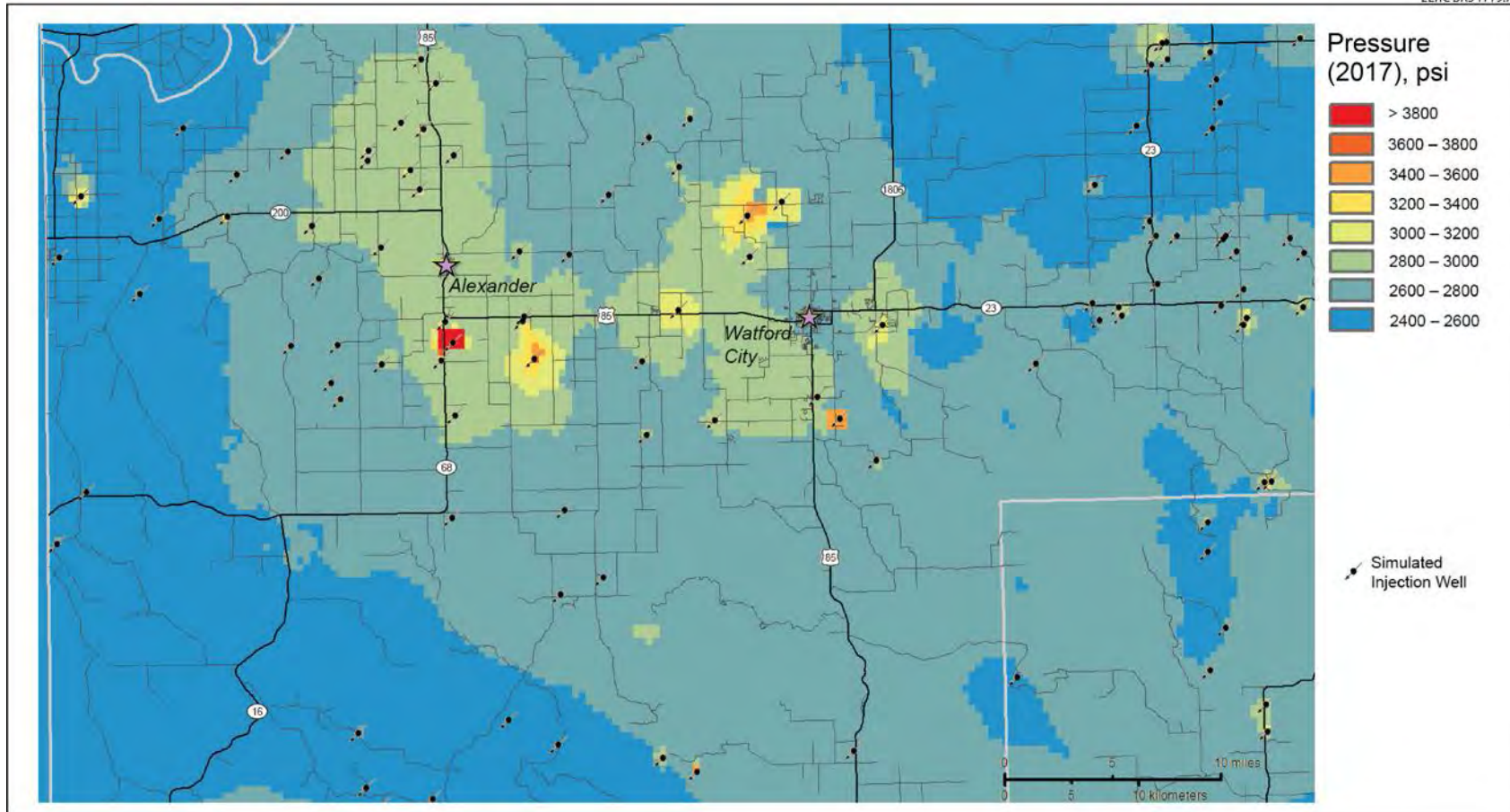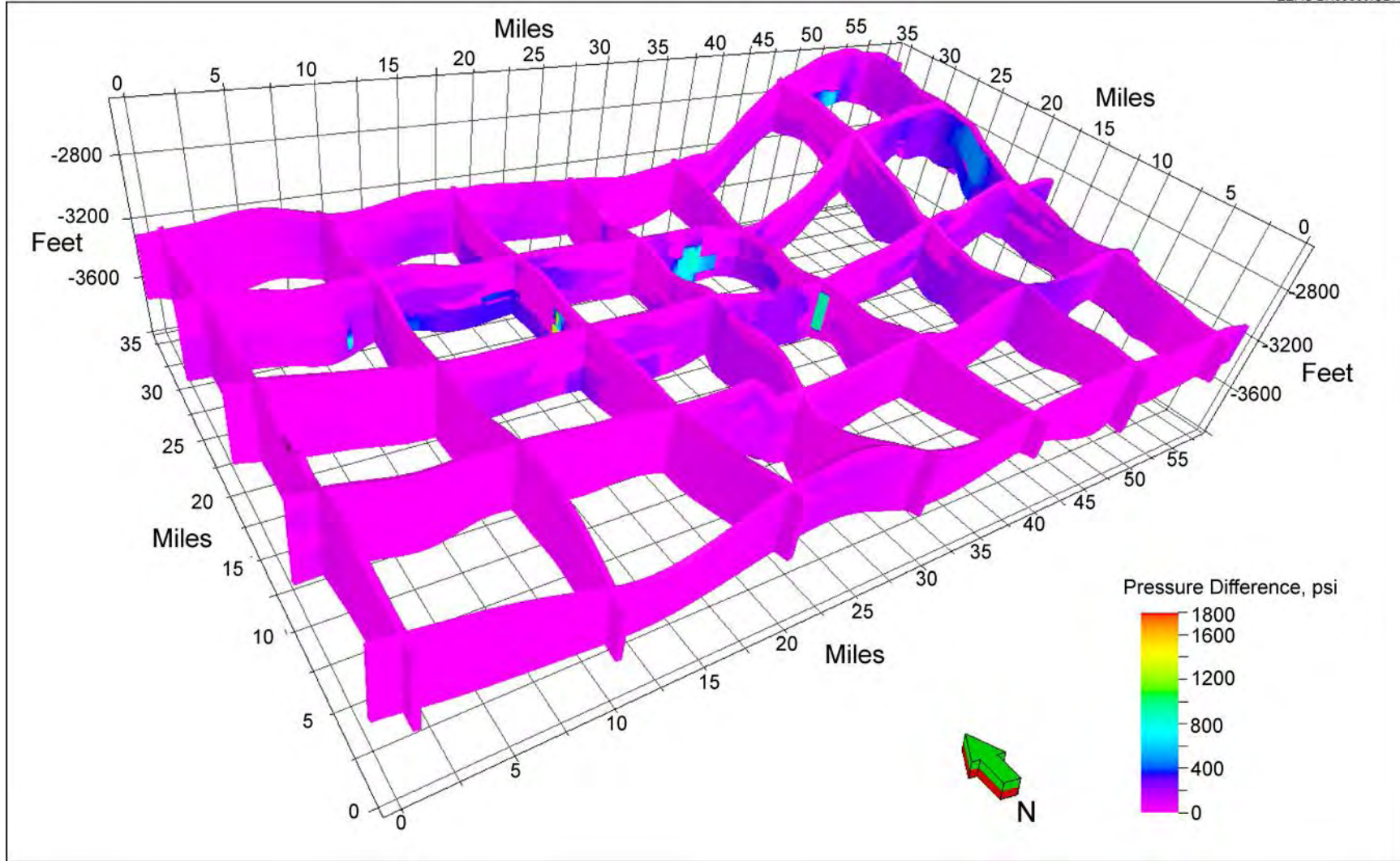
Figure 20. Maximum hypothetical pressure distribution exhibited by any of the 40 model layers in each grid cell. This represents the model-predicted conditions for 2017.

Figure 21. Fence diagram illustrating the simulated pressure change between the first injection date (1961) and 2017.
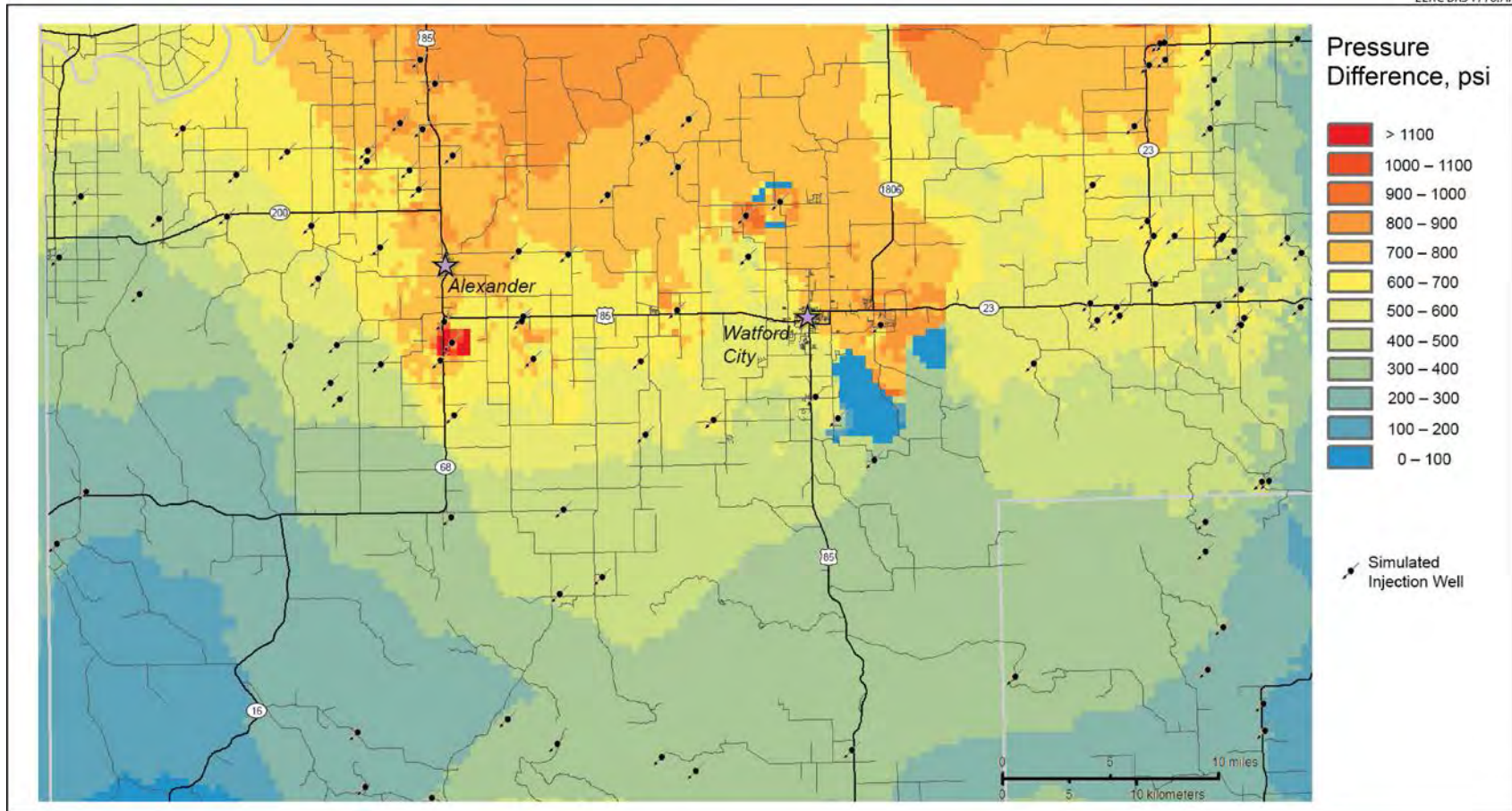
Figure 22. Maximum hypothetical pressure increase exhibited by any of the 40 model layers in each grid cell. This represents the change between 2017 and 2050 for Case 2_C.
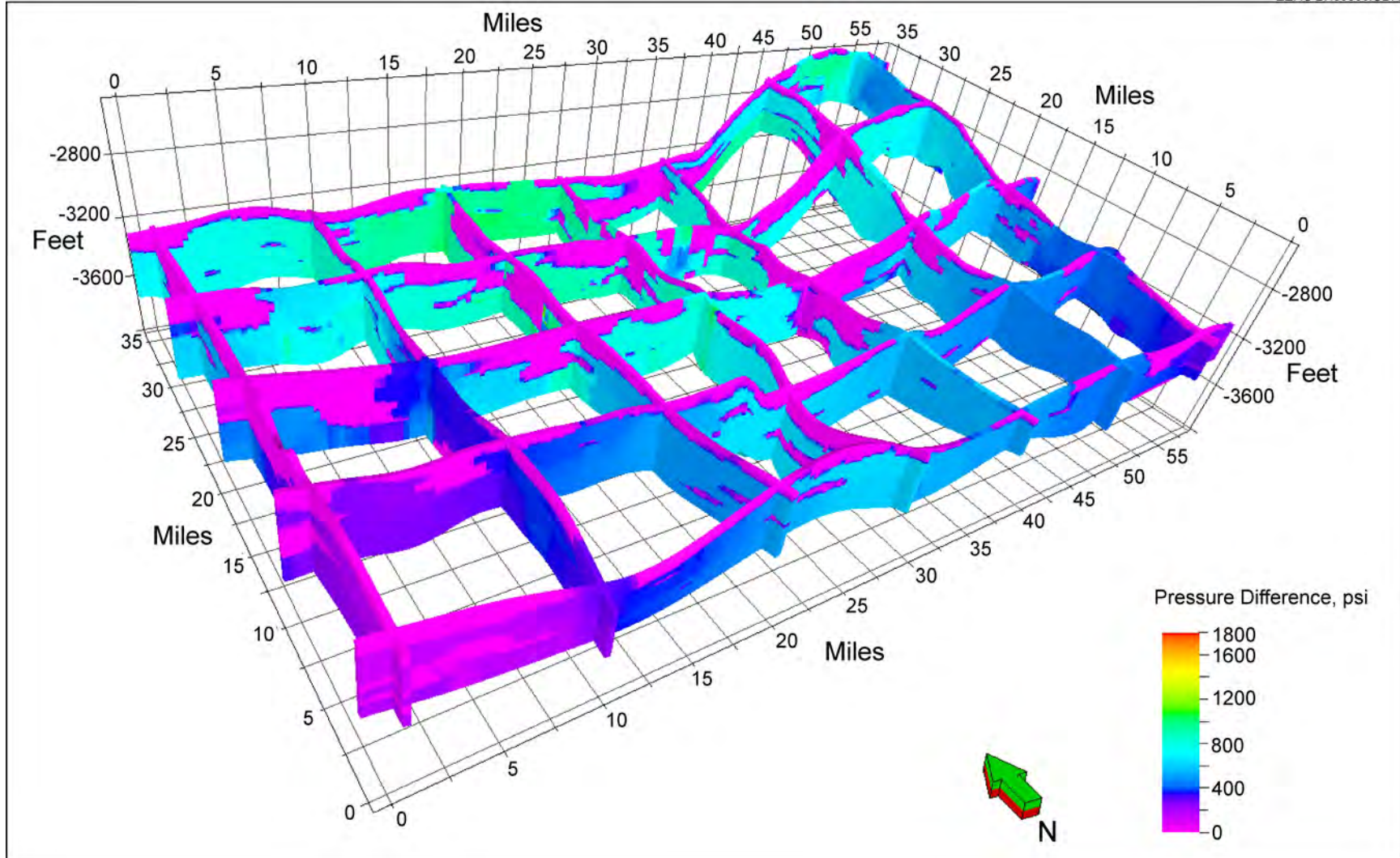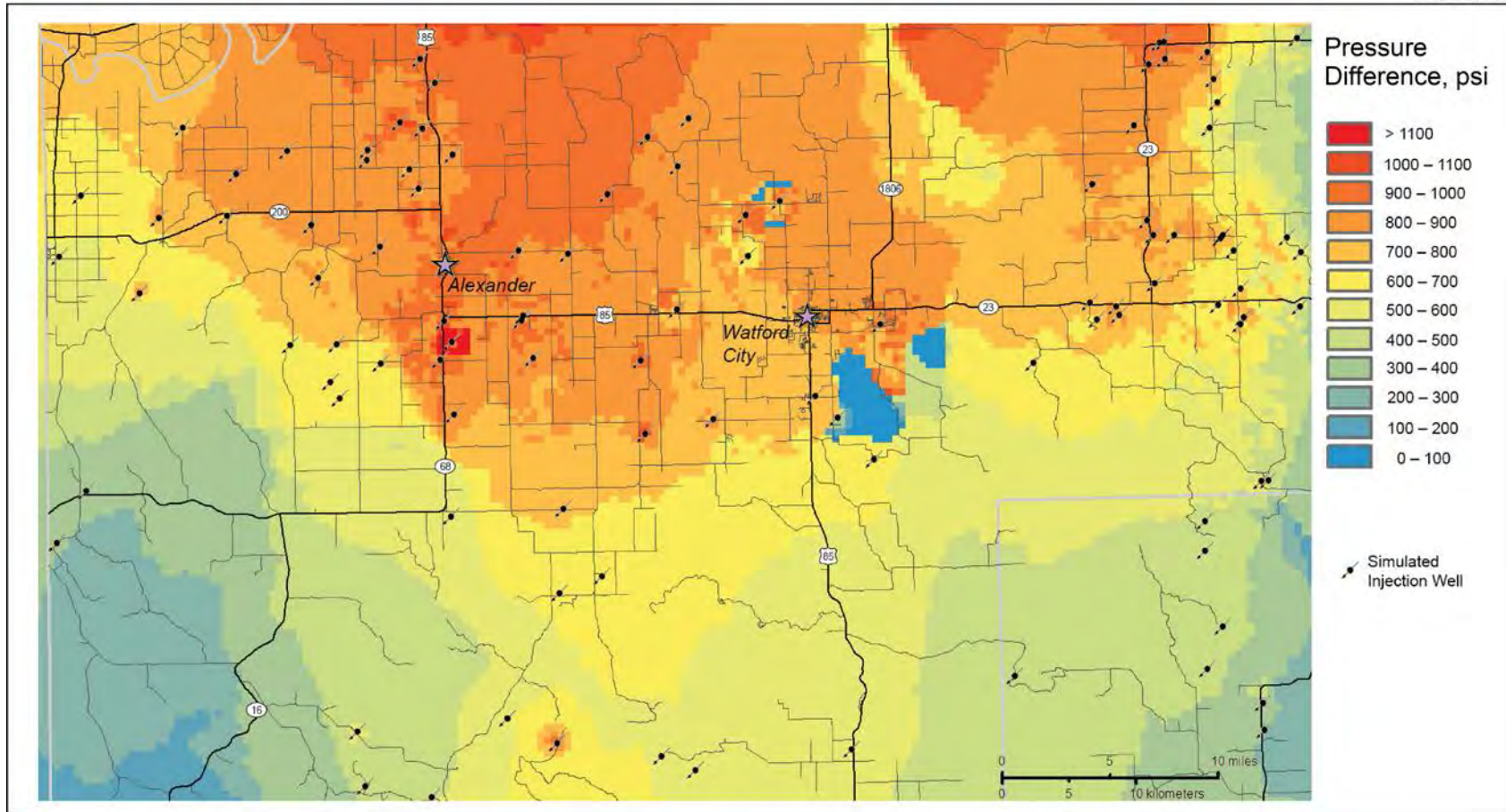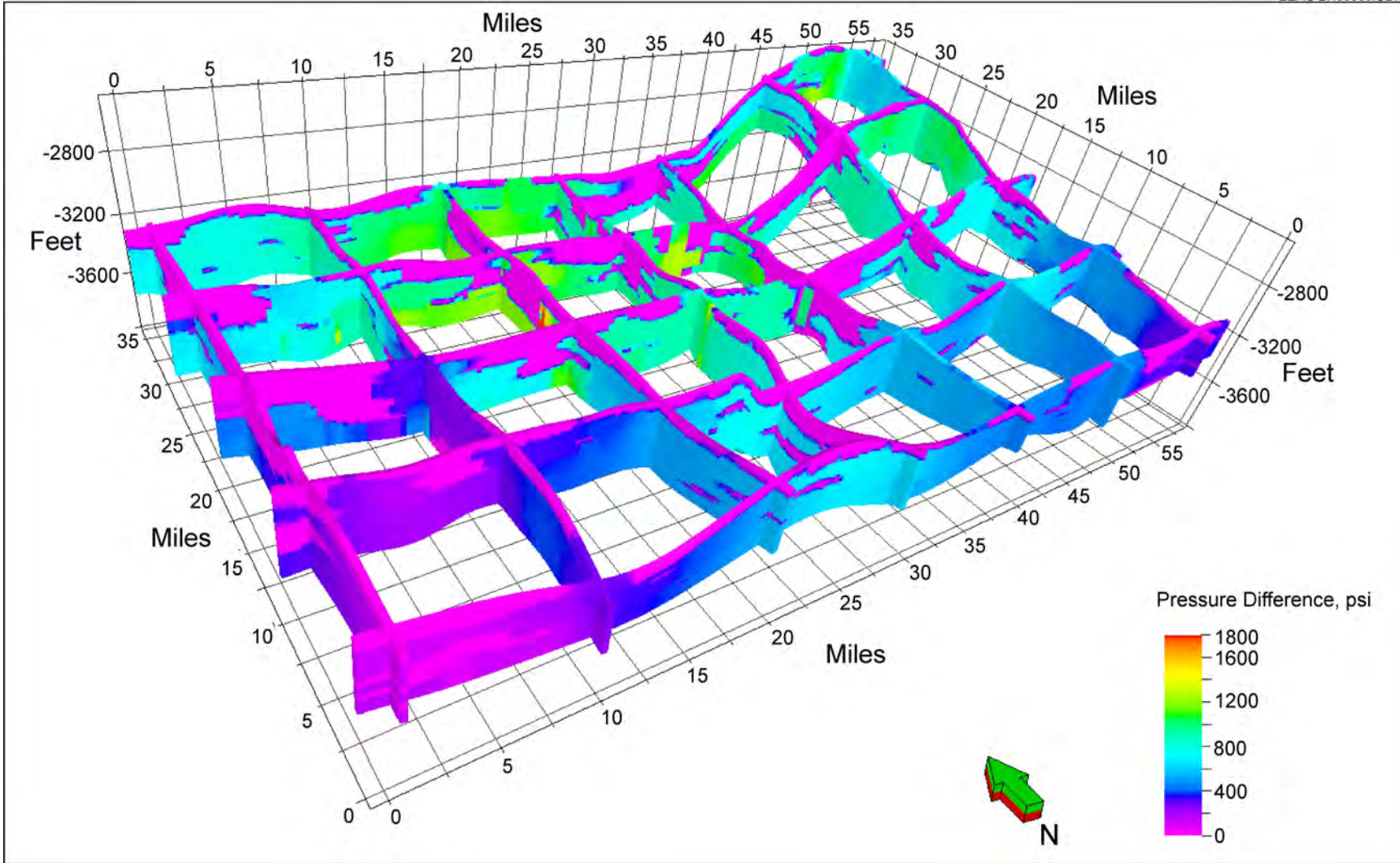
Figure 23. Fence diagram illustrating the hypothetical pressure change between 2017 and 2050 for Case 2_C.

Figure 24. Maximum hypothetical pressure increase exhibited by any of the 40 model layers in each grid cell. This represents the change between 2017 and 2050 for Case 3_C.

Figure 25. Fence diagram illustrating the hypothetical pressure change between 2017 and 2050 for Case 3_C.

In addition to the pressure difference maps, it is also worth discussing the absolute pressure distribution at each simulated time step. As an example, the maximum hypothetical fluid pressure exhibited for any of the model layers for year 2050 of Case 3_C is shown in Figure 26, and the predicted fluid pressure distribution for the same scenario and year is illustrated by the fence diagram in Figure 27. The pressure distribution map in Figure 26 suggests that the pressure is greater in some of the northern areas of the modeled extent. These areas may have reached or are close to the maximum allowable injection pressure based on the decline of water injection rate in Figure 19. As was seen in the pressure difference maps, the pressure is highest around the SWD well sites and decreases with distance from the well. Intuitively, the areas with greater future injection potential occur in areas with no or few SWD wells, mostly in the southern half of the simulated area.

The pressure distribution fence diagram shown in Figure 27 illustrates a trend of increased pressure in the higher porosity and permeability layers shown in Figures 12 and 13. This demonstrates that the zones with higher porosity and permeability, which are the targets for SWD, have experienced the largest change in pressure as a result of long-term injection. Using fence diagrams to depict hypothetical pressure changes in the Inyan Kara as a result of injection may have utility in broadly identifying potential areas to target (or avoid) for future SWD well locations.

The discussion of results has largely focused on the predicted cumulative injection volumes and associated fluid pressure increase. Another output of the model that has not yet been discussed is the predicted change in formation fluid salinity as a result of brine injection. Because subsurface reservoirs exhibit pressure changes long before injected fluids (whether brine or CO_2) have migrated, the footprint of brine injection into the formation is much smaller than the pore pressure changes (Gorecki et al., 2015).

The predicted shape and distribution of the brine plumes for each SWD well vary significantly from layer to layer within the model based on the location of perforations within each well and on the targeted injection zones. To better illustrate the extent of the injected brine throughout the entire thickness of the reservoir, the salinity distribution for each cell in each layer of the model was determined and normalized by the porosity in each cell. The equation used to determine this is similar to one used to illustrate gas per unit area as defined in the CMG Results 3-D user guide (2014). The equation used to determine the salinity per unit area is shown in Equation 4:

$$\text{Salinity per Unit Area} = \text{Salinity} * \text{Initial Porosity} * \text{Pay Thickness} \qquad \text{[Eq. 4]}$$

where salinity is expressed by NaCl molarity (moles/liter) and the pay thickness is in feet; thus the units for this parameter are NaCl molarity feet. Although this parameter is derived and does not have a clear physical analog, it is a way to compare the three-dimensional footprint of the injected brine extent between SWD wells by distributing the moles of the solute within the pore spaces for the entire thickness of the reservoir.
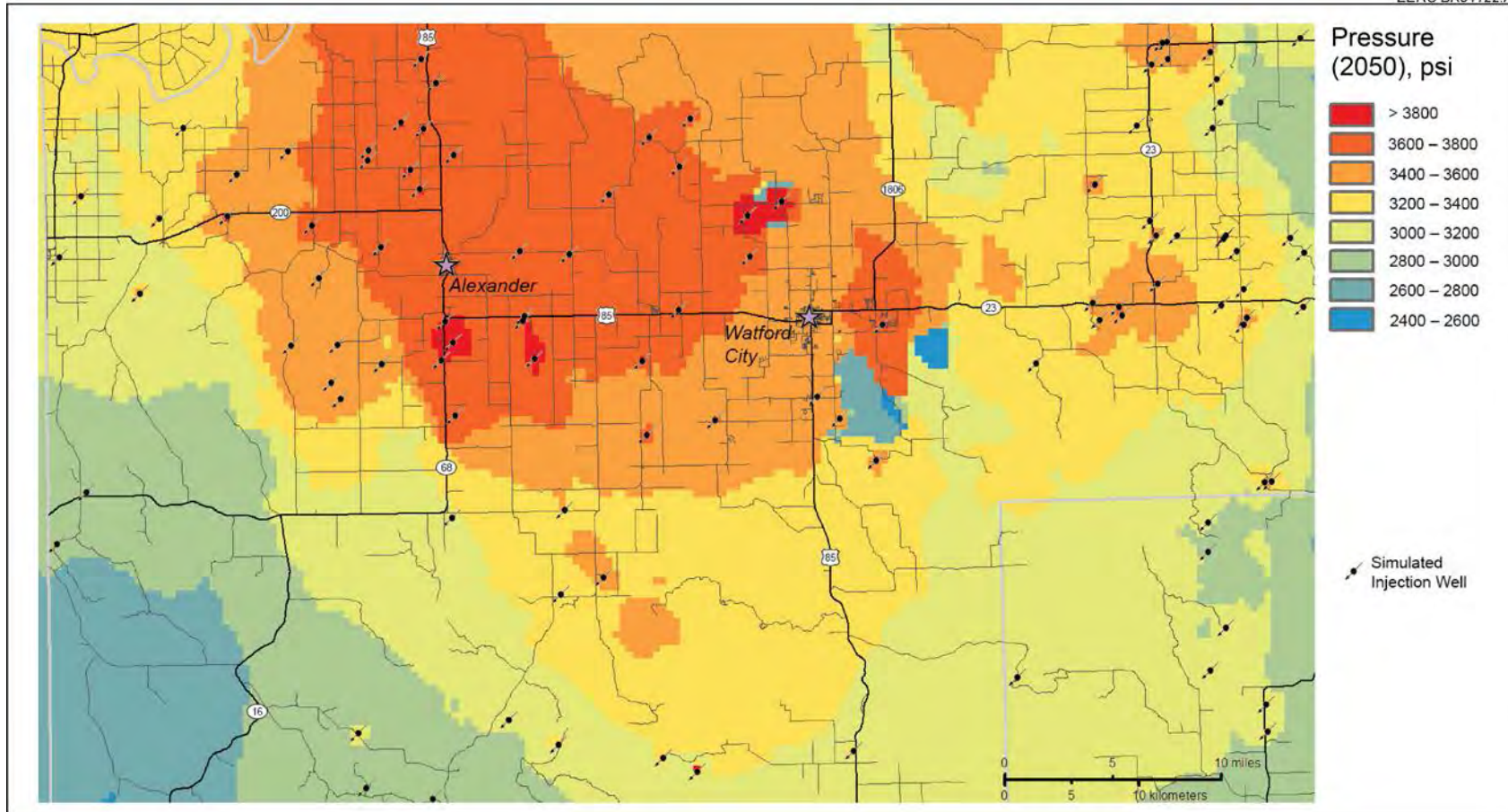
Figure 26. Maximum hypothetical pressure distribution exhibited by any of the 40 model layers in each grid cell. This represents year 2050 for Case 2_C.
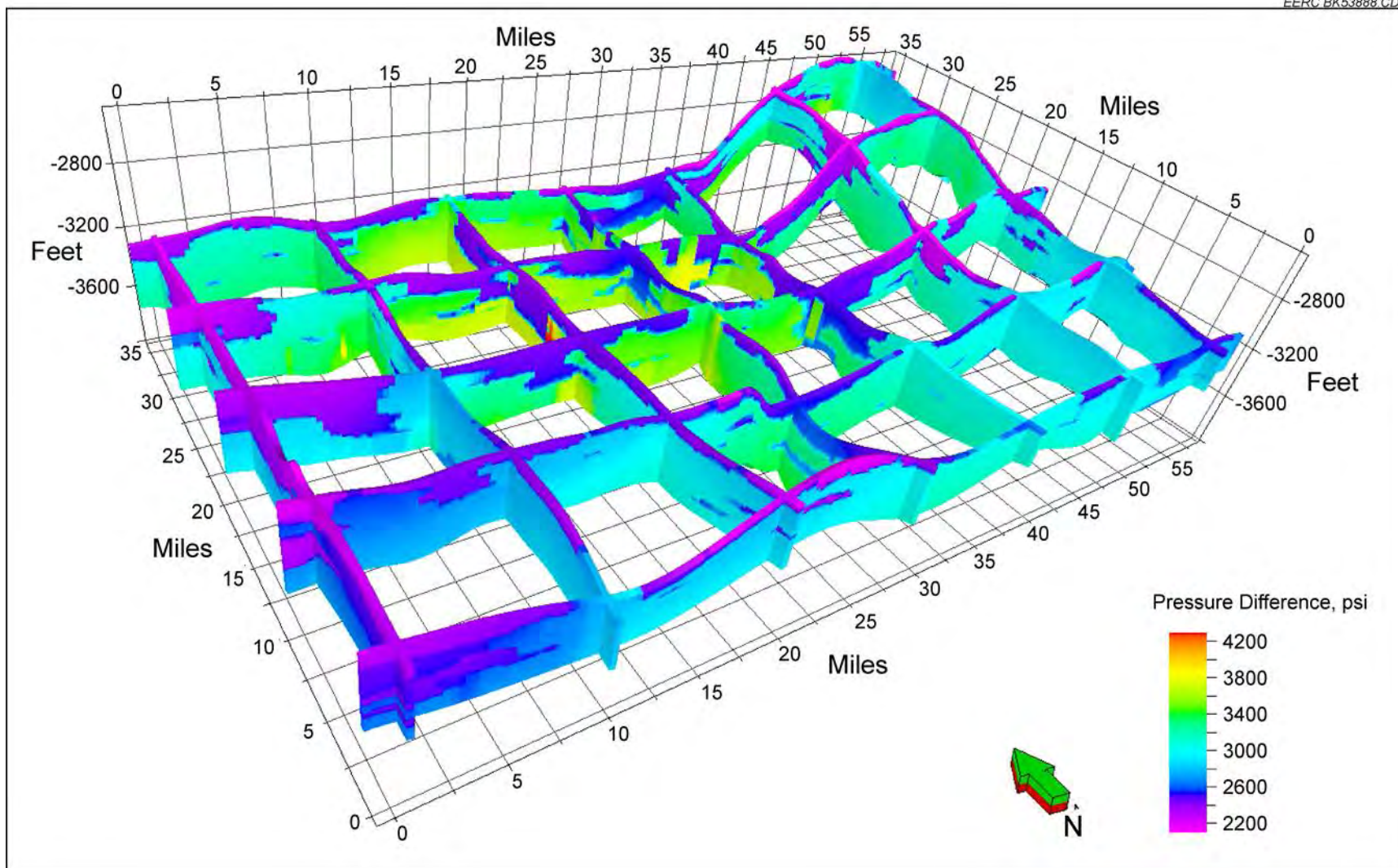
Figure 27. Fence diagram illustrating hypothetical pressure distribution in 2050 for Case 3_C.

Figure 28 is an illustration of the salinity per unit area distribution map for the year 2050 for Case 3_C. This figure clearly depicts the potential irregularity in plume shape that can result from anisotropy and heterogeneity in the reservoir matrix, as well as pressure interference from other nearby injectors. The extent of the area affected by salinity changes is relatively small when compared to the area affected by changes in pressure. Additional figures illustrating formation fluid pressure and salinity distributions are included in Appendix B.
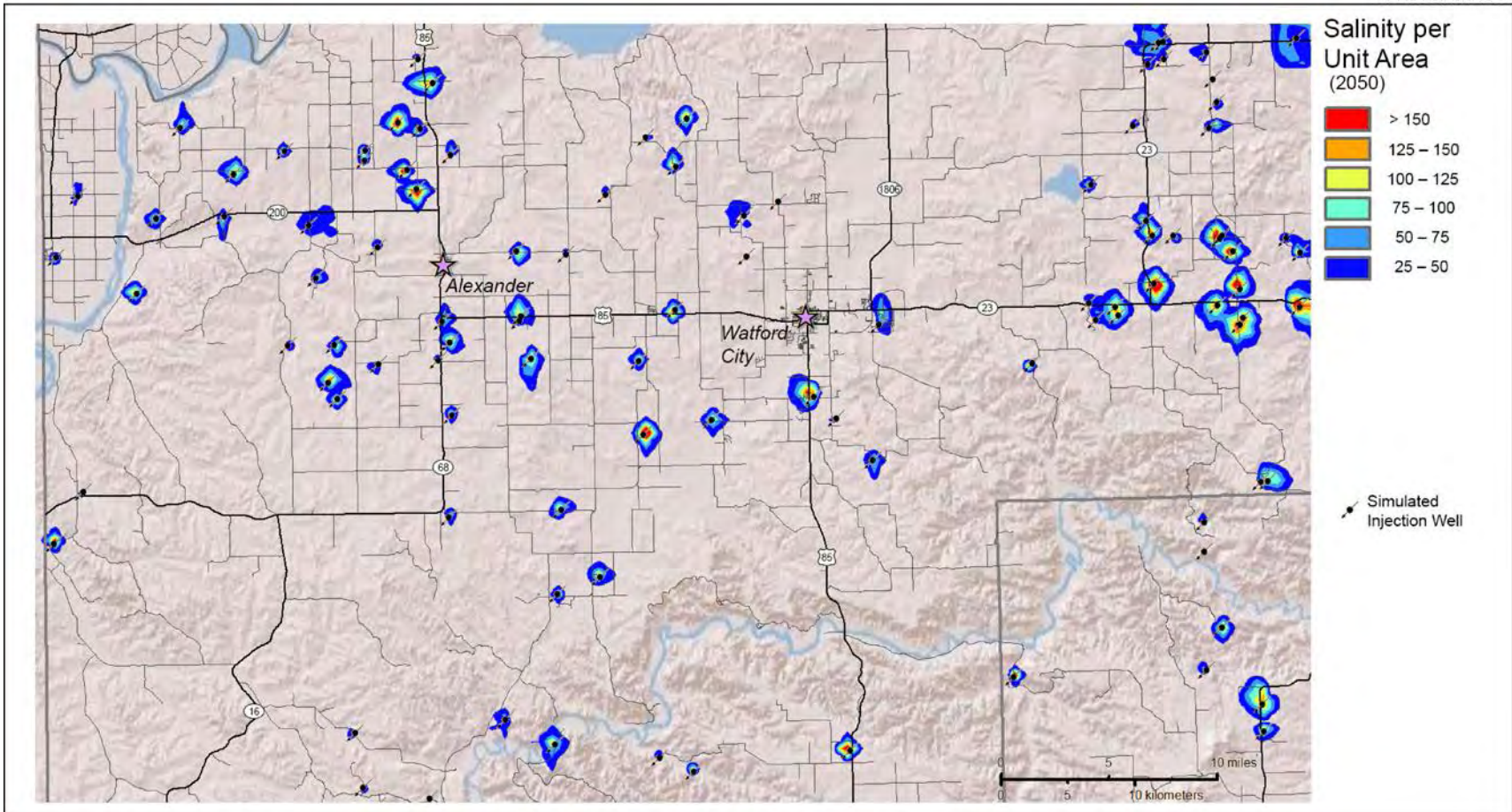
Figure 28. Salinity per unit area total in 2050 for Case 3_C.

SUMMARY AND CONCLUSIONS

The primary goal of this effort was to identify areas within the Inyan Kara reservoir that may already exhibit pressurization effects as a result of SWD disposal and to evaluate hypothetical future injection scenarios and their possible effects on reservoir fluid pressure. An additional goal was to evaluate the long-term disposal potential of the Inyan Kara as a SWD target in the modeled extent. To accomplish these goals, the following work was performed:

1. A geologic model was developed for the Inyan Kara Formation. The model's areal extent encompassed most of McKenzie County and a portion of northwestern Dunn County.

2. A volumetric method was used to estimate SWD potential in a closed system, and the result was used for comparison to the dynamic simulation results.

3. A simulation model was constructed and history-matched using the field injection and pressure data from 103 SWD wells in the modeled area.

4. The simulation model was used to run several predictive cases to evaluate long-term disposal potential and pressure effects in the Inyan Kara.

Based on the results of the prediction simulation cases, there remains a very large SWD potential of approximately 4 to 5 billion bbl within the Inyan Kara modeled area based only on existing SWD well locations (5 to 6 times the current cumulative water injected). If additional SWD wells are drilled and operated within the study area, the total water disposal potential may be considerably higher. In fact, even the closed-system-equation-based approach estimates a disposal potential of 7.19 billion bbl in the modeled portion of the Inyan Kara.

Despite the large predicted storage potential of the Inyan Kara, localized areas of pressurization have already occurred within the formation as indicated by the model predictions and supported by anecdotal evidence from SWD well operators. Predictive model simulations indicate that the areas of elevated pressure could expand in size and magnitude with continued long-term injection, especially in the northern portion of McKenzie County. These areas exhibit behavior of a closed or semiclosed system when injection occurs with dozens of wells at the current injection rate. Continued injection at the present or increased rates could result in operators curtailing injection rates and/or injected volumes to avoid exceeding the injection pressure limitations established by the DMR. The model predictions also suggest that there is a large portion (e.g., southern half) of the simulated area that could support an additional pressure increase even after more than 30 years of injection.

Maps depicting the brine plume extents surrounding individual SWD wells illustrate the influence of geology of the brine migration pathways. Many of the brine plumes appear to follow preferential flow pathways which result from variability in the extent and thickness of the sandstone layers. The model results reinforce the importance of understanding the local geology prior to siting a SWD well.

FUTURE WORK

As previously stated, the goal of this modeling effort was not to conduct a comprehensive analysis of multiple potential injection scenarios, but rather to provide a tool that can be used to evaluate scenarios of interest to BPOP members. In addition, this model was meant to evaluate broad-scale SWD into the Inyan Kara, not to precisely evaluate the effects of individual SWD wells. As such, there remains considerable work that could be done to further assess SWD in the Inyan Kara, including the following:

1. The simulations could be focused on a local site rather than at a regional scale. For a specific field, performing pressure analyses during simulated water injection would be helpful in (better) estimating the local injection potential. This may be of particular assistance to individual SWD well operators.

2. This regional scale model has relatively large grid cell size ($1640 \times 1640 \times 11$ feet). According to the study by Pekot and others (2016), larger grid cells result in lower injection rates and lower cumulative storage. For a specific field, the grid cell size could be smaller, which gives better estimated cumulative storage potentials.

3. As additional Inyan Kara isopach maps are completed by the DMR, the EERC could develop a statistical method to evaluate current and potential future SWD wellsites in the areas beyond the current simulated extent.

4. Further simulation work could be performed to evaluate additional injection well locations to optimize storage potential within the formation. Potential well locations could be selected based upon both the simulation results and real-world logistical considerations, such as proximity to access roads for the convenience of drilling and fluid transport or in close proximity to areas with a greater need for additional SWD wells.

5. The output from the reservoir simulation could be used to identify and develop relationships between key reservoir parameters and the projected performance of individual SWD wells. These relationships could be used to extend insights to other areas of the Inyan Kara in western North Dakota that have not been intensively studied.

REFERENCES

Bader, J.W., 2015, Inyan Kara sandstone isopach map: Watford City 100K Sheet, North Dakota. North Dakota Department of Mineral Resources, www.dmr.nd.gov/ndgs/documents/ Publication_List/pdf/GEOINV/GI-189.pdf (accessed December 2016).

Bourgoyne, A.T., Millheim, K.K., Chenevert, M.E., and Young, F.S., 1986, Applied drilling engineering: Society of Petroleum Engineers.

Computer Modelling Group, 2014, Results 3-D user guide.

Craig, J., Gorecki, D.C., Ayash, S.C., Liu, G., and Braunberger, J.R., 2014, A comparison of volumetric and dynamic storage efficiency in deep saline reservoirs—an overview of IEAGHG study IEA/CON/13/208: 12th International Conference on Greenhouse Gas Control Technologies.

Gorecki, C.D., Ayash, S.C., Liu, G., Braunberger, J.R., and Dotzenrod, N.W., 2015, A comparison of volumetric and dynamic CO_2 storage resource and efficiency in deep saline formations: International Journal of Greenhouse Gas Control, v. 42, p. 213–225.

Gorecki, C.D., Liu, G., Braunberger, J.R., Klenner, R.C.L., Ayash, S.C., Dotzenrod, N.W., Steadman, E.N., and Harju, J.A., 2014, CO_2 storage efficiency in deep saline formations—a comparison of volumetric and dynamic storage resource estimation methods (IEA/CON/13/208): Final report (May 1, 2013 – April 30, 2014) for IEA Greenhouse Gas R&D Programme, Grand Forks, North Dakota, Energy & Environmental Research Program, August.

Gorecki, C.D., Sorensen, J.A., Bremer, J.M., Ayash, S.C., Knudsen, D.J., Holubnyak, Y.I., Smith, S.A., Steadman, E.N., and Harju, J.A., 2009, Development of storage coefficients for carbon dioxide storage in deep saline formations: Final report (August 25, 2008 – June 30, 2009) for IEA Greenhouse Gas R&D Programme, EERC Publication 2009-EERC-07-06, Grand Forks, North Dakota, Energy & Environmental Research Center, July.

Hall, H.N., 1953, Compressibility of reservoir rocks: Petroleum Transactions, AIME, 198, 309-311.

Kurz, B.K., 2016, Summary of the Bakken water assessment report: Presentation given to the North Dakota Legislative Water Topics Overview Committee, Bismarck, North Dakota, September 23, 2016.

Kurz, B.K., Stepan, D.J., Glazewski, K.A., Stevens, B.G., Doll, T.E., Kovacevich, J.T., and Wocken, C.A., 2016, A review of Bakken water management practices and potential outlook: Final report prepared for members of the Bakken Production Optimization Program. EERC Publication, Grand Forks, North Dakota, Energy & Environmental Research Center, 42 pp.

Murphy, E.C., Nordeng, S.H., Juenker, B.G., and Hoganson, J.W., 2009, North Dakota stratigraphic column: North Dakota Geological Survey.

Pekot, L.J., Ayash, S.C., Bosshart, N.W., Dotzenrod, N.W., Ge, J., Jiang, T., Jacobson, L.L., Vettleson, H.M., Peck, W.D., and Gorecki, C.D., 2016, CO_2 storage efficiency in deep saline formations – Stage 2: EERC Publication for IEA Greenhouse Gas R&D Programme, Grand Forks, North Dakota, Energy & Environmental Research Program.

Schlumberger, 2016, Petrel 2016: Petrel E&P Software Platform.

U.S. Department of Energy, 2007, National Energy Technology Laboratory carbon sequestration atlas of the United States and Canada.

U.S. Department of Energy, 2008, National Energy Technology Laboratory carbon sequestration atlas of the United States and Canada, 2nd ed.

U.S. Department of Energy National Energy Technology Laboratory, 2010, Carbon sequestration atlas of the United States and Canada, 3rd ed.

Zhou, Q., Birkholzer, J.T., Tsang, C.-F., and Rutqvist, J., 2008, A method for quick assessment of CO_2 storage capacity in closed and semiclosed saline formations: International Journal of Greenhouse Gas Control, v. 2, no. 4, p. 626–639.

APPENDIX A

HISTORY-MATCHING RESULTS OF THE 103 SWD WELLS AND EXAMPLE HISTORY-MATCHING PLOTS

Table A-1. History-Matching Results of the 103 SWD Wells

Well No.	Well Name in Model	Starting Date	Current Operator	HM[1] Result
1606	D	6/1/2011	Abraxas Petroleum Corp.	M[2]
10525	D8	7/1/2013	Abraxas Petroleum Corp.	N/A[3]
90251	K4	5/1/2013	Alati Arnegard LLC	M
90241	J9	11/1/2012	Alexander SWD, LLC	MP[4]
90216	J3	8/1/2012	Aqua Terra Water Management USA, LLC	M
90131	H3	2/1/2010	Arrow Water, LLC	M
90266	K8	7/1/2013	Arrow Water, LLC	M
11295	E4	5/1/2012	Bennett SWD, LLC	M
16929	G1	1/1/2015	Bennett SWD, LLC	M
90285	K9	10/1/2013	Big Disposal Cartwright, LLC	MP
90243	K1	11/1/2012	Bosque Disposal Systems, LLC	M
8267	O	11/1/2011	Buckhorn Energy Services, LLC	MP
8681	S	1/1/2012	Buckhorn Energy Services, LLC	M
90288	I9	6/1/2013	Buckhorn Energy Services, LLC	MP
90204	L2	7/1/2012	Buckhorn Energy Services, LLC	MP
10734	E1	11/1/2003	Burnett Energy Inc.	MP
3614	I	12/1/2012	C & J Well Services, Inc.	MF[5]
9388	Z	4/1/2012	Caliber Midstream North Dakota LLC	M
11027	E2	8/1/2014	Caliber Midstream North Dakota LLC	MP
90222	J4	1/1/2013	Caliber Midstream, LLC	M
8839	V	4/1/1982	Citation Oil & Gas Corp.	MP
11540	E6	9/1/1996	Citation Oil & Gas Corp.	MP
13617	F2	10/1/1994	Citation Oil & Gas Corp.	M
16177	F7	8/1/2014	Cypress Energy Partners – Bakken, LLC	M
90179	I2	5/1/2012	Cypress Energy Partners – Bakken, LLC	M
7041	L	4/1/2013	Dakota Fluid Solutions, LLC	M
10461	D6	1/1/2006	Deep Creek Adventures, CO.	MP
8761	T	3/1/1984	Denbury Onshore, LLC	N/A
11719	E5	3/1/1986	Enduro Operating, LLC	M
11729	E7	3/1/1991	Enduro Operating, LLC	N/A
11536	E8	12/1/1998	Enduro Operating, LLC	M
8945	W	4/1/1993	Energyquest II, LLC	M
90165	H5	10/1/2011	Enerplus Resources USA Corporation	N/A
90184	I4	7/1/2012	Enerplus Resources USA Corporation	N/A

[1] HM: history-matching.
[2] M: well-matched.
[3] N/A: not matched.
[4] MP: poorly matched.
[5] MF: fairly matched.

Table A-1. History-Matching Results of the 103 SWD Wells (continued)

Well No.	Well Name in Model	Starting Date	Current Operator	HM Result
90233	J8	7/1/2013	Environmentally Clean Systems, LLC	M
90245	K2	2/1/2013	EOG Resources, Inc.	M
90229	J7	12/1/2012	Flatland Resources I, LLC	M
2724	G	9/1/1966	Flying J Oil & Gas, Inc.	MF
90290	L3	7/1/2013	Hanna SWD, LLC	MP
16581	F9	2/1/2015	Hep HB Disposal, LLC	MF
9539	C	3/1/1999	Hess Bakken Investments II, LLC	MF
9764	E	12/1/2002	Hess Bakken Investments II, LLC	M
1317	D1	5/1/2006	Hess Bakken Investments II, LLC	N/A
90077	D2	10/1/1992	Hess Bakken Investments II, LLC	M
1831	G5	9/1/2007	Hess Bakken Investments II, LLC	MP
90206	J1	11/1/2012	HJG North Dakota–Cartwright, LLC	M
90213	J2	11/1/2012	Hunt Oil Company	M
90011	G3	5/1/1980	Kerr–McGee Corp.	M
9774	M	4/1/2006	Landtech Enterprises, LLC	M
16189	D3	9/1/2007	Landtech Enterprises, LLC	M
90123	D5	10/1/2008	Landtech Enterprises, LLC	M
90134	F8	9/1/2010	Landtech Enterprises, LLC	M
7429	H2	11/1/1980	Landtech Enterprises, LLC	M
10128	H4	10/1/1984	Landtech Enterprises, LLC	M
6323	K	12/1/1999	Legacy Reserves Operating LP	MF
90177	I1	1/1/2012	Madison Disposal 2-1, L.L.C.	M
1167	B	8/1/2009	MBI Oil & Gas, LLC	M
90186	I5	7/1/2012	Mckenzie Energy Partners, LLC	M
90190	I7	11/1/2012	Mckenzie Energy Partners, LLC	M
90200	I8	9/1/2012	Mckenzie Energy Partners, LLC	M
2028	F	7/1/1962	Missouri Basin Well Service, Inc.	M
8977	X	1/1/2012	Missouri Basin Well Service, Inc.	M
90302	L4	2/1/2014	Missouri Basin Well Service, Inc.	M
8399	P	10/1/2010	Murex Petroleum Corporation	MF
8440	R	5/1/2006	Murex Petroleum Corporation	M
90183	I3	6/1/2012	NGL Water Solutions Bakken, LLC	M
90257	K6	8/1/2013	NGL Water Solutions Bakken, LLC	M
15766	F5	8/1/2011	OASIS Petroleum North America LLC	M
16134	F6	4/1/2009	OASIS Petroleum North America LLC	M

[1] HM: history-matching.

[2] M: well-matched.

[3] N/A: not matched.

[4] MP: poorly matched

[5] MF: fairly matched.

Table A-1. History-Matching Results of the 103 SWD Wells (continued)

Well No.	Well Name in Model	Starting Date	Current Operator	HM Result
90002	G2	11/1/1981	OASIS Petroleum North America LLC	M
90087	G6	9/1/1996	OASIS Petroleum North America LLC	M
90107	G7	2/1/2005	OASIS Petroleum North America LLC	MF
90112	G8	3/1/2006	OASIS Petroleum North America LLC	M
90116	G9	9/1/2007	OASIS Petroleum North America LLC	MF
90261	K7	9/1/2013	OASIS Petroleum North America LLC	M
10720	D9	2/1/1985	Paul Rankin Inc.	M
12806	F1	10/1/2012	PETRO-Hunt Dakota, LLC	MP
2764	H	9/1/2001	PETRO-HUNT, LLC	MP
11093	E3	11/1/1987	PETRO-HUNT, LLC	MP
10104	D4	3/1/2010	QC Environmental Services, Inc.	M
8163	N	3/1/1985	Ranch Oil Company	MP
8816	U	5/1/1983	RIGEL, Inc.	MP
9481	C9	7/1/1998	Rim Operating, Inc.	M
90166	H6	2/1/2012	Secure Energy Services USA, LLC	MF
90250	K3	11/1/2013	Secure Energy Services USA, LLC	MF
90173	H9	2/1/2012	Statoil Pipelines, LLC	M
90252	K5	9/1/2013	Statoil Pipelines, LLC	M
90189	A	7/1/2012	Tervita, LLC	MF
1156	Y	8/1/2008	Tervita, LLC	M
9081	I6	3/1/2011	Tervita, LLC	MF
5336	J	3/1/1981	True Oil LLC	M
15121	F4	9/1/2012	True Oil LLC	M
90170	H7	12/1/2011	White Owl Energy Services (US) Inc.	M
90172	H8	1/1/2013	White Owl Energy Services (US) Inc.	M
90228	J6	10/1/2012	White Owl Energy Services (US) Inc.	MP
13684	F3	7/1/1995	White Rock Oil & Gas, LLC	MF
8435	Q	1/1/1982	Whiting Oil And Gas Corporation	MP
10503	D7	5/1/2011	XTO Energy Inc.	M
90015	G4	6/1/1979	XTO Energy Inc.	M
90117	E9	12/1/2007	Zavanna, LLC	MF
90226	H1	12/1/2012	Zavanna, LLC	MP
90287	J5	11/1/2013	Zavanna, LLC	M
12498	L1	8/1/1999	Zavanna, LLC	MP

[1] HM: history-matching.
[2] M: well-matched.
[3] N/A: not matched.
[4] MP: poorly matched
[5] MF: fairly matched.
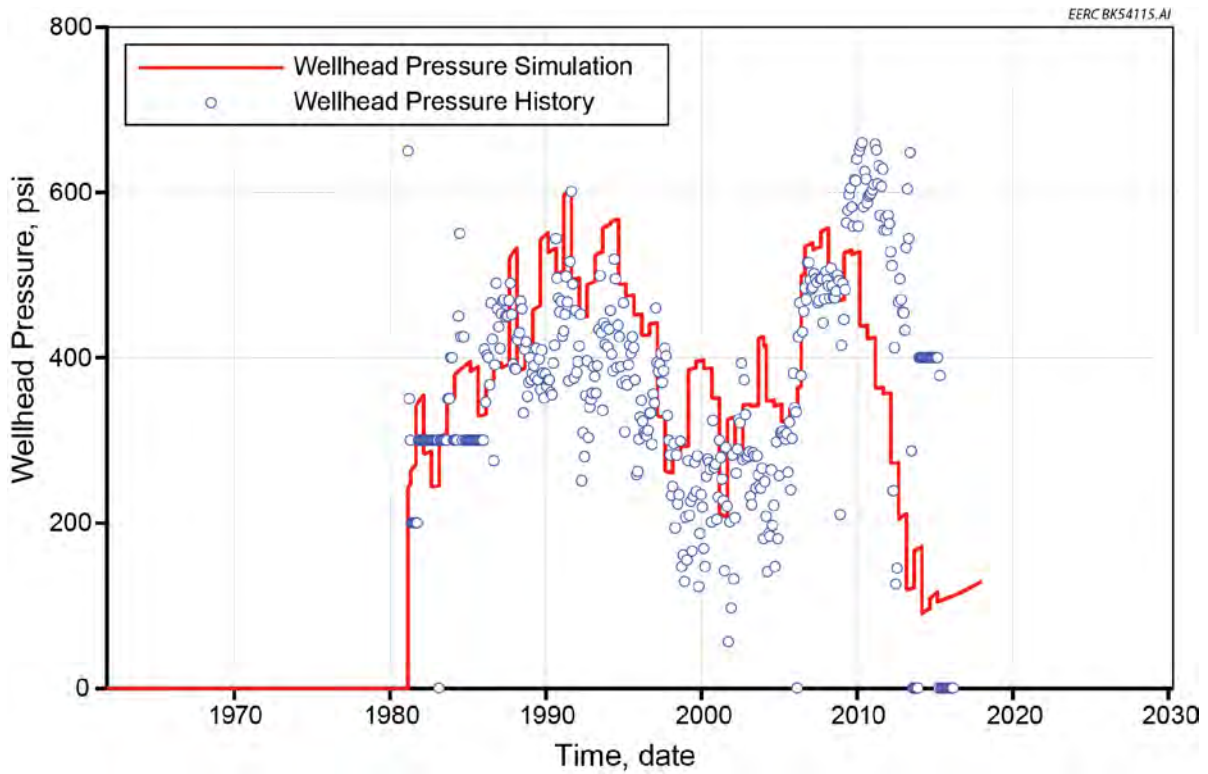
Figure A-1. Good-quality wellhead pressure history match for Well 5336.
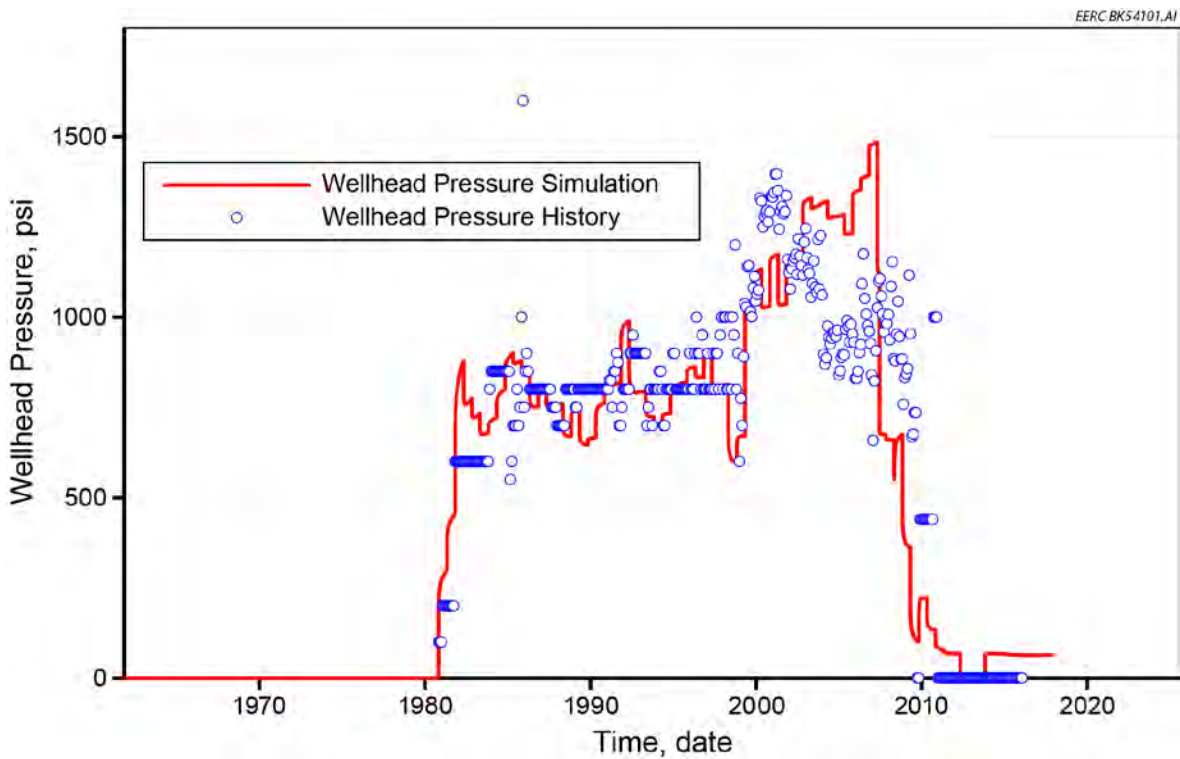
Figure A-2. Good-quality wellhead pressure history match for Well 7429.

A-4
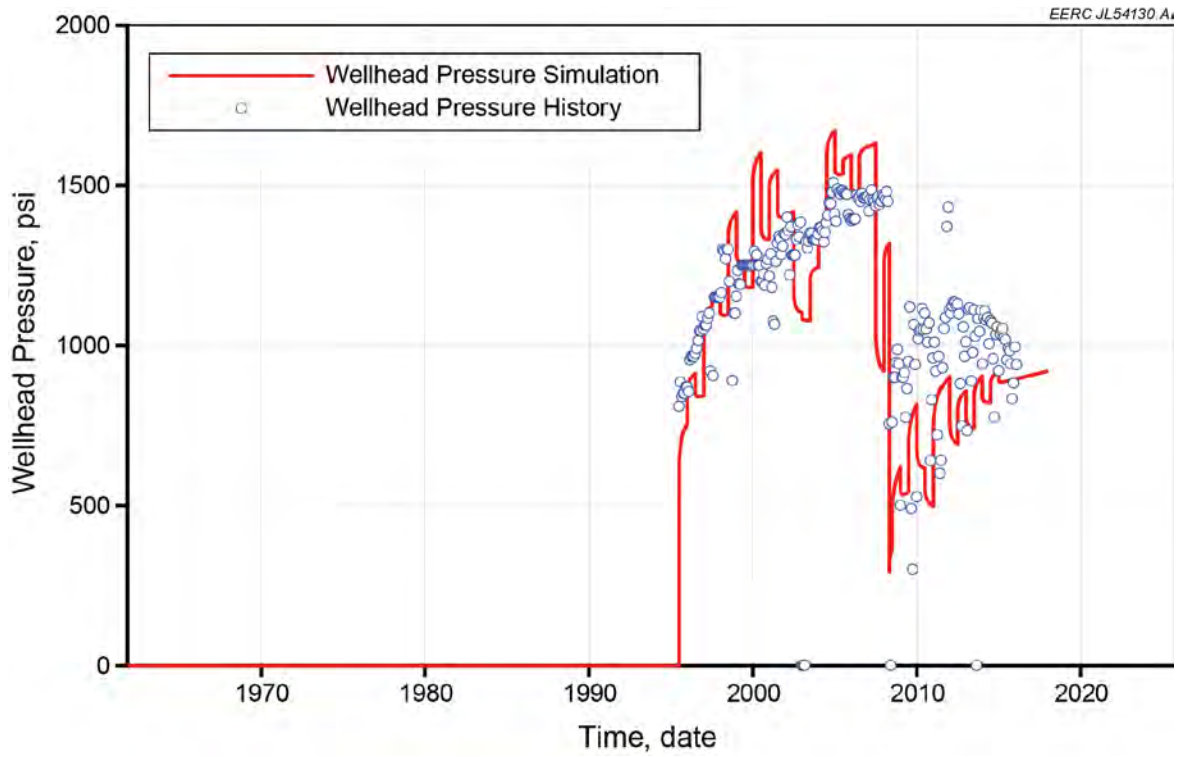
Figure A-3. Good-quality wellhead pressure history match for Well 13684.
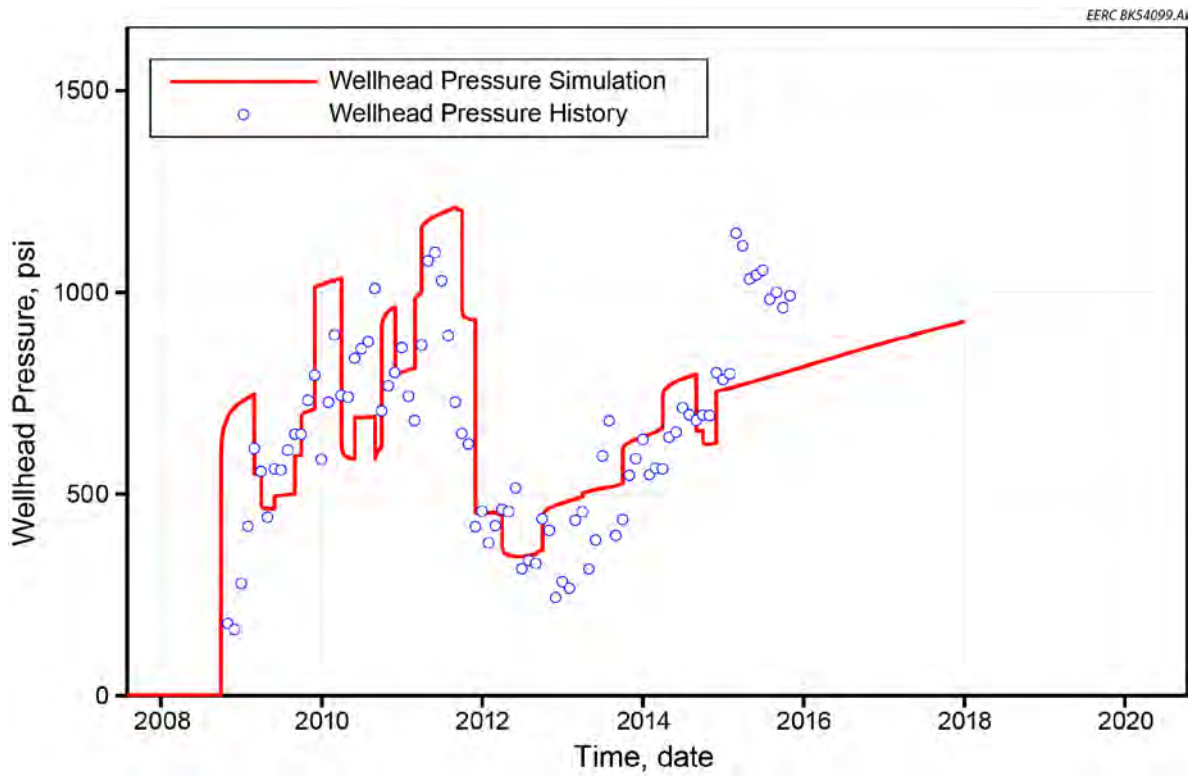
Figure A-4. Good-quality wellhead pressure history match for Well 90123.
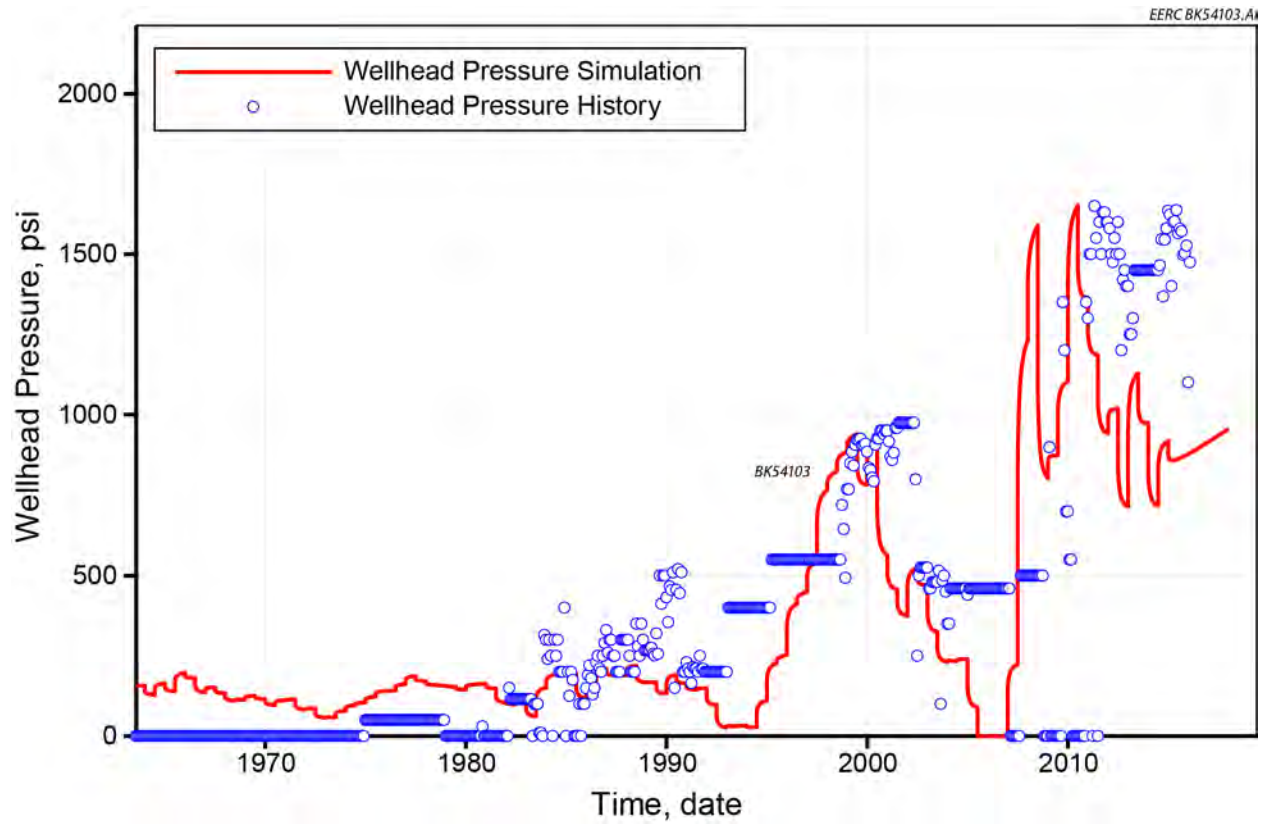
Figure A-5. Fair-quality wellhead pressure history match for Well 2028.
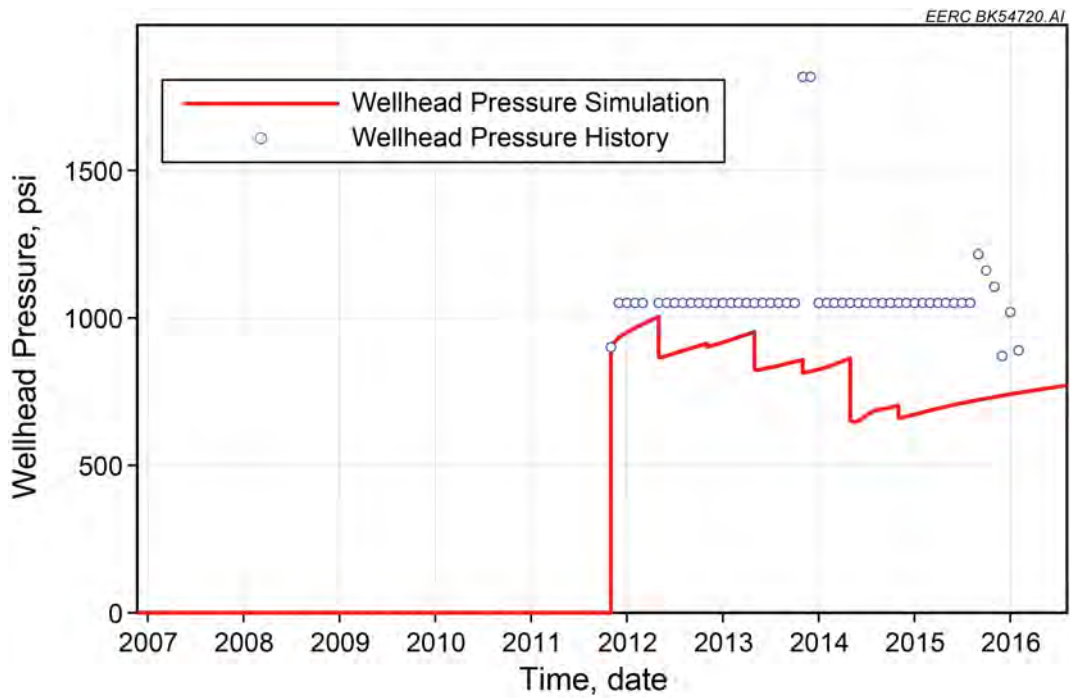
Figure A-6. Poor-quality wellhead pressure history match for Well 8267.

A-6
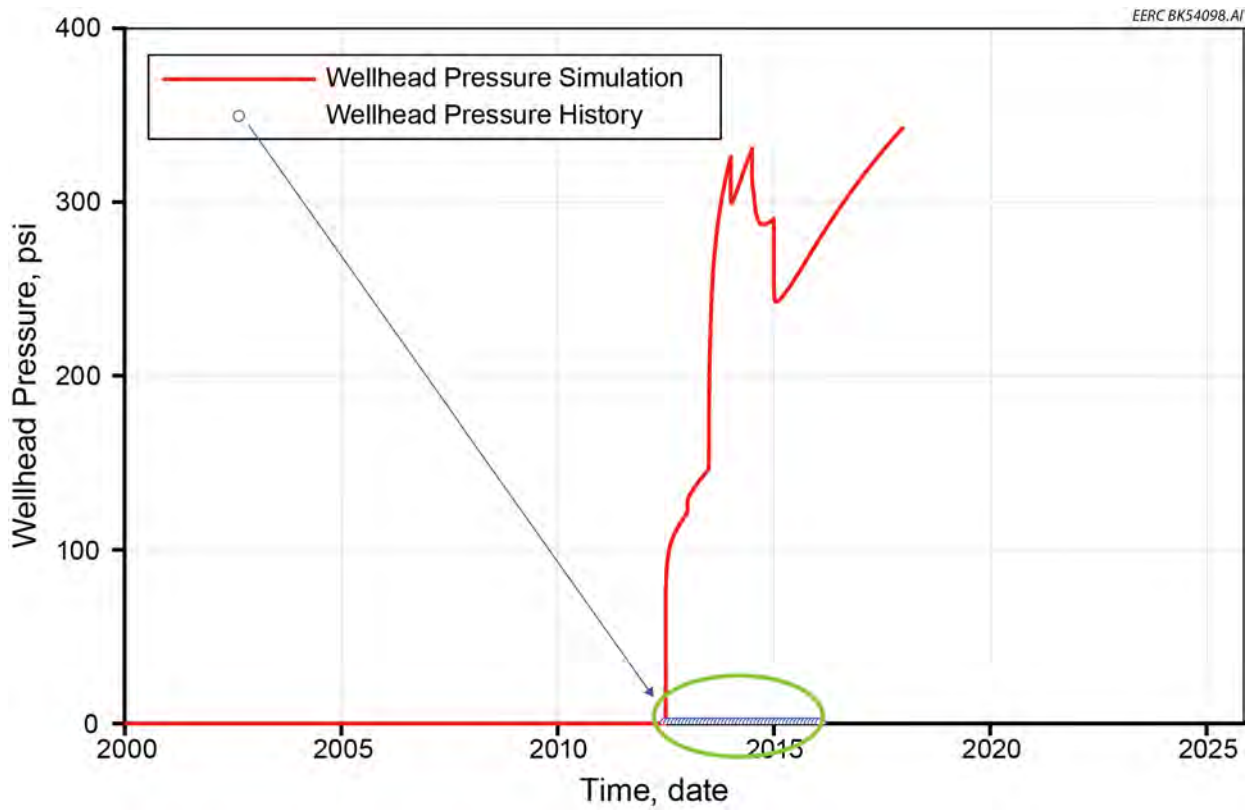
Figure A-7. Unmatched wellhead pressure for Well 90123 because of unreliable field data.
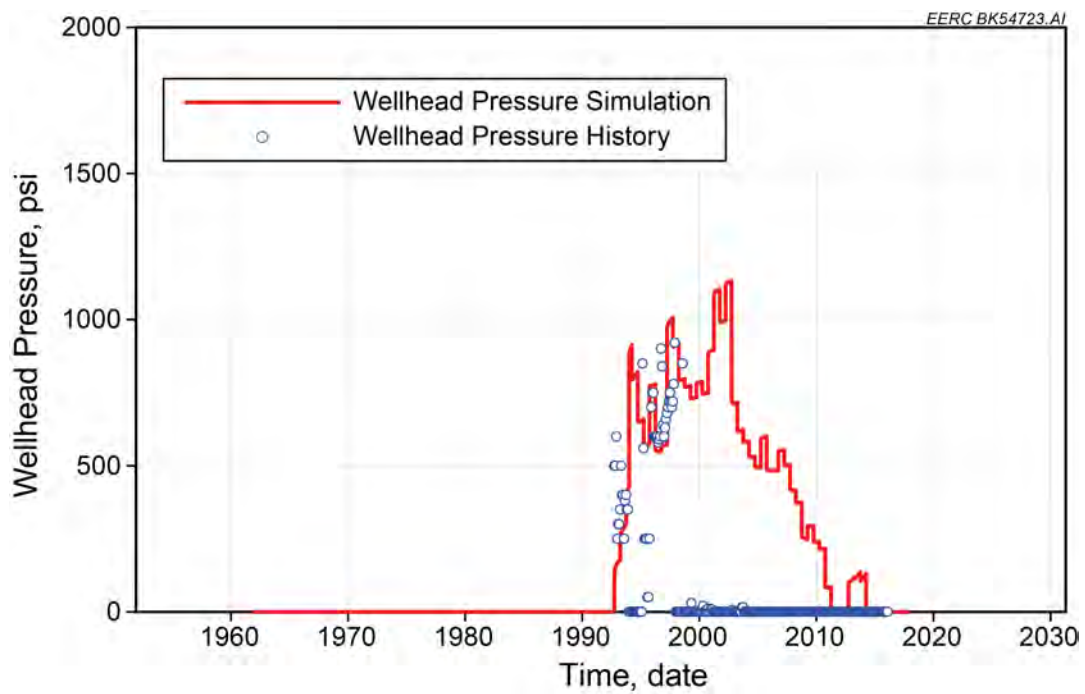
Figure A-8. Wellhead pressure history match for Well 90077.
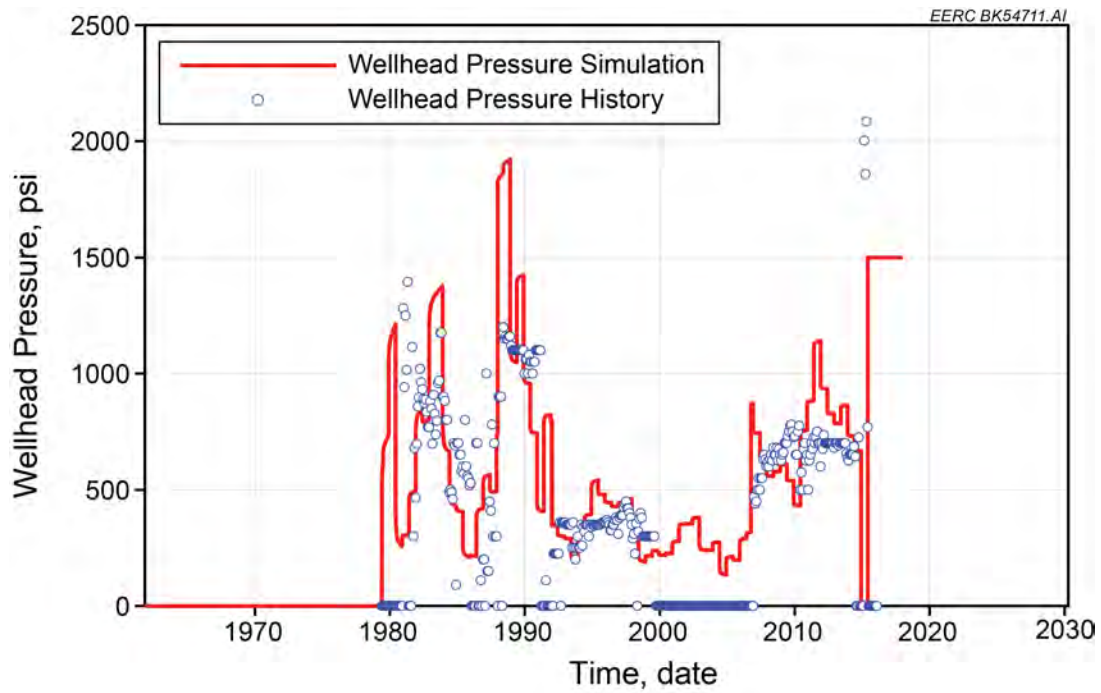
Figure A-9. Wellhead pressure history match for Well 90015.
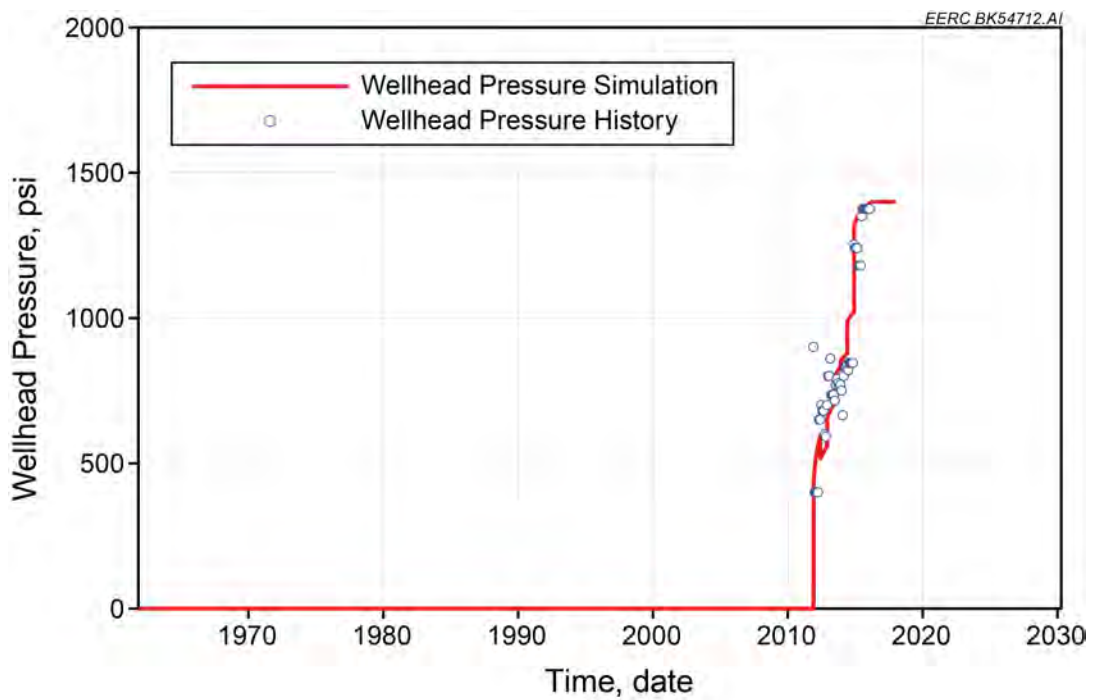
Figure A-10. Wellhead pressure history match for Well 90170.
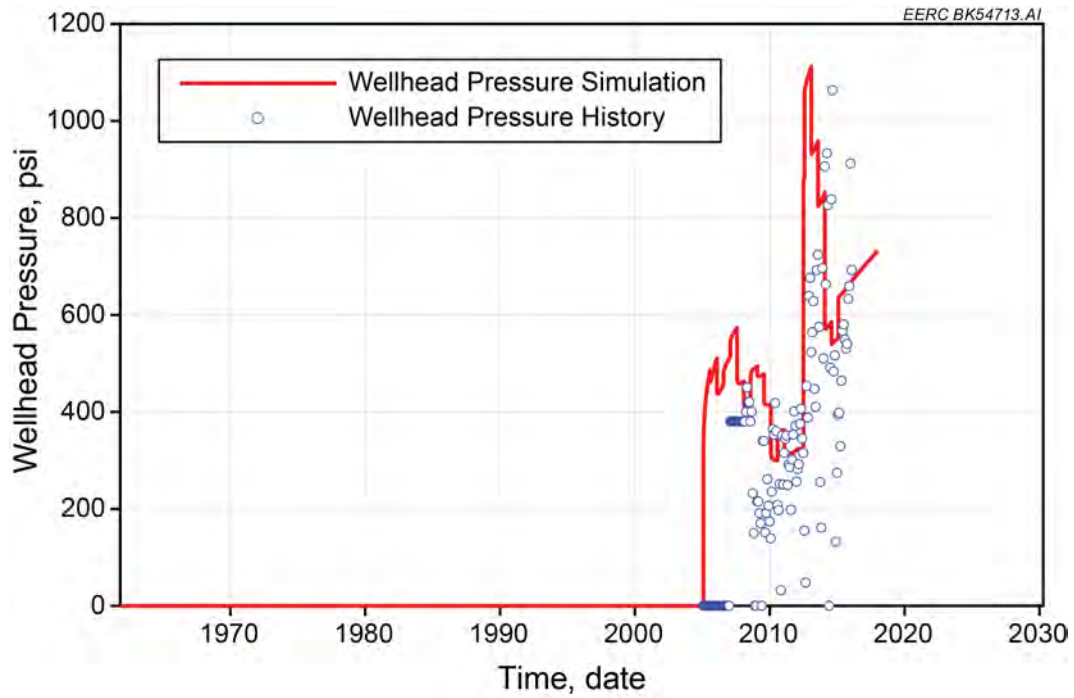
Figure A-11. Wellhead pressure history match for Well 90107.
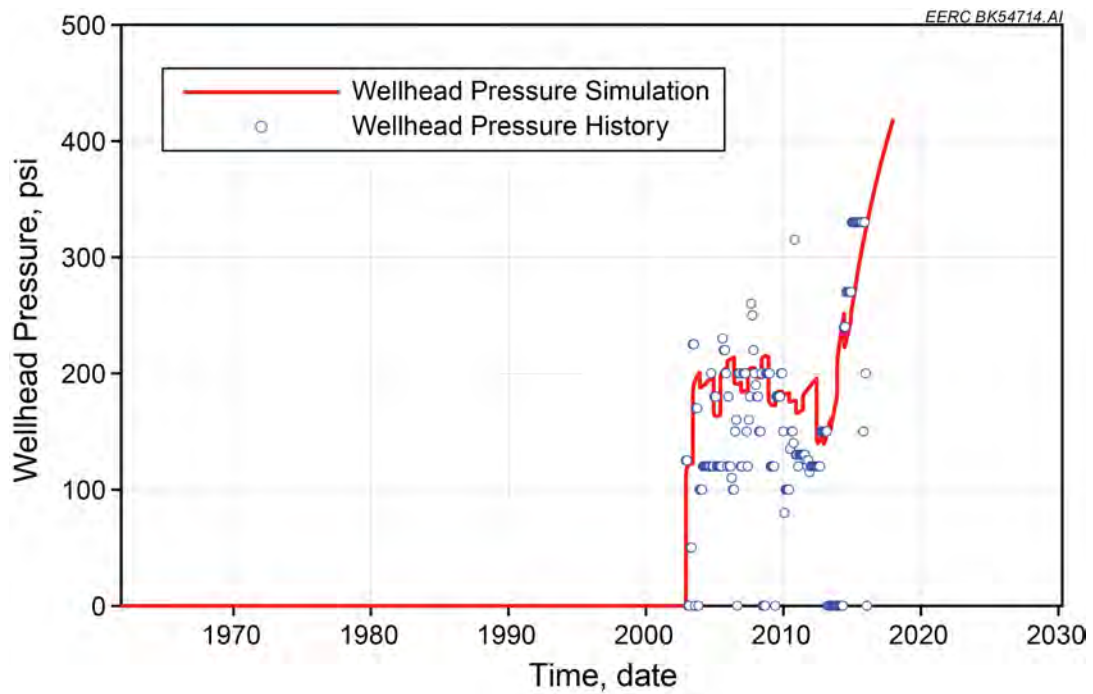
Figure A-12. Wellhead pressure history match for Well 9764.

A-9
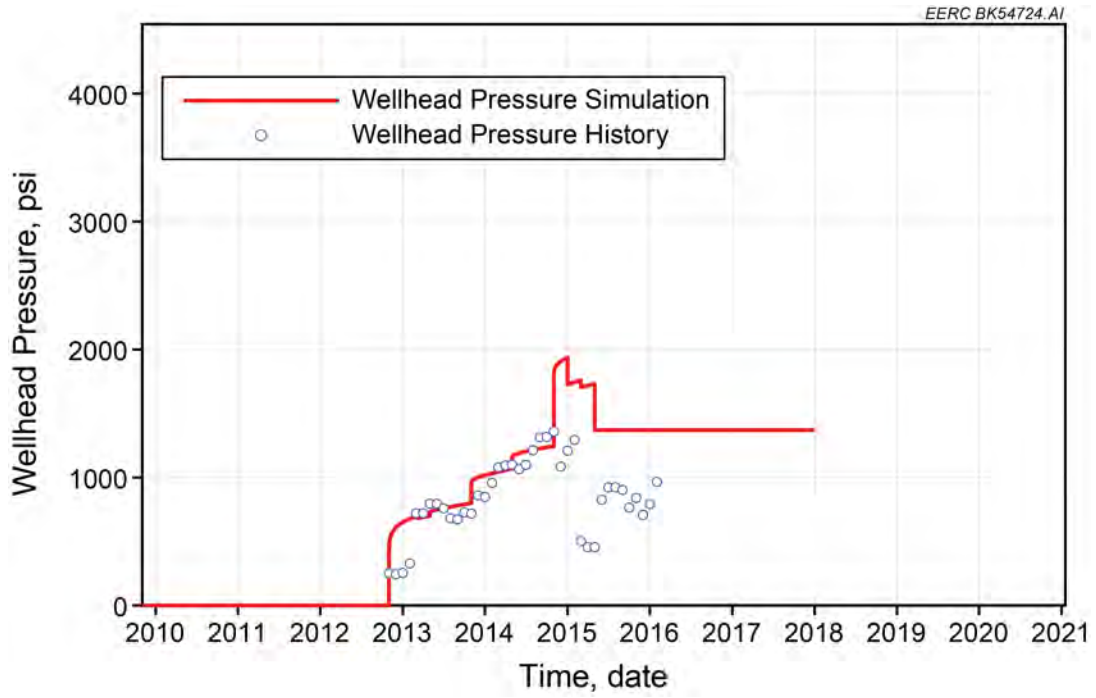
Figure A-13. Wellhead pressure history match for Well 90243.
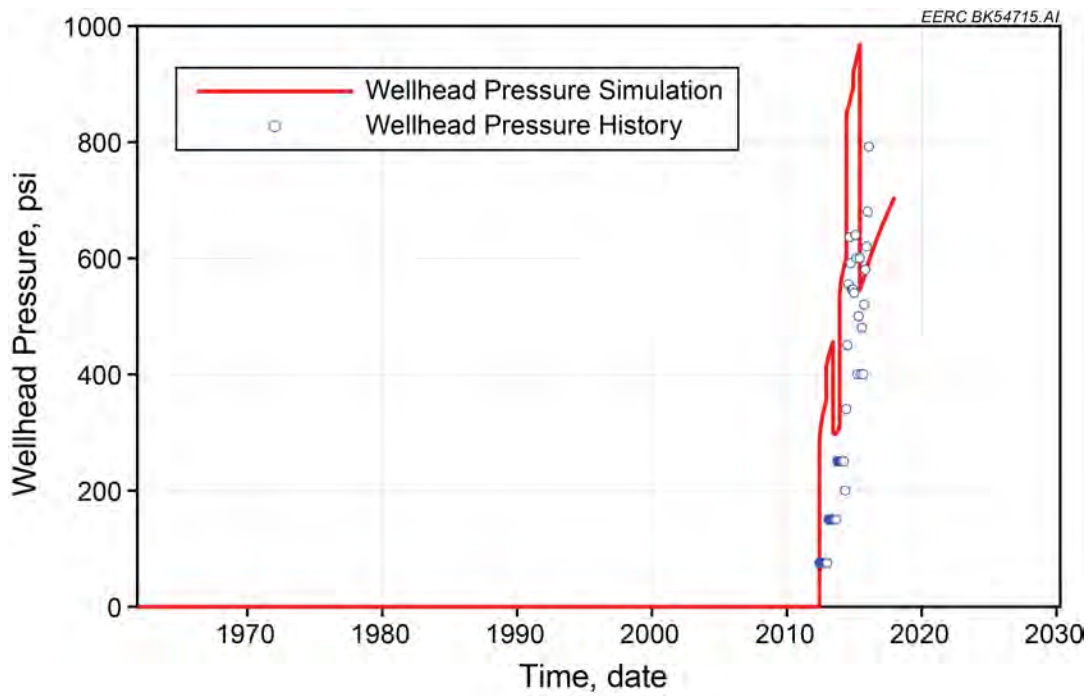
Figure A-14. Wellhead pressure history match for Well 90183.
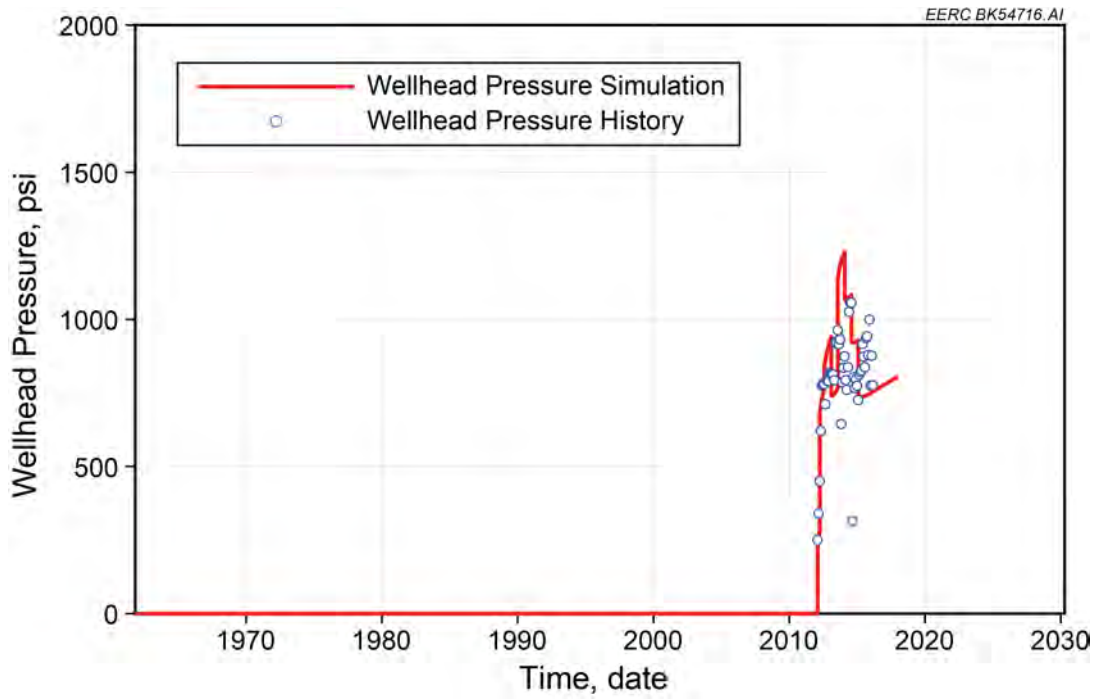
Figure A-15. Wellhead pressure history match for Well 90166.
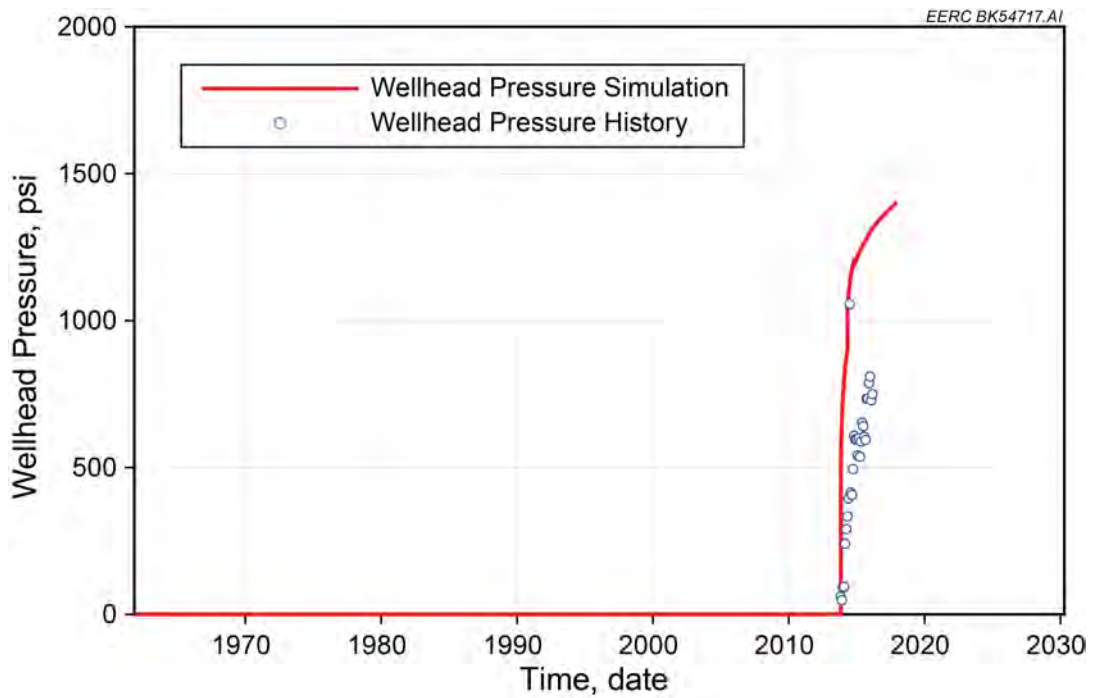
Figure A-16. Wellhead pressure history match for Well 90250.

A-11
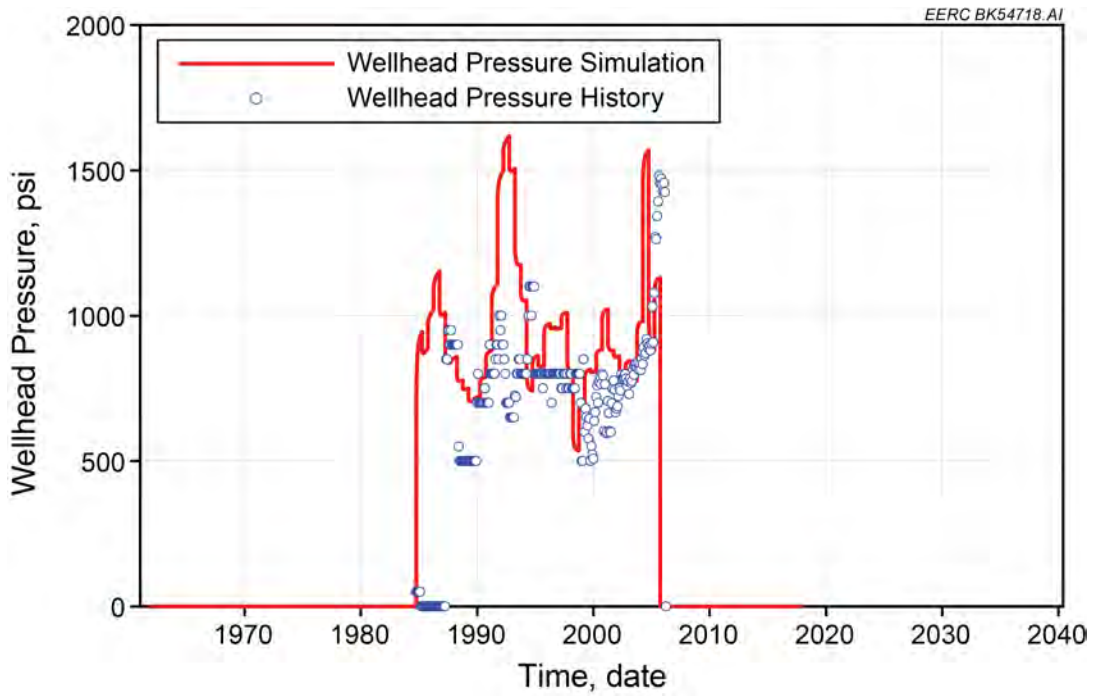
Figure A-17. Wellhead pressure history match for Well 10128.
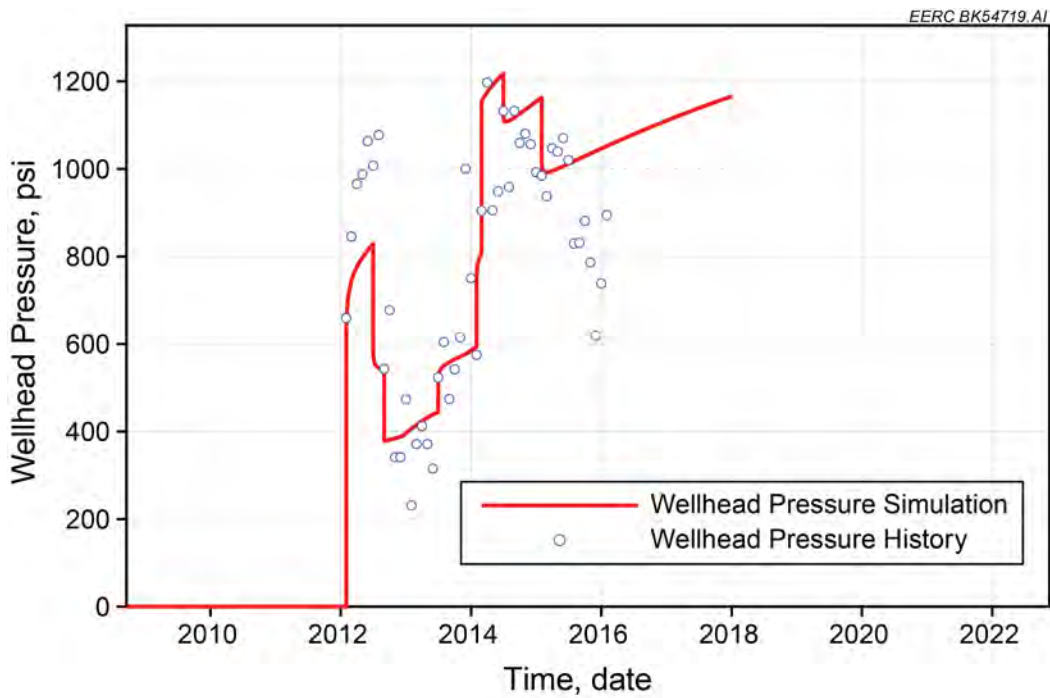
Figure A-18. Wellhead pressure history match for Well 90173.
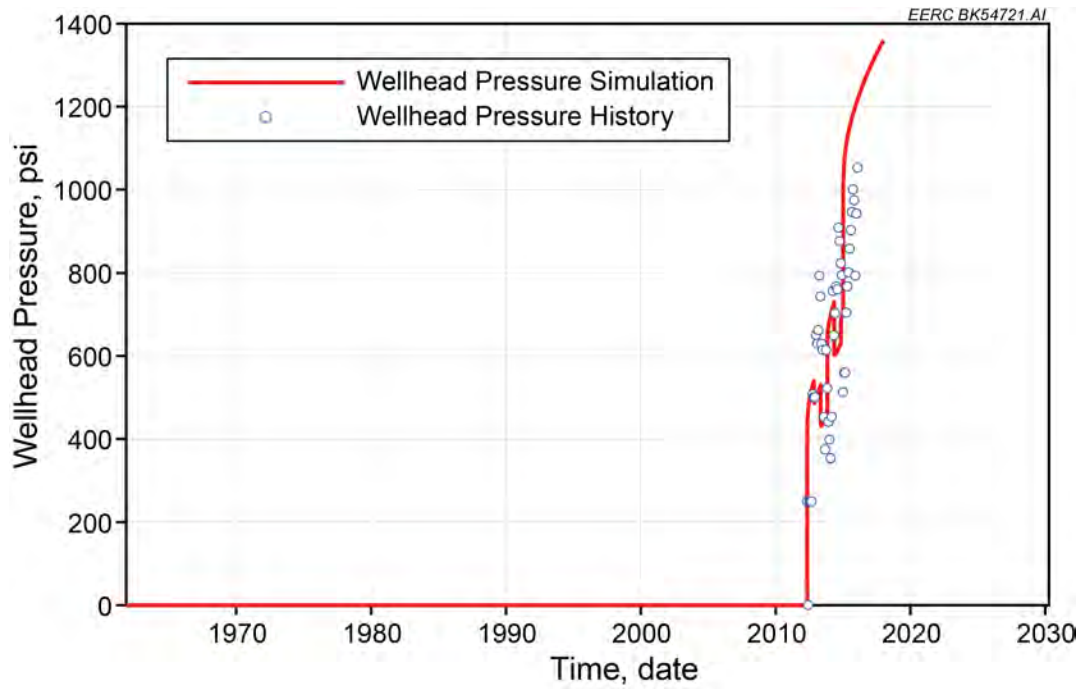
Figure A-19. Wellhead pressure history match for Well 11295.
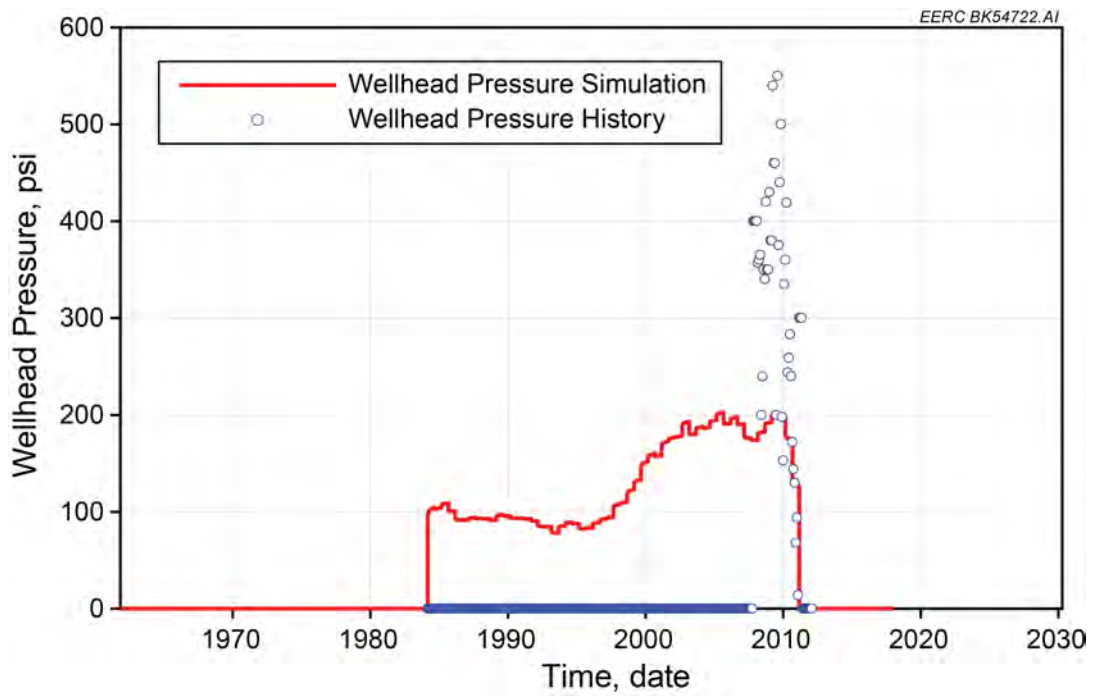
Figure A-20. Wellhead pressure history match for Well 8761.

APPENDIX B

ADDITIONAL FIGURES ILLUSTRATING HYPOTHETICAL PRESSURE AND SALINITY DISTRIBUTIONS
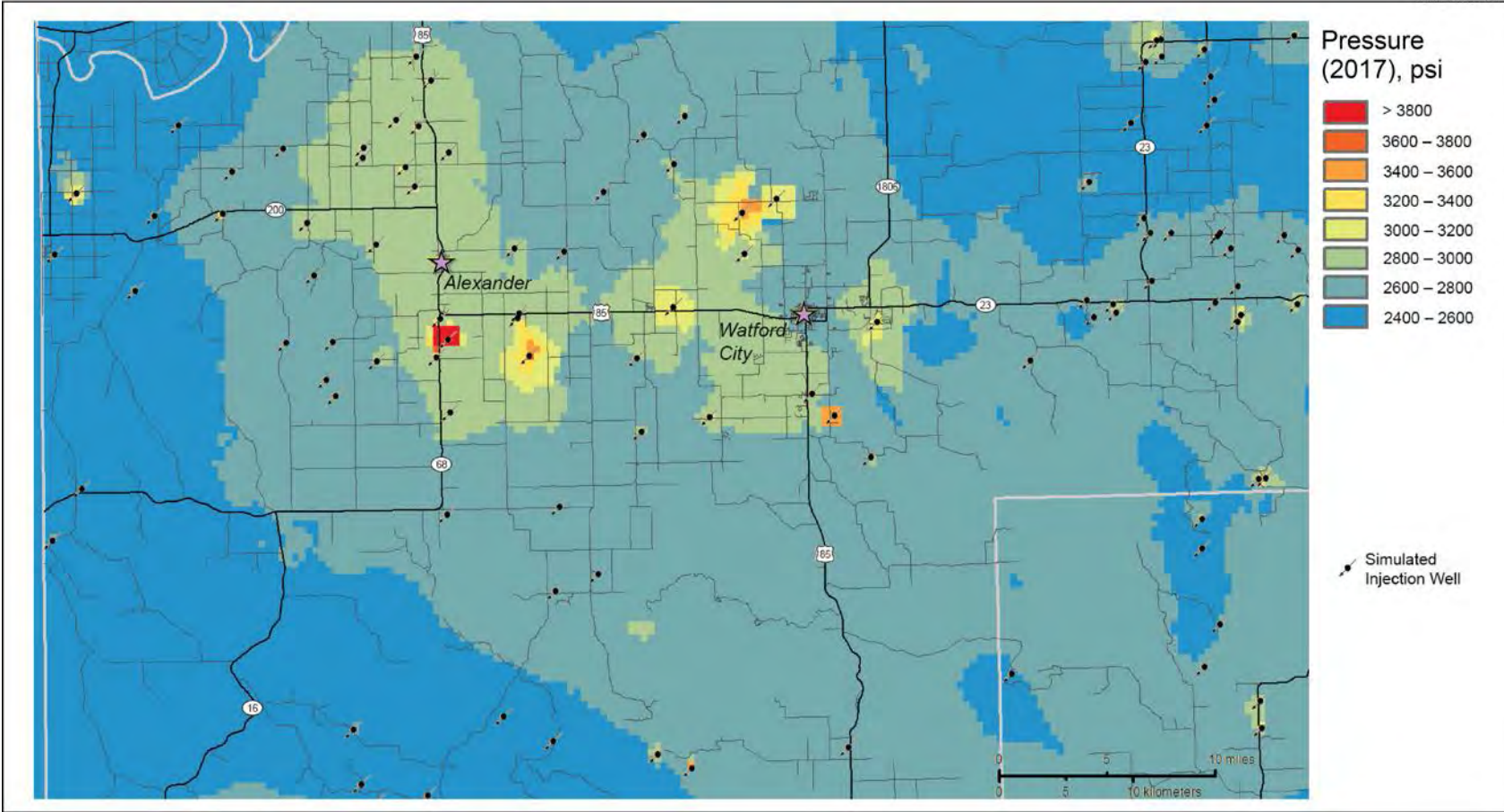
Figure B-1. Maximum hypothetical pressure distribution exhibited by any of the 40 model layers in each grid cell. This represents the model-predicted conditions for 2017.
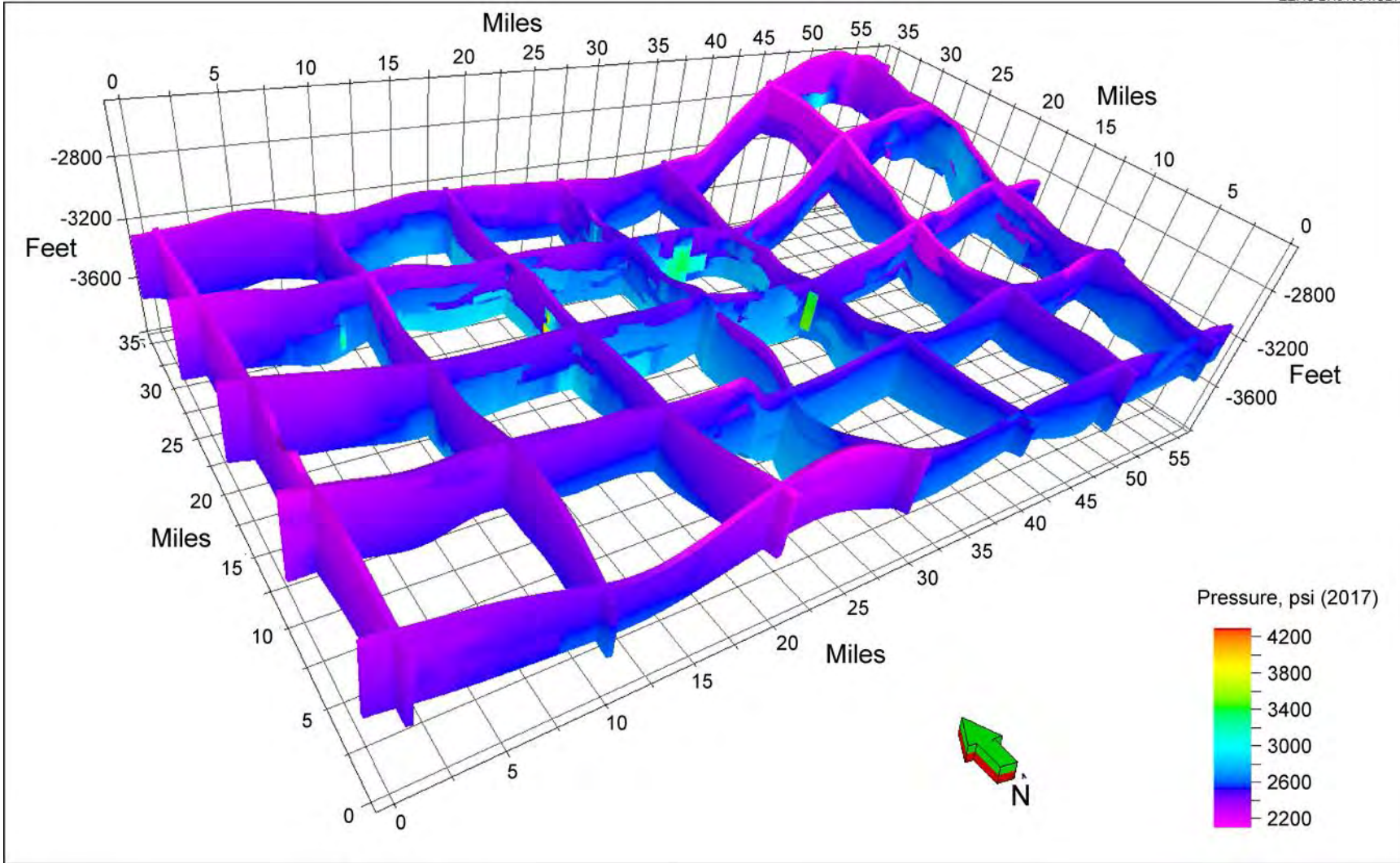
Figure B-2. Fence diagram illustrating simulated pressure distribution in 2017 for Case 3_C
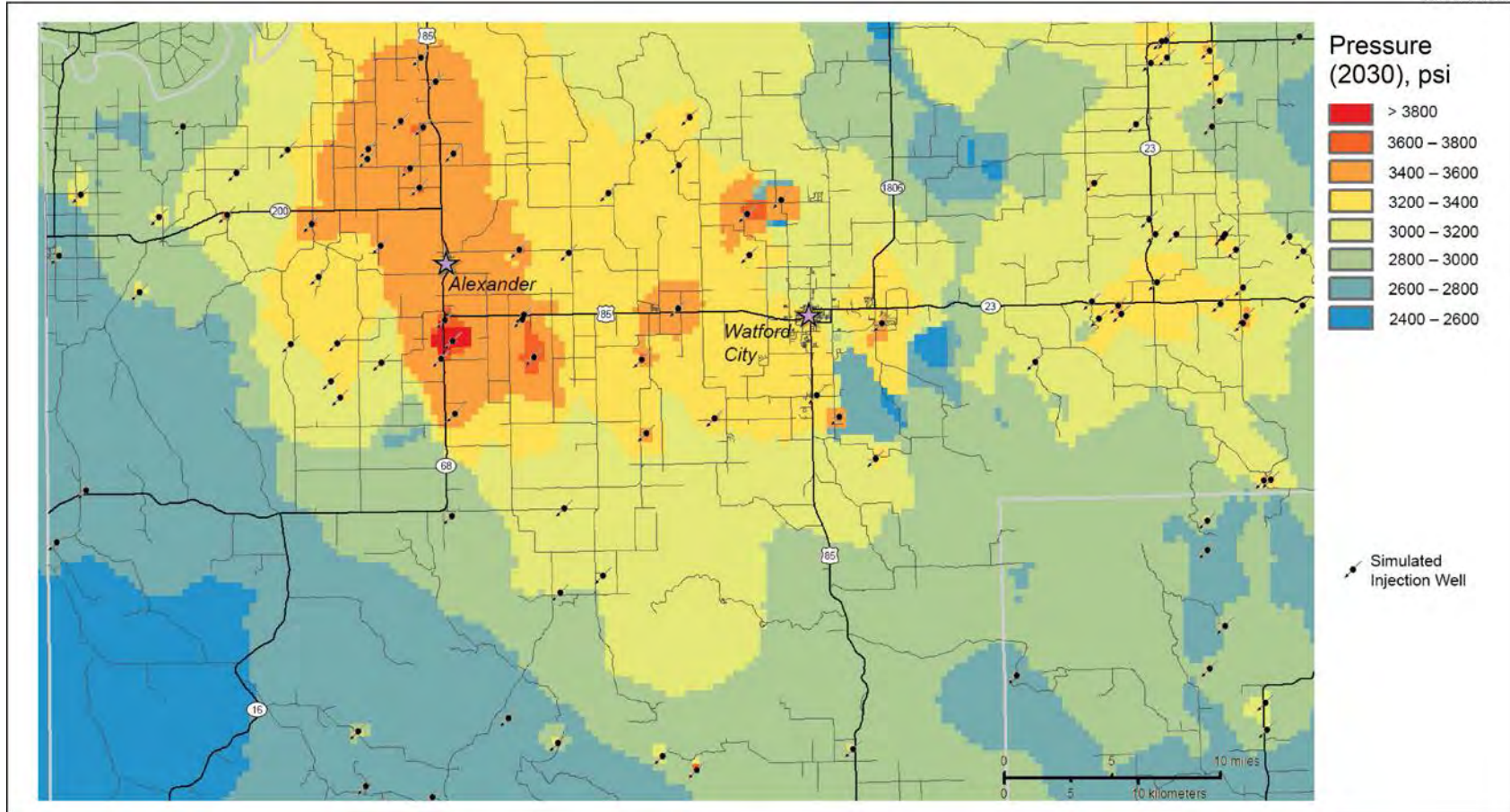
Figure B-3. Maximum hypothetical fluid pressure exhibited by any of the 40 model layers in each grid cell. This represents the pressure distribution in 2030 for Case 3_C.
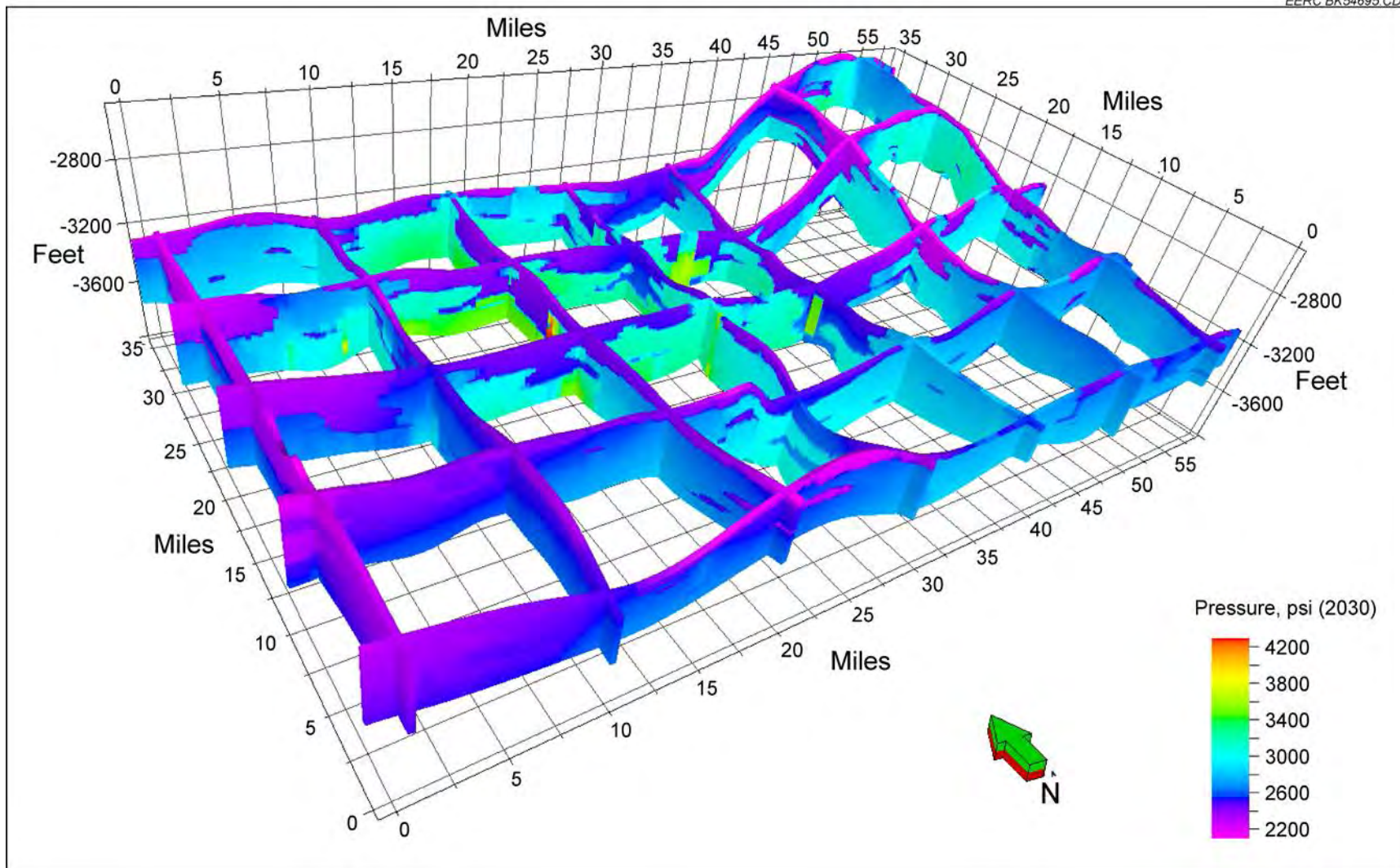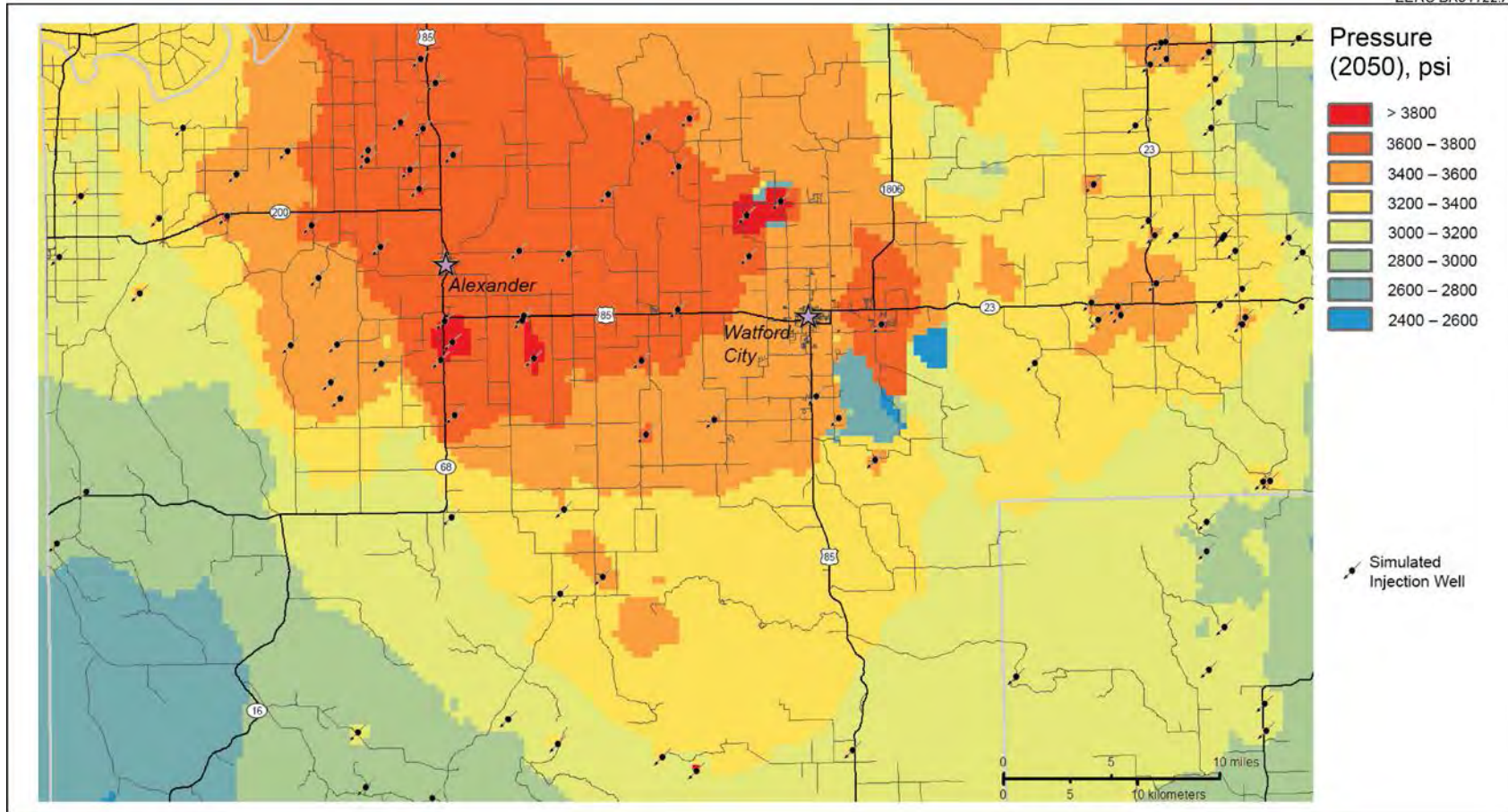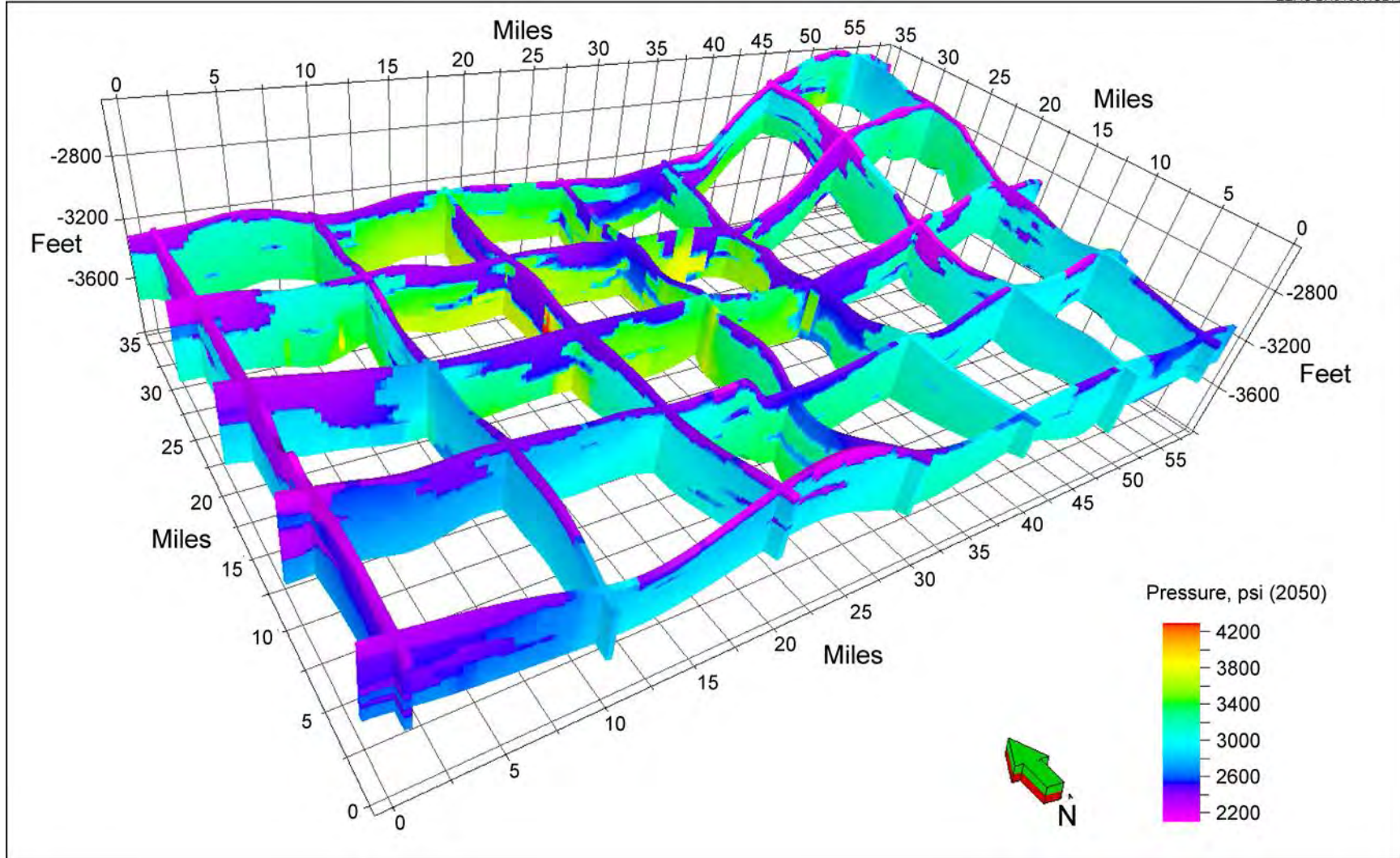
Figure B-4. Fence diagram illustrating the hypothetical pressure distribution in 2030 for Case 3_C.
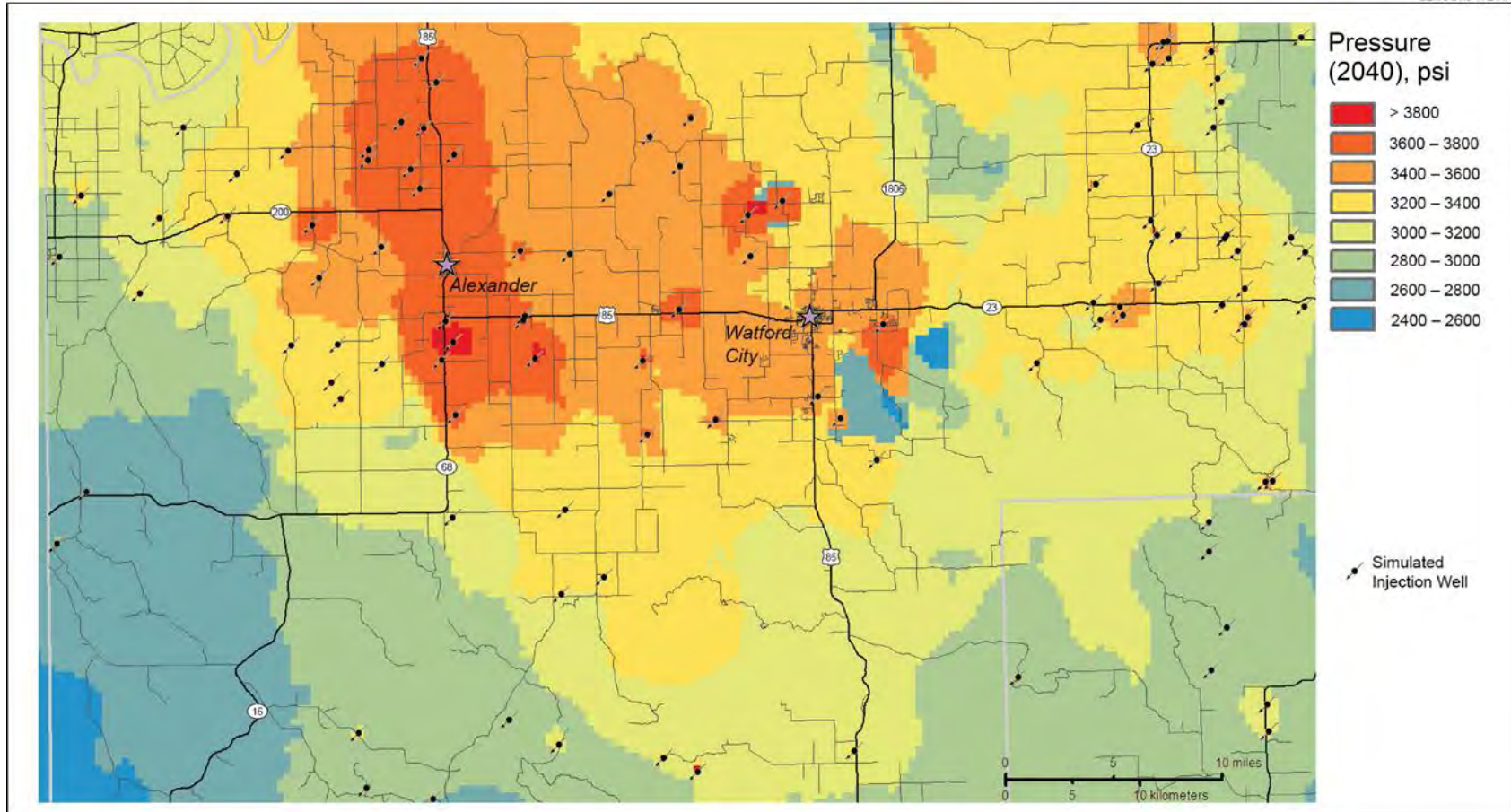
Figure B-5. Maximum hypothetical fluid pressure exhibited by any of the 40 model layers in each grid cell. This represents the pressure distribution in 2040 for Case 3_C.
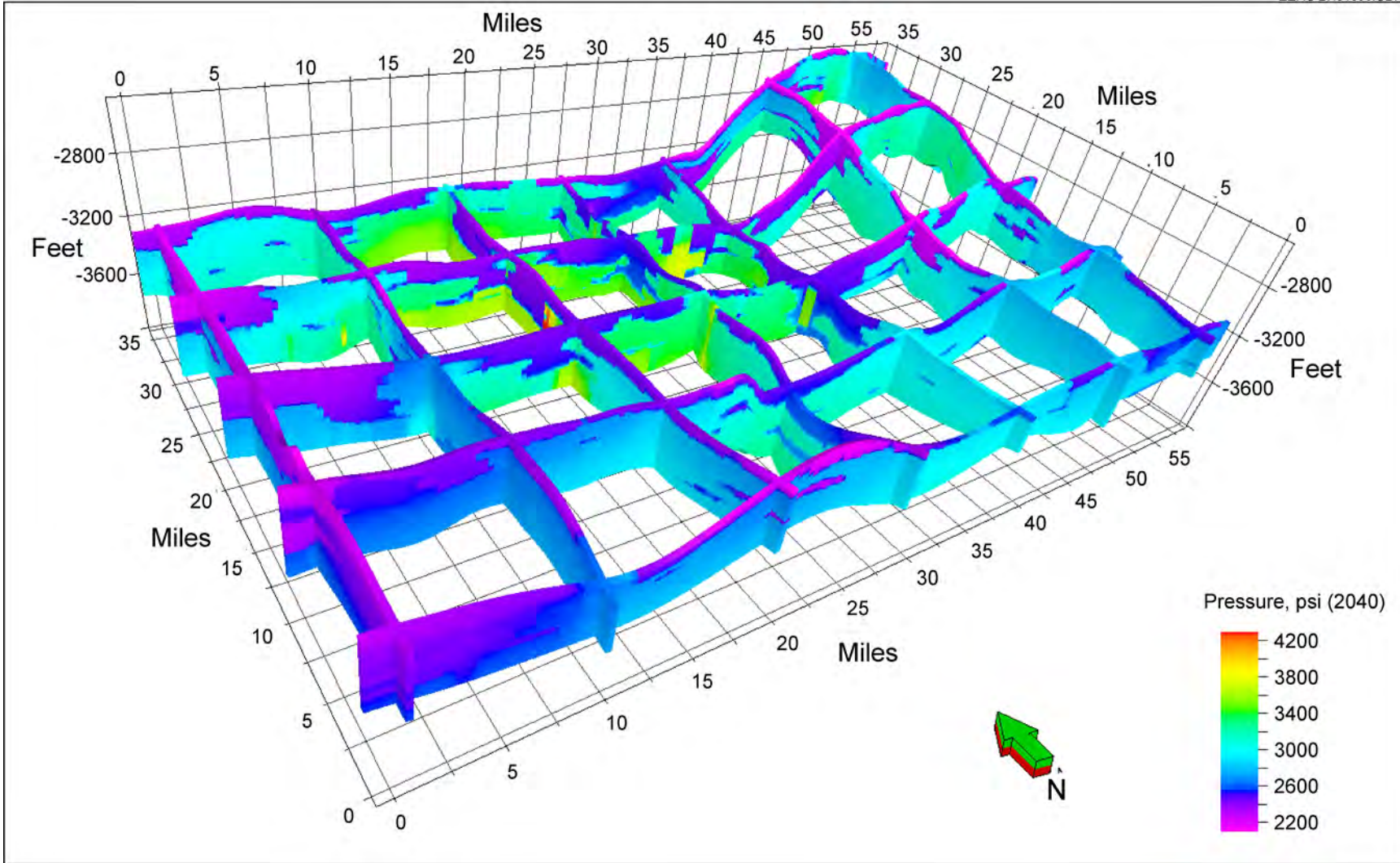
Figure B-6. Fence diagram illustrating the hypothetical pressure distribution in 2040 for Case 3_C.

Figure B-7. Maximum hypothetical fluid pressure exhibited by any of the 40 model layers in each grid cell. This represents the pressure distribution in 2050 for Case 3_C.

Figure B-8. Fence diagram illustrating the hypothetical pressure distribution in 2050 for Case 3_C.
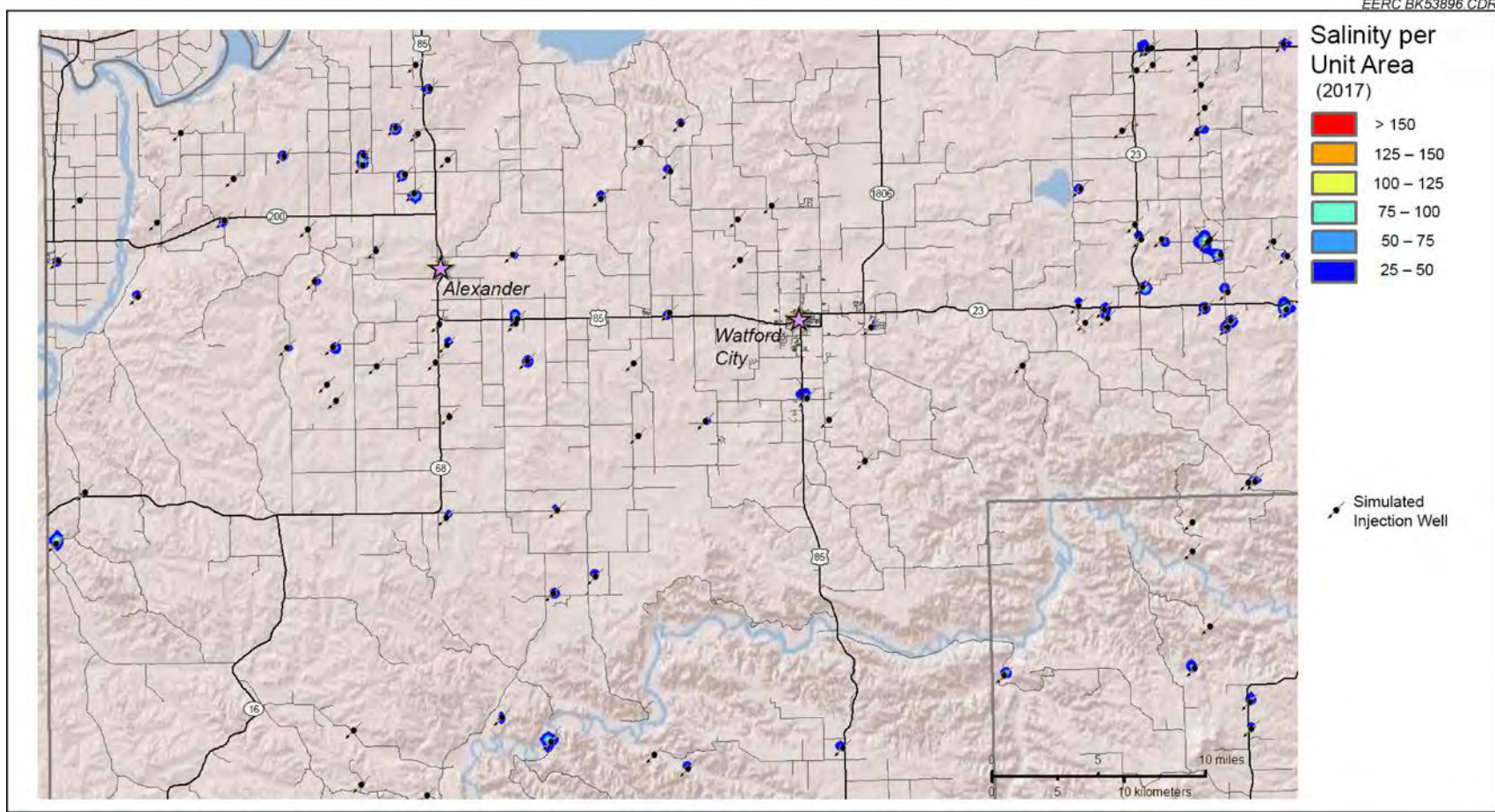
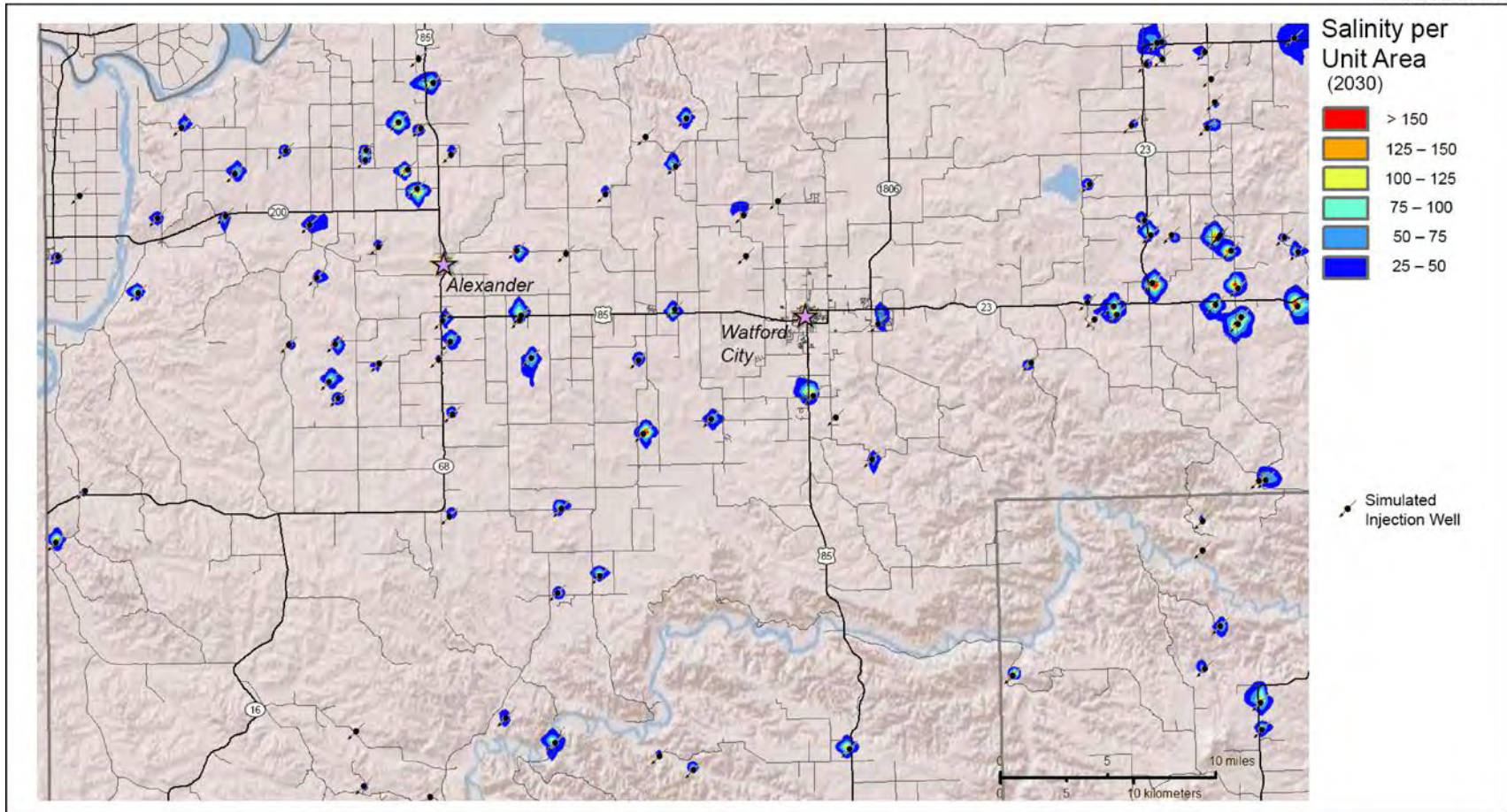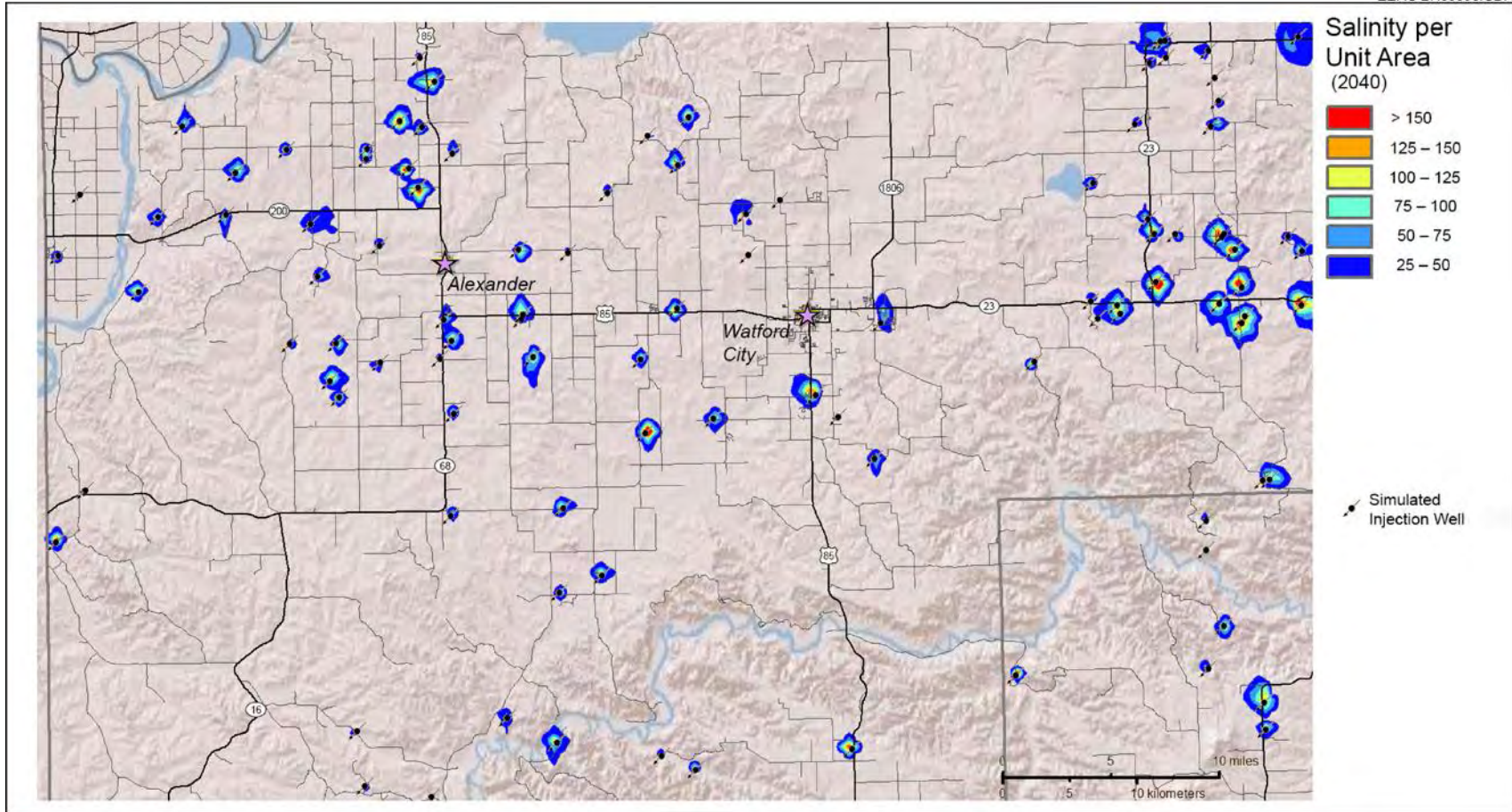Figure B-9. Hypothetical salinity per unit area in 2017 for Case 3_C.
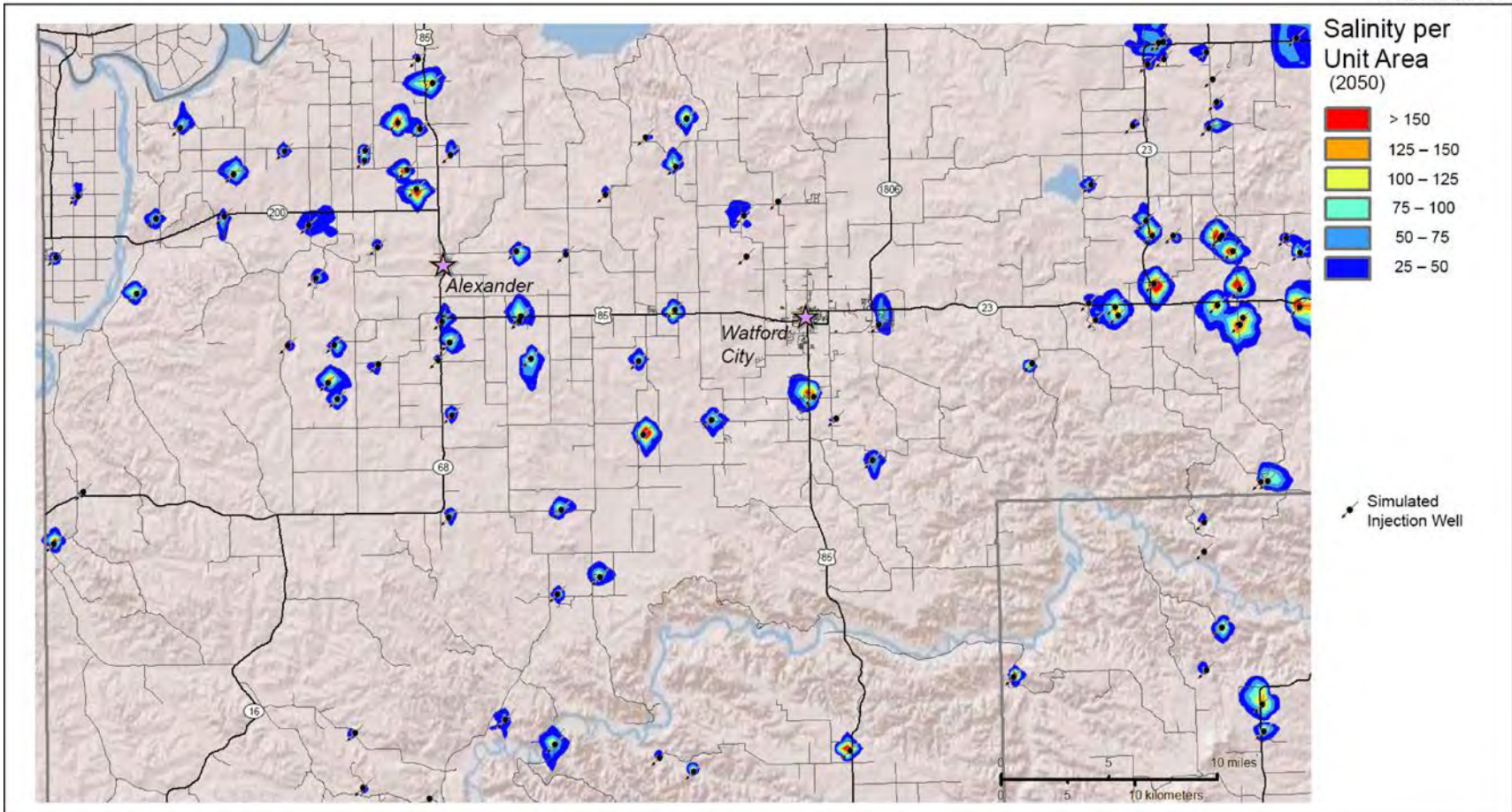
Figure B-10. Hypothetical salinity per unit area total in 2030 for Case 3_C.

Figure B-11. Hypothetical salinity distribution in 2040 for Case 3_C.

Figure B-12. Hypothetical salinity per unit area total in 2050 for Case 3_C.